

UNCLASSIFIED

AD 4 6 4 2 6 1 L

DEFENSE DOCUMENTATION CENTER

FOR

SCIENTIFIC AND TECHNICAL INFORMATION

CAMERON STATION ALEXANDRIA, VIRGINIA



UNCLASSIFIED

NOTICE: When government or other drawings, specifications or other data are used for any purpose other than in connection with a definitely related government procurement operation, the U. S. Government thereby incurs no responsibility, nor any obligation whatsoever; and the fact that the Government may have formulated, furnished, or in any way supplied the said drawings, specifications, or other data is not to be regarded by implication or otherwise as in any manner licensing the holder or any other person or corporation, or conveying any rights or permission to manufacture, use or sell any patented invention that may in any way be related thereto.

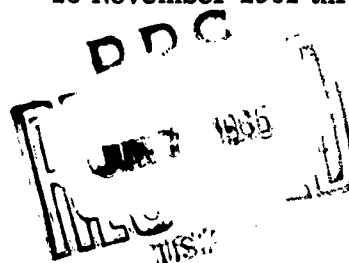
464261L

CATALOGED BY: DDC

AS AD N7

464261

AVAILABLE COPY WILL NOT PERMIT  
FULLY LEGIBLE REPRODUCTION.  
REPRODUCTION WILL BE MADE IF  
REQUESTED BY USERS OF DDC



**Exploration and  
Evaluation  
of  
New Glasses  
In  
Fiber Form**

16 November 1961 through 15 February 1965

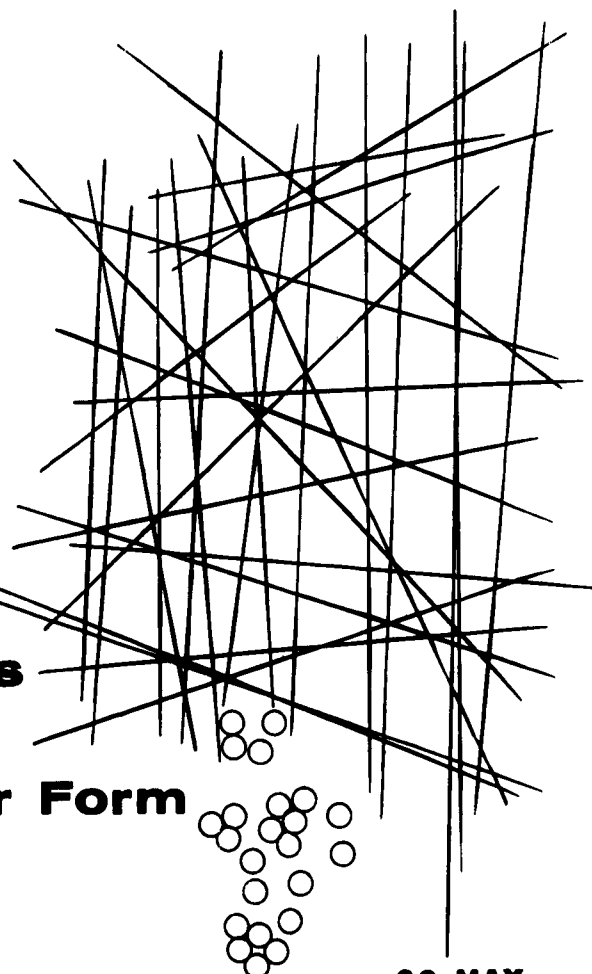
20 MAY  
1965



A Division of International Harvester Company

**U.S. Naval Research Laboratory**  
contract **NONR 3654(00)(X)**

final summary report



EXPLORATION AND EVALUATION  
of  
NEW GLASSES IN FIBER FORM

Prepared under U. S. Naval Research Laboratory  
Contract NONR 3654(00)(X)

FINAL SUMMARY REPORT

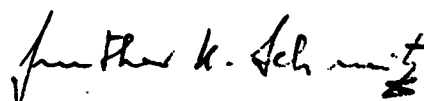
16 November 1961 through 15 February 1965

Issued: 20 May, 1965

This report applies to work on:

NRL Project 62 R05 19A  
Technical Memo 258

Prepared by:

  
Gunther K. Schmitz  
Senior Research Engineer

Approved by:

  
A. G. Metcalfe  
Associate Director  
of Research

  
John V. Long  
Director of Research

SOLAR

A Division of International Harvester Company  
2200 Pacific Highway, San Diego, California 92112

**NOTICE**

**This document may not be reproduced or published in any form in whole or in part without prior approval of the Government.**

## FOREWORD

This report covers the work performed by Solar over roughly a three-year period, from 16 Nov. 1961 to 15 Feb. 1965, under the direction of J. A. Kies, Scientific Officer, Naval Research Laboratories, Contract Nonr-3654(00)(X), Problem 62R05-19A.

The work was performed by Gunther K. Schmitz as Principal Investigator, under the general guidance of John V. Long, Director of Research Laboratories, and Arthur G. Metcalfe, Associate Director of Research. The experimental work was performed by Donald G. Clark, Senior Research Technician. The computer program was executed by Robert M. Gardner, Engineer.

## ABSTRACT

The strength of E- and S-glass fibers was investigated by tensile tests and static fatigue (constant load) tests. The principal variables were: gage length, strain rate, applied stress in static fatigue, and humidity. The gage length study led to identification of two types of surface flaws and a structural flaw type related to the heterogeneity of the glass network. Severity and distribution of flaws were derived from failure probability plots and strength-length plots at one strain rate in laboratory atmosphere. The effects of strain rate and of humidity on the flaw characteristics was studied.

Extensive static fatigue tests provided insight into the stress corrosion processes. Fibers retained the initial tensile strength over 95 percent of the static fatigue exposure. It was postulated that chemical events during this incubation period had to reach a critical stage before stress corrosion could occur, and that corrosion originated on sites of structural flaws located near the surface. These findings are in disagreement with the current theory on stress corrosion and a new model is proposed.

Additional work included investigation of damage resistance of the two glasses, and a study of the effect of gage length on strength of E- and S-glass strands.

## C O N T E N T S

	Page
FOREWORD	111
ABSTRACT	v
GENERAL INTRODUCTION	xi

### P A R T 1.

#### LENGTH EFFECT ON STRENGTH

##### SECTION

I	LENGTH EFFECT ON STRENGTH OF E- AND S- GLASS FIBERS	1
1.1	"Effect of Length on the Strength of Glass Fibers"	1
1.2	Addendum	21
1.3	Summary of Flaws on Glass Fibers	25
II	DAMAGE RESISTANCE OF E- AND S- GLASS FIBERS	27
III	LENGTH EFFECT ON STRENGTH OF STRANDS	29

### P A R T 2.

#### ENVIRONMENTAL EFFECTS ON STRENGTH

IV	EFFECT OF STRAIN RATE	31
V	STRESS CORROSION ON E- GLASS FIBERS	35
5.1	Static Fatigue Tests	35
5.2	Tensile Tests	53
5.3	Conclusions	55
VI	GENERAL CONCLUSIONS	56
VII	RECOMMENDATIONS	57
	REFERENCES	59

#### LIST OF FIGURES AND TABLES

##### Figure

1	General Strength-Length Relationship for Glass Fibers	2
2	Tension Test Equipment Block Diagram	5
3	Single Fiber Tester Set-Up For Short Fiber Testing	5 and 63
4	Multiple Fiber Tester	6 and 63
5	Length Effect on Strength of S- Glass Fibers	9
6	Length Effect on Strength of E- Glass Fibers	9
7	Effect of Distribution Functions on Probability Plot	10



# C O N T E N T S (Cont'd 1 )

Figure		Page
8	Gaussian Failure Distribution at Different Gage Lengths	11
9	Systematic Change of Failure Distribution Curves with Gage Length	12
10	Frequency Distribution of Failure Strength at Different Gage Lengths	12
11	Effect of Narrow Distribution of Stress Concentration Factors	13
12	Effect of Wide Distribution of Stress Concentration Factors	14
13	Graphical Separation of Two Flaw Populations on Gaussian Probability Paper	16
14	Bi-Modal Summation Curves for Virgin S- Glass Fibers	17
15	Distribution Curves for Virgin E- Glass Fibers	20
16	Flaw Analysis for Virgin E- Glass Fibers	20
17	Strength-Length Relationship for Virgin E- Glass Fibers	22
18	Flaw Analysis of OCF Data on Gaussian Probability Paper	22
19	Strength Reduction of Strand Fibers and Artificially Damaged Fibers	26
20	Damage Marks from Garnet Grains on E- Glass	26
21	Length Effect on Breaking Strength of Strands with and without Resin	28
22	Degrading Effect of Poor Fiber Collimation on Strand Strength	28
23	Strength versus Strain Rate Curves for Two Gage Lengths	32
24	Gaussian Failure Distribution Plots at Different Strain Rates	32
25	Strain Rate Curves Obtained from Various Groups of 20 cm Fibers	32
26	Effect of Annealing on Shape of Failure Distribution	34
27	Strength Behavior of Fibers and of Pressure Vessels	34
28	Static Fatigue Data from 2.5 cm Virgin E-Glass Fibers in 100% RH	40
29	Failure Time Probability Plots at Various Applied Stresses	41
30	Static Fatigue Curve for 100% RH	42
31	Tensile Strength Distribution of Unbroken Fibers (Test Series III)	42
32	Tensile Strength Distributions of Unbroken Fibers	48
33	Growth of Flaw Depth with Time	48
34	Static Fatigue Failure Time versus Inverse Applied Stress	50
35	Delay of Corrosion in Static Fatigue Due to Presence of Water	50
36	Time Relationship Between Tensile and Static Fatigue Test	52
37	Comparison of Strain Rate and Static Fatigue Data	52

## LIST OF TABLES

### Table No.

I	Materials Tested	3
---	------------------	---

# C O N T E N T S (Cont'd 2)

Table No.	Page
II Effect of Fiber Separation on Strength	4
III Summary of Sample Sizes at Different Test Lengths	8
IV Characteristics of Flaws on E- Glass Fibers	24
V Characteristics of Flaws on S- Glass Fibers	24
VI Theoretical Expressions for the Static Fatigue Curve	36
VII Static Fatigue Program Summary	36
VIII Strength of Control Fibers in Static Fatigue Tests	44
IX Strength Retention of Stress Corrosion Tested Fibers	44
X Cumulative Damage from Stress Corrosion in Tensile Test	54
XI Stress Corrosion Time Equivalence of Tensile Tests	54
 APPENDIX A - Photographs of Test Instrumentation	 61-69
APPENDIX B - Application of Single Fiber Data to Composite Structures	71
APPENDIX C - List of Reports	77
- Reference Chart for Test Series and Failure Probability Plots	79
 Distribution List -	 a b c d
 D D Form 1473	 e f

## GENERAL INTRODUCTION

The work performed under this contract can be divided conveniently into two parts: Length Effect on Strength, and Environment Effect on Strength.

Part 1, Length Effect on Strength, is comprised of the work accomplished during the first two years. This work included: length effect studies on E- and S-glass (994 glass) fibers; length effect studies on strands; and investigation of damage resistance of the two glasses. One of the questions to be answered by the length effect study was "how to determine the strongest fiber for particular applications." Results soon indicated that there was no direct answer; it became increasingly clear that strength properties were rather complex and that the commonly used term "Strength of Fibers" applies only to a relatively narrow set of experimental strength data. The meaning of "strength" must be interpreted in a broader sense because of the many influencing factors.

Some of these factors were investigated following the length effect study. This work is reported in Part II. The primary factor investigated was humidity. Its effect on strength was determined for the case of constant stress (static fatigue) and for variable stress (tensile tests). Another series of tests was concerned with the effect of strain rate where the change in test time leads to different exposures to atmospheric moisture.

A few remarks concerning the organization of this Final Summary Report may be helpful. The primary subject of Part 1, Strength of Single Fibers, is presented in Section I as a reprint of a paper delivered at ASTM(22), followed by an addendum reporting on subsequent single fiber work. This section concludes with a summary of flaws on glass fibers. This method of reporting has been chosen for the convenience of both reader and writer, since it presents the essential results in a condensed form.

The two subsequent sections, Damage Resistance, and Strength of Strands, are reported in Part 1 because the method of strength evaluation, and environmental conditions were the same as for the previous study.

Part 2 presents the results from strain rate tests in Section IV, and from static fatigue tests in Section V. The title of Section V, "Stress Corrosion of E-Glass Fibers," indicates that the stress corrosion problem constitutes the major theme. An analysis of stress corrosion in tensile tests is part of this section.

Photographs of test instrumentation are shown in Appendix A. Appendix B contains a contribution by J. A. Kies, NRL, concerning the application of single fiber data (such as reported here) to composite structures.

Bi-monthly progress reports and yearly reports are listed in Appendix C with reference to the respective Technical Memo numbers. Key words indicate major subjects. A reference chart for test series is included in Appendix C because the designation of earlier test series has been changed for reason of publication. The last column of this chart lists the reports where the failure probability plots of the respective test series can be found.

## PART 1.

### LENGTH EFFECT ON STRENGTH

Part 1 is concerned with the effect of gage length on the strength of single fibers and strands for one experimental condition, i.e., strain rate  $0.06 \text{ min}^{-1}$  (referred to as standard strain rate) and laboratory atmosphere of approximately 50% RH.

#### I. LENGTH EFFECT ON STRENGTH OF E- AND S-GLASS FIBERS

##### 1.1 "EFFECT OF GAGE LENGTH ON THE STRENGTH OF GLASS FIBERS"

The purpose of this work was to investigate (1) the importance of gage length in tension testing of glass fibers, including verification of a proposed damage model, and (2) the applicability of Weibull-type analyses to study flaws governing failure. E- and S-glass fibers, both virgin and from strands, were examined.

A marked effect of gage length was found on the strength of glass fibers. The logarithmic strength-length plots were not linear over the entire length range from 0.025 to 30 cm. For a given fiber, a slope change occurred at a critical gage length due to varying contributions of mixed flaw populations to failure strength. Different flaws could be identified through a specially developed analysis of failure distribution plots. Single exponent failure distribution functions, such as the Weibull function, are inadequate to describe failure in glass for the conditions investigated. At least two different exponents are needed to fully describe the observed strength behavior. As a result, it does not appear possible to substantiate a generalized model to describe damage of glass fibers.

The percentage of the strength of virgin glass monofilaments that can be retained in a glass-fiber reinforced structure has increased steadily in the past few years. For example, a glass with a strength of 700,000 psi as a monofilament will permit a 10 cm (4-in.) diameter bottle to be made that fails at 400,000 psi stress in the wall, or a larger motor case that fails at a stress of 270,000 psi.<sup>2</sup> The size effect indicated by such results

on pressure bottles has not been studied in detail, partly because the basic information on the effect of size on the strength of monofilaments has not been available. Although certain data have indicated an effect of gage length on the breaking strength of monofilaments, there have been no standards adopted for tension testing of glass fibers. Recent publications report tests on fibers from 2.5 to 7 cm in length; therefore, one objective of the work reported in this paper was to establish the importance of gage length in tension testing so that the groundwork would be laid for adoption of a standard gage length. A second objective of the work was to apply Weibull-type analyses to the data to

\* Presented at the Sixty-seventh Annual Meeting of the Society, June 21-26, 1964.

† This work was performed under Navy Contract Nonr-3654(00)(X).

<sup>1</sup> Solar, Division of International Harvester, San Diego, Calif.

<sup>2</sup> Based on information supplied by Owens-Corning Fiberglass Corp., Granville, Ohio.

learn more about the flaws governing failure.

#### THEORETICAL BACKGROUND

The theoretical strength of glass may be estimated in several ways. A mechanical model leads to a strength equal to  $\frac{1}{10}$  of the elastic modulus, and a chemical approach derives the strength from the bond energy. Both approaches lead to values above 1,000,000 psi. To explain

when the stress at any one flaw becomes larger than the ability of the surrounding material to resist the local stresses. Weibull assumed a reasonable distribution function and derived the expression:

$$S = 1 - \exp \left[ -V \left( \frac{\sigma}{\sigma_0} \right)^m \right] \dots (1)$$

where:

$S$  = probability of failure,

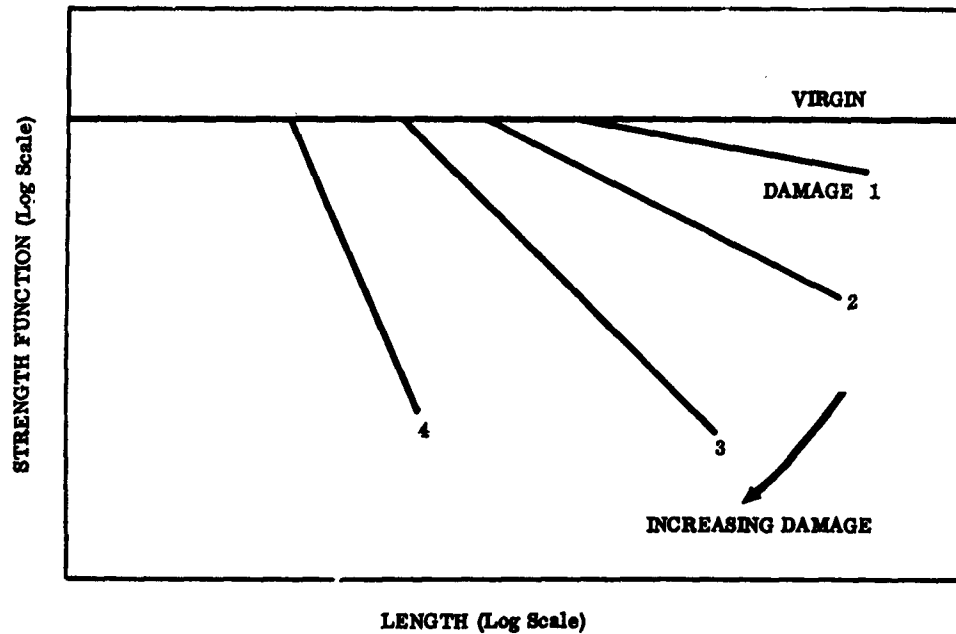


FIG. 1—General Strength-Length Relationship for Glass Fibers.

the observed lower values, Griffith (1)<sup>3</sup> introduced the concept that glass contains pre-existing flaws so that the fracture process is one of crack propagation rather than initiation. In agreement with this concept, Griffith found a size effect for glass of different diameters. Weibull (2) proposed a statistical theory of failure based on randomly distributed flaws of random severity. The “weakest link” approach was adopted as a criterion of failure, that is, a brittle material fails

<sup>3</sup> The boldface numbers in parentheses refer to the list of references appended to this paper.

$\sigma$  = applied stress to a volume of material,  $V$ ,

$\sigma_0$  = upper limiting strength, and

$m$  = index of relative number of flaws.

This relationship is deficient because the applied stress must approach infinity if the probability of failure is to approach unity (certainty of failure). Kies (3) suggested that a simple solution to this problem would be to modify the Weibull relationship:

$$S = 1 - \exp \left[ -V \left( \frac{\sigma - \sigma_u}{\sigma_0 - \sigma} \right)^m \right] \dots (2)$$

where:

$\sigma_u$  = lower limiting strength of glass  
(may be zero),

$\alpha$  = damage coefficient,

and the other variables have the same meaning as in the original Weibull expression.

Apart from the early work of Griffith (1) on the effect of diameter, there have been few attempts to apply statistical theories to the failure of glass. Whereas

The deficiencies of the Weibull relation (Eq 1) had led Kies (3) to develop the modified Eq 2. However, it was recognized by Kies that the upper limiting strength  $\sigma_o$  was not equal to the virgin strength of glass, but was twice this value. Accordingly, the physical behavior of glass monofilaments could be represented empirically by a plot such as Fig. 1. Examination of this representation was an inherent part of this work.

TABLE 1—MATERIALS TESTED.

Glass	Source of Fiber	Manufacturer	Average Dia, in.	Finish	Remarks
E....	As drawn:	Solar			drawn in 1963
	EM 1	from OCF marbles	$40 \times 10^{-4}$	none	preliminary study
	EM 2	from OCF marbles	$39 \times 10^{-4}$	none	final virgin data
	Strand:	OCF			1962, commercial E
	ES 1	spool 1	$37 \times 10^{-4}$	A-1100	glass, ECG 150-1/0
	ES 2	spool 2	$37 \times 10^{-4}$	A-1100	
S....	As drawn:	OCF			drawn in 1963 from
	SM1		$42 \times 10^{-4}$	none	single hole bushing
	Strand:	OCF			
	SS 1	(experimental X-994)	$42 \times 10^{-4}$	195	received in 1962
	SS 2	(semi-production S-994)	$39 \times 10^{-4}$	195	drawn in 1962

\* Diameters held within  $\pm 5$  per cent (905 fibers).

<sup>b</sup> No diameter survey, average diameter from OCF (470 fibers).

<sup>c</sup> All fiber diameters within  $\pm 5$  per cent (180 fibers).

<sup>d</sup> 99 per cent of fiber diameters within  $\pm 12$  per cent (678 fibers).

Griffith found the strength of glass to decrease as the size increased, Thomas (4) in a series of carefully controlled experiments found no effect over the diameter range 20 to  $60 \times 10^{-5}$  in. Thomas attempted to compensate for the size change by variation in drawing speed and adopted careful precautions to avoid damage after drawing. Variation of gage length, rather than diameter, to study the flaw distribution as in Ref. (3) has the advantage that specimens can be taken from a single drawing of glass fibers, so that the mixed flaw populations that result from the different drawing conditions necessary for different diameters are avoided.<sup>4</sup> This approach has been used in the present work.

#### EXPERIMENTAL APPROACH

A wide range of gage lengths is necessary in order to investigate the length effect on properties. It was desired to cover, among others, the previously unexplored range between 0.5 cm and approximately 0.015 cm. Anderegg (5) has performed conventional tension tests from 100 to 0.5 cm, and the gage length of approximately 0.015 cm was obtained as the equivalent gage length (to uniaxial tension) in the loop test developed

<sup>4</sup> Another point was brought out by J. A. Kies upon review of this paper: "Also, the differences in drawing conditions for different diameters of filaments produces uncontrolled degrees of compaction so that aside from the flaws the glasses are physically different."

by Sinclair (6). The complex bending stress condition in the loop test does not lead to completely unambiguous interpretation in terms of a tension test because of the stress gradients.

Because this work has been performed with gage lengths an order of magnitude lower than those studied previously in tension tests, it has been necessary to pay unusual attention to the experimental techniques. The most difficult problem has been the determination of the exact gage length below 1 mm.

from which individual fibers are separated. Thus, 50 fibers are obtained for each gage length from a population of 65. Separation of individual fibers was carried out in the following manner: One end of a bundle is taped to a holder (in front of a dark background for better visibility). A fiber is separated from the free end by means of a slender, sharply-pointed needle. Fiber and remaining bundle are then slowly pulled apart by exerting a constant, gentle pull outward-downward on both ends. Separation

TABLE 2—EFFECT OF FIBER SEPARATION ON STRENGTH.

Fiber	Test Length, cm	Avg Strength, total <sup>a</sup>	Avg Strength <sup>a</sup>		Variation from Avg Total <sup>b</sup>	
			First	Second	First	Second
SS 1.....	0.75	455	462	447	+1.5	-1.7
	1.5	435	450	419	+3.5	-3.7
	3	388	380	396	-2.0	+2.0
	6	346	382	310	+10.1	-10.4
	12	310	323	292	+4.1	-4.5
	24	325	324	327	-0.3	+0.6
SS 2.....	0.5	526	542	511	+3.1	-2.8
	0.5	491	485	499	-1.2	+1.7

<sup>a</sup> Ksi.

<sup>b</sup> Per cent.

#### Materials Tested:

Two glasses, E and S, were investigated. Table 1 summarizes the materials tested and also includes other necessary information such as average diameters, manufacturer, and finish. Good sampling technique is important and will be discussed in detail later.

#### Sampling from Strands:

Assuming a desired specimen of 50 fibers for each of nine different test lengths, a sufficient amount (3 ft of strand) is taken from the spool. A bundle of approximately 65 fibers (to allow for fiber separation loss) out of a total of 204 in the strand is separated, cut into nine parts, and labeled in ascending order of the programmed gage lengths. Each part is subdivided into three groups

takes place in short leaps depending on amount and tenacity of finish. This mode of separation seems to indicate that a finish-finish separation took place rather than finish-glass.

In order to investigate the effect of the separation process on the strength of fibers, a comparison was made between the average strength of the first half of the population of 50 fibers with the second half. Table 2 shows that the average strength of the first 25 fibers separated was not significantly different from that of the second 25 fibers separated.

#### Sampling from Monofilaments:

The sampling procedure differed from the above in that only three gage lengths out of the programmed nine were as-

signed to one monofilament 1.6 meters (62 in.) long, but four or five fibers are sampled for each gage length. This ap-

setup time for different gage lengths in the test equipment. Such changes are difficult below 0.25 cm, where micro-

#### SPEED CONTROL

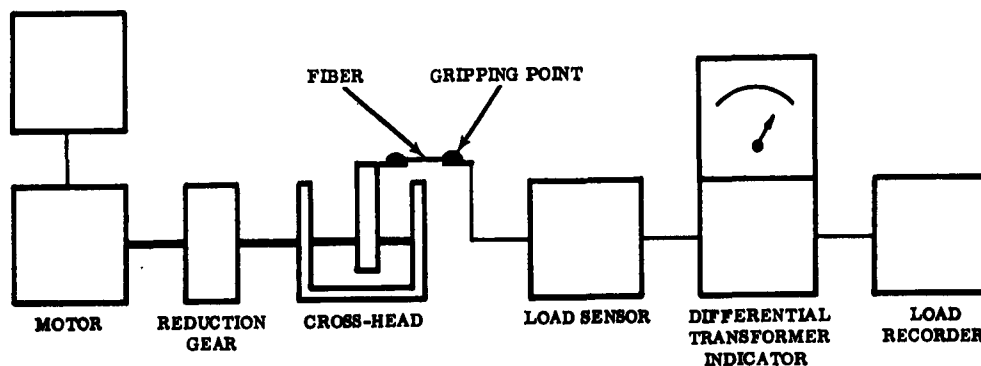


FIG. 2—Tension Test Equipment Block Diagram.

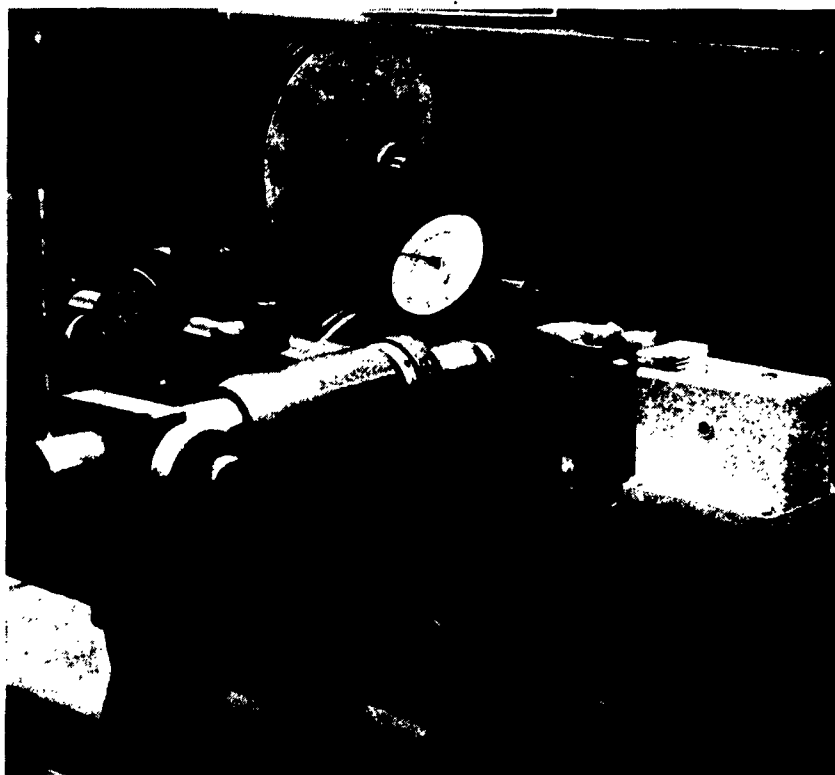


FIG. 3—Single-Fiber Tester Setup for Short Fiber Testing.

proach was necessary because of the time factor involved in testing large sample sizes, and the need to reduce the

scopic observation is required to adjust the gripping points to the desired gage lengths. A certain bias was introduced



by this sampling method because of strength variations between filaments that affect four or five fibers simultaneously. However, analysis revealed that bias is negligible for specimens between 70 and 100.

#### *Tension Test Equipment:*

A single-fiber tester was built, based on a design by Otto (7). Some modifications included: gripping wax carriers, type of wax, reduction gears for various

microscope at 20 $\times$  to determine gage length. The dial indicator served as a crosshead zero position index as well as a head travel measuring device.

The entire equipment was powered by a constant voltage source. Accuracy of the load recording was found to be  $\pm 1$  per cent; this included systems, calibrations, and readout errors.

To handle large specimens, a multiple-fiber tester was designed to test four fibers simultaneously. Figure 4 shows



FIG. 4—Multiple-Fiber Tester.

fiber lengths, and arrangement on an optical bench to accommodate change in gage length.

The block diagram in Fig. 2 illustrates the sequence of components, while the photograph, Fig. 3, shows the actual apparatus in a setup for short-gage-length testing.<sup>5</sup> Here the gripping points (wax carriers  $\frac{1}{2}$  in. (1 cm) diameter) are in line-of-sight of the bifilar micrometer

this equipment. The lower gage limit in multiple testing was 0.5 cm.

#### *Testing Procedures:*

Tension testing was conducted at a laboratory temperature of  $77 \pm 2$  F ( $25 \pm 1$  C) and relative humidity between 40 and 50 per cent. These conditions are generally regarded as satisfactory if the fibers are tested within a few days. In this work, monofilaments were tested within 24 hr after drawing.

Extreme care was taken in the handling of fibers. No contact was permitted with the center section of the fibers used as gage length. Frames were used to transfer fibers to the tensile machine and

<sup>5</sup> Load-measuring components were: (1) load sensor—Schaevitz, LVDT-TDC-3,  $\pm 350$  g; (2) differential transformer indicator—Daytronic 300 B; and (3) load recorder—Texas Instrument, Servo-riter, PSR, chart speed 1 in./10 sec. A Minarik  $\frac{1}{8}$ -hp speed-controlled Bodin motor (240:1 ratio) operated the drive spindle via double-belt reduction gears.

were not removed until the wax gripping medium had solidified. Horizontal and longitudinal alignment was ensured to avoid bending stresses at the point of fiber exit from the wax. It was found that the commonly used red sealing wax did not grip the fiber adequately. At short gage lengths, fiber slippage led to uncertainty in the exact length under stress. A search led to superior wax (Hi-Test Chemical Co. Wax No. 3066). This wax requires the fiber to be exposed to 350 F for approximately 30 sec; the absence of preferential failures at the fiber exit from the wax was taken as proof that this exposure had no detrimental effect.

Tests were conducted at a strain rate of 0.06 to 0.07 per min; this led to the failure of virgin E- and S-glasses within the same time (about 45 sec) and ensured approximately equal exposures to the atmosphere during stressing.

Fiber diameters were measured with a Leitz microscope at 500X by means of a bifilar eyepiece with micrometer readout. The fiber is immersed in methylphenol ether (Anisole) with a refractive index of 1.518. The fibers had refractive indexes in the range 1.49 to 1.55. Self-consistent diameter readings were obtained by limiting the readout to one operator. It is estimated that the average diameter error did not exceed  $\pm 1$  per cent of the fiber diameter of  $40 \times 10^{-5}$  in. Since the purpose of this work was the comparison of strengths at different lengths, reproducibility was more important than absolute values. A com-

parison with another laboratory showed somewhat larger differences.<sup>6</sup>

Combination of the error due to diameter readout and the error due to load measurement leads to an over-all maximum error in the stress of  $\pm 3.5$  per cent. This includes only self-consistency errors.

#### *Determination of Gage Length:*

Gage length is an important variable in this study and must be known accurately. Above 0.25 cm there appears to be no problem if the gage length is taken between the fiber exit points from the wax. Further support for this approach is provided by the small percentage of failures at the exit point or in the wax (less than 7 per cent).

For gage lengths below 0.25 cm, the number of failures at the exit point or in the wax increases slowly at first, reaching 15 per cent at 0.05 cm, and then increases more rapidly to 25 per cent at 0.025 cm. Such tests are rejected. In view of the large number of rejections at 0.05 cm and below, a study was made of the wax solidification process and its effect on gripping. The standard fiber mounting process included fan cooling to reduce the waiting time between tests. First, it was shown that stress buildup (up to 10 per cent of failure strength) in the fiber by contraction on cooling did not affect strength; continuous reduction of the stress during cooling had no effect. Second, the solidification pattern was changed by replacing accelerated fan cooling with natural convective cooling. More uniform cooling resulted, and much more effective gripping of the fiber was indicated because the percentage of failures in the wax fell markedly, the elastic pullout of the wax was reduced, and load-elongation curves departed to a lesser extent from a straight line. The improvement was very marked at 0.025-cm gage lengths, but the natural convective cooling time was 20 min so that

<sup>6</sup> This comparison was made with Narmco Research and Development, San Diego, Calif., by arrangement with W. H. Otto. It was found that individual readout of the four participants was self-consistent (less than one per cent), but actual values varied by up to 2.8 per cent. This leads to a maximum strength difference of 5.6 per cent due to diameter readout; this figure corresponds to an average difference of 5 per cent in strength based on many years of observations by Otto (7).

the method was somewhat impractical. However, the interpretation of results that are presented later is not critically dependent on the strength values for the 0.025-cm gage length, so that limited determinations were made with this method of cooling. In the case of fibers separated from strands, it was found that these problems were less apparent, suggesting that the finish applied in stranding aids in wax gripping.

earlier. Some wax pullout is inevitable because the elastic modulus of the mounting medium is low, but such pullout indicates good adherence of the wax to the fiber. This was indicative of a good test, and fracture within the pulled-out wax cone occurred very infrequently. In these cases, the gage length was measured between the tips of the cones. The gage length measured immediately prior to fracture for good tests was approxi-

TABLE 3—SUMMARY OF SAMPLE SIZES AT DIFFERENT TEST LENGTHS.\*

Length, cm	EM 1	EM 2	ES 1	ES 2	SM 1	SS 1	SS 2
0.025.....	...	...	...	...	31	...	48
0.5.....	...	81	...	...	18	12	25
0.1.....	28	85	...	...	13	25	25
0.25.....	14	92	...	...	5	25	25
0.5.....	37	93	...	...	25	...	25
0.75.....	...	...	...	...	...	75	...
1.0.....	29	96	...	...	27	...	25
1.5.....	...	...	25	79	...	75	25
2.....	36	77	...	...	24	...	...
3.....	...	...	...	50	...	75	25
4.....	28	85	...	...	19	...	...
6.....	...	...	25	79	...	50	25
8.....	40	84	...	...	18	...	...
12.....	...	...	...	83	...	43	...
24.....	...	...	25	79	...	50	...
30.....	...	...	...	25	...	...	...

\* Total: 2233 fibers.

Fiber breakage within the wax makes the gage length indeterminate, and, as discussed earlier, such failures are rejected. Other problems in the determination of gage length arise from slippage in the wax and wax pullout. Slippage implies separation at the fiber-wax interface so that the true gripping point (that is, where stress attenuation begins) is within the wax, and the gage length is indeterminate. Such slippage is clearly indicated by a sawtooth pattern in the load-elongation diagram; the respective results were rejected and have been included in the rejection percentages cited

previously. Some wax pullout is inevitable because the elastic modulus of the mounting medium is low, but such pullout indicates good adherence of the wax to the fiber. This was indicative of a good test, and fracture within the pulled-out wax cone occurred very infrequently. In these cases, the gage length was measured between the tips of the cones. The gage length measured immediately prior to fracture for good tests was approxi-

#### EXPERIMENTAL RESULTS

Table 3 shows the total number of tests performed on various glasses at different gage lengths. Average strengths were calculated from the individual re-

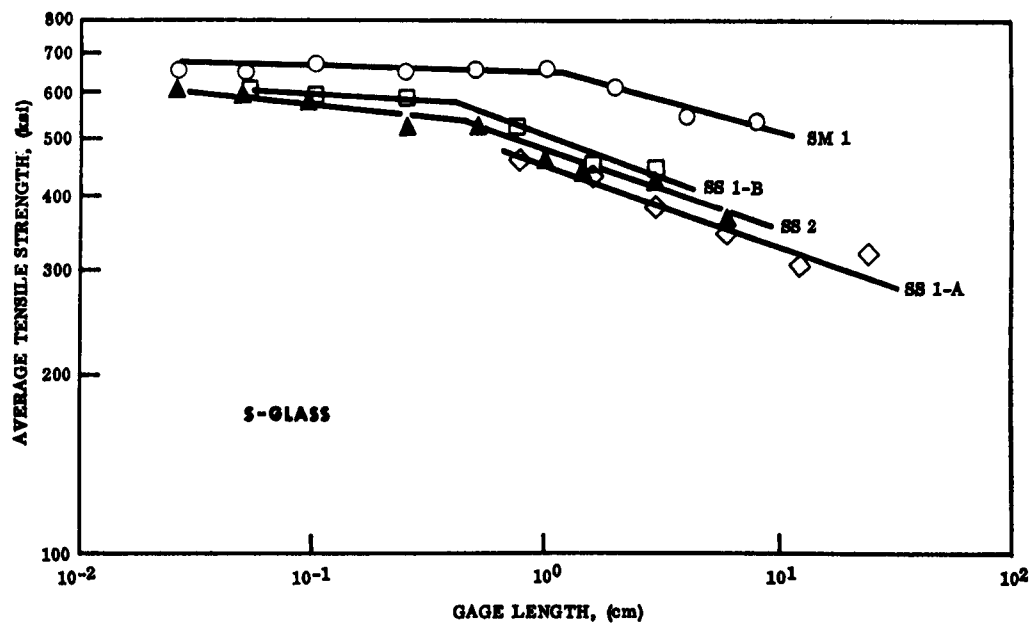


FIG. 5—Length Effect on Strength of S-Glass Fibers.

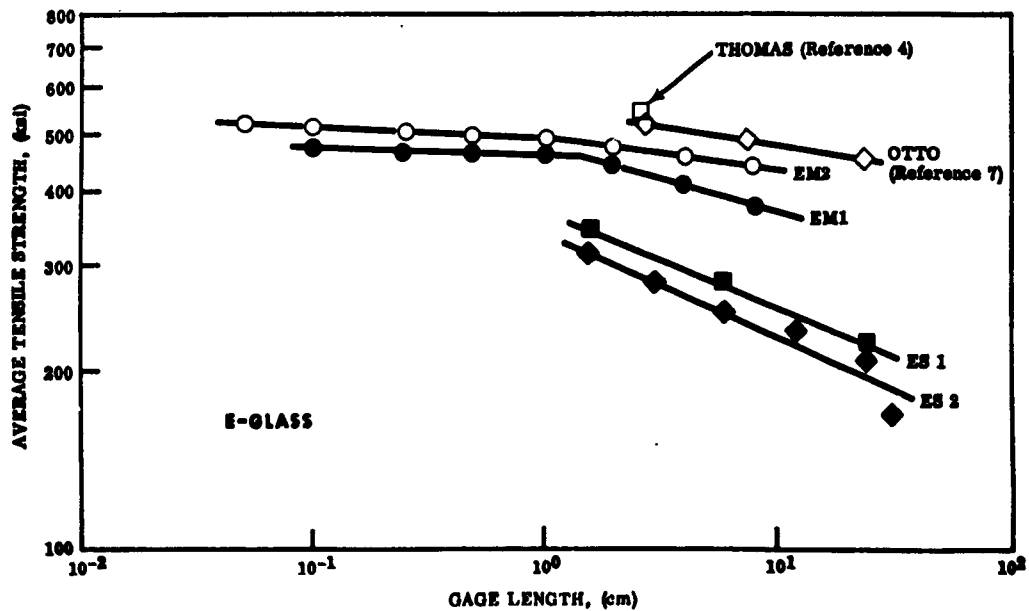


FIG. 6—Length Effect on Strength of E-Glass Fibers.

sults and plotted against length on logarithmic paper.<sup>7</sup> Figures 5 and 6 show the results for the two glass compositions.

## DISCUSSION OF RESULTS

### *Characteristics of Defects in Glass Fibers:*

The results presented in Figs. 5 and 6 generally support the model advanced in Fig. 1. One marked difference is that the strength at short gage lengths is not

2. Greater damage may tend to increase the slope of the curve.

3. Greater damage tends to move the position of the slope change to shorter gage lengths.

Although there appears to be general agreement with the simple model proposed in Fig. 1, more detailed examination shows that this model has certain limitations.

The general relationship between the

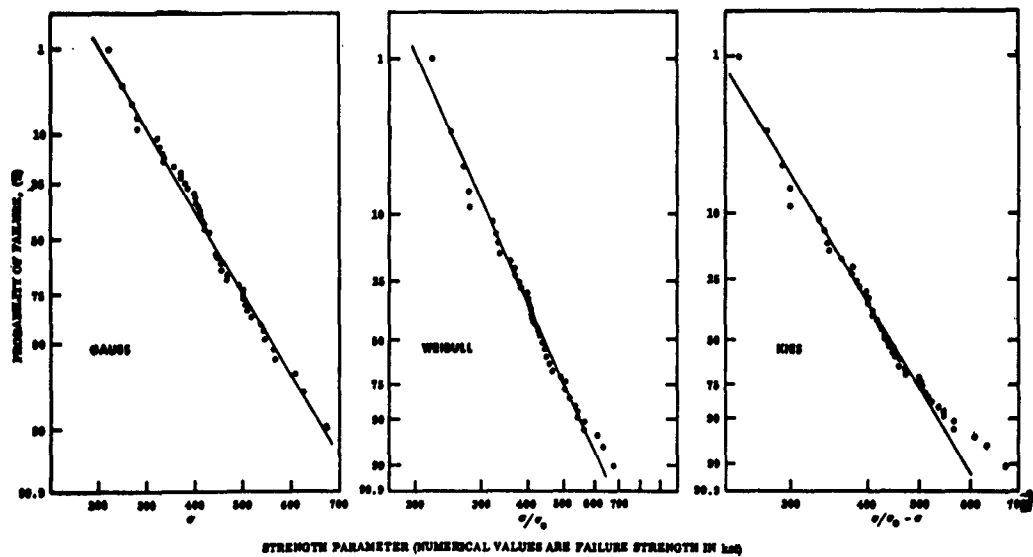


FIG. 7—Effect of Distribution Functions on Probability Plot.

constant, as proposed in the model. At longer gage lengths, the strength decrease is in general agreement with the model. Making the reasonable assumption that fibers separated from strands contain greater damage than virgin monofilaments, then:

1. Greater damage causes increasing loss of strength at long gage lengths (compare SS1 with SM1 in Fig. 5, or ES1 with EM1 or EM2 in Fig. 6).

<sup>7</sup> It will be shown later that more complex functions than  $\log$  (average strength) may be appropriate, such as  $\log ((\sigma - \sigma_u)/(\sigma_s - \sigma))$  for the Kies distribution. However, such changes have no effect on the conclusions that will be drawn from these results in the succeeding paragraphs.

probability of failure,  $S$ , and the applied stress,  $\sigma$ , is given by:

$$S = 1 - e^{-Lf(\sigma)} \dots \dots \dots (3)$$

where  $f(\sigma)$  is chosen for the statistics selected. The function of stress must be one that will give close to a straight line on a  $\log f(\sigma) - \log L$  plot.

For constant length,  $L$ , it is possible to design graph paper so that a plot of  $S$  against  $\sigma$  gives a straight line. The Gaussian (Normal) probability paper is the best known example, but for the purposes of this work, special paper was constructed for other functions. Scales were chosen so that a straight line would

result if the distribution would follow the appropriate statistics.

Figure 7 compares a typical set of data on the Gaussian, Kies, and Weibull

to examine the data obtained at each gage length. It was realized at the time of this selection that certain inconsistency is introduced by this choice be-

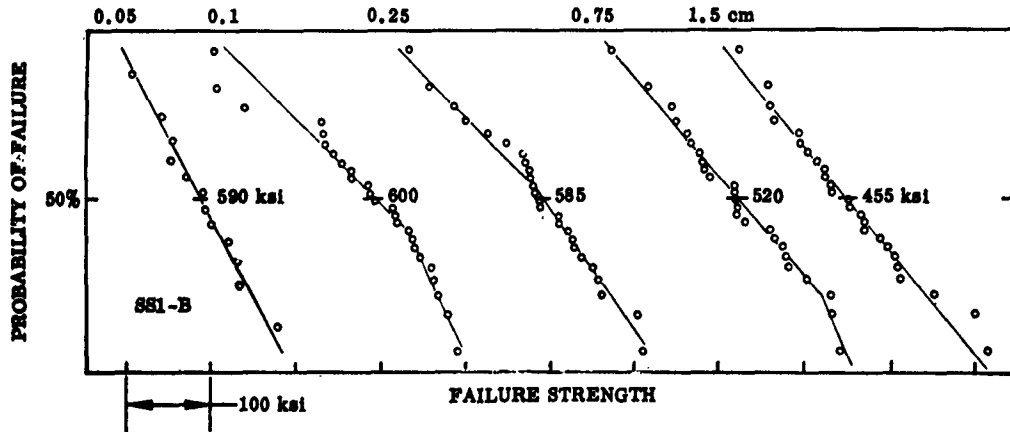


FIG. 8—Gaussian Failure Distributions at Different Gage Lengths.

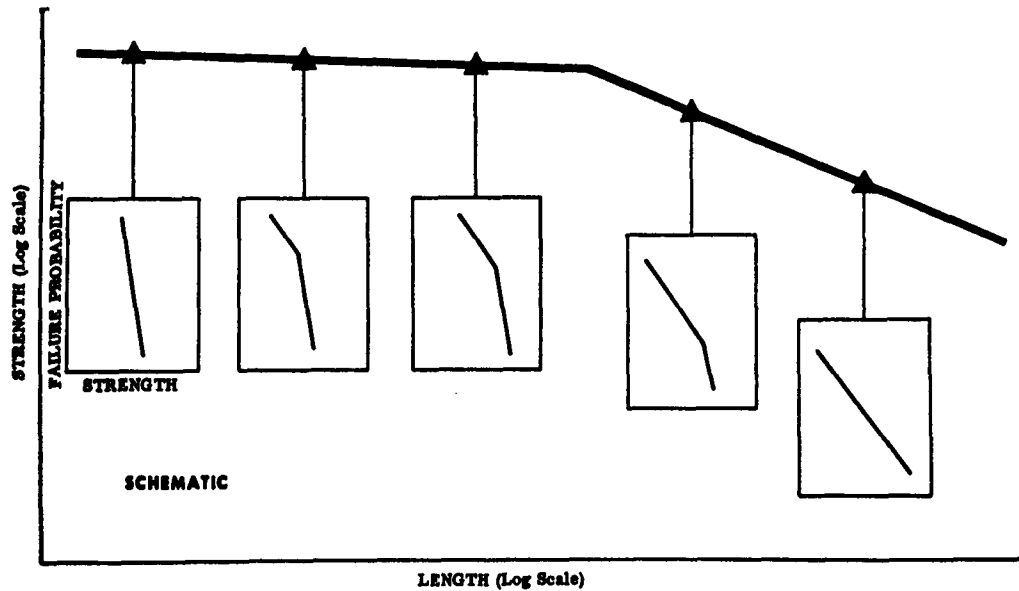


FIG. 9—Systematic Change of Failure Distribution Curves with Gage Length.

distributions. As a result of examination of many sets of data, it was found that the Gaussian distribution best fitted the results for gage lengths removed from the position of the slope change (Figs. 5 and 6). Therefore, the Gaussian distribution was used in all subsequent work

cause the strength must approach infinity for zero probability of failure. The purpose of the work at this stage was not to develop a mathematical model to fit the data, but rather to determine the physical model. For this reason, the generalized Eq 3 was introduced.

Analysis of Gaussian distribution plots covering the range of gage lengths across the slope change (Figs. 5 and 6) revealed a systematic trend. Figure 8 shows the failure probability plots for test series SS1-B between 0.05 and 1.5 cm. Figure 5 shows that the slope change occurs at 0.5 cm. In Fig. 8, straight-lines are obtained at lengths of 0.05 and 1.5 cm indicative of failure strengths following a Gaussian distribution, whereas increasing irregularity occurs at intermediate lengths. Figure 9 shows these failure probability plots superimposed on

strengths to another and is, therefore, not a sharp break but a gradual change of slope.

A distribution of strengths can be represented equally by a distribution of stress concentrators that cause failure at the observed strength. A scratch or other surface damage on virgin glass with a stress concentration factor of 1.25 will reduce the failure stresses to 80 per cent of that of virgin glass. The average strength of the S-glass (strand fibers) at 1.5-cm gage length was 455,000 psi (Figs. 5 and 10) so that the average

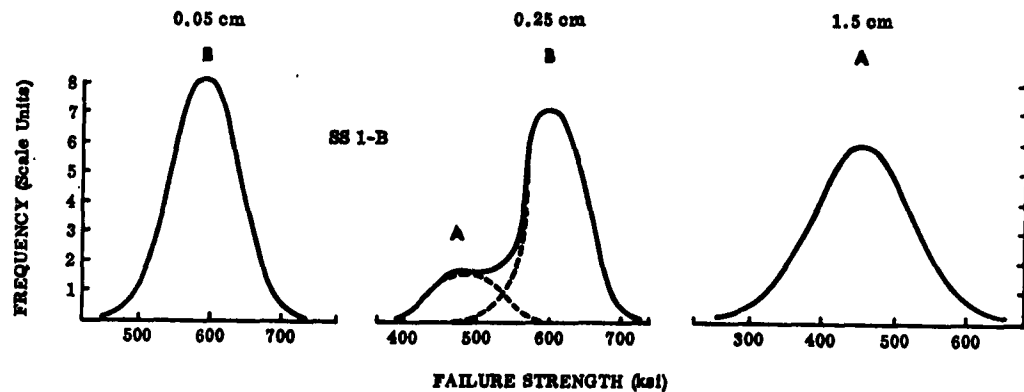


FIG. 10—Frequency Distribution of Failure Strength at Different Gage Lengths.

the logarithmic strength-length relationship. It is obvious that the failure strengths fall on a normal distribution at both short and long lengths, but on a mixed distribution at intermediate lengths. Comparison of the slopes of the failure probability versus strength curves (Fig. 8) for 0.05 and 1.5 cm shows that the normal distribution is much wider, that is, has a wider dispersion at the longer 1.5-cm length. Figure 10 presents these distributions in the more usual form and includes the bimodal distribution curve for an intermediate length. The meaning of the slope change in logarithmic strength-length relationships (Figs. 5 and 6) is now clear; it represents a transition from one distribution of

stress concentration factor introduced by stranding is 650/455 or 1.43.<sup>8</sup>

The wide dispersion of the strength distributions shown in Fig. 10 indicates that the stress concentration factors of those defects causing failure must also have a wide dispersion. In other words, stranding causes surface damage that varies considerably in magnitude. The separation of these defects along the fiber must be on the order of 1 cm. This statement is based on the shape of the failure probability versus strength plots in Fig. 8, where it can be seen that in

<sup>8</sup> At this time, S-glass was drawn on an experimental basis (X994) and the virgin fiber strength was 650,000 psi according to the manufacturer. Current values are 670,000 to 720,000 psi.

the 0.5-cm range approximately half of the fibers do not contain these severe defects and fall on a strength distribution characteristic of very short lengths. Thus the defects controlling failure at long gage lengths for fibers from strands have the following characteristics:

1. A wide range of stress concentration factors. Typical values for 10 cm length are 1.2 to 5.4 for 99 and 1 per cent probability, respectively.

to both monofilaments and fibers from strands, and to commercially produced as well as laboratory specimens. Conclusions are possible as to the influence of drawing and stranding processes on flaw and damage formation.

#### *Damage Model for Glass Fibers:*

It has been shown that two distributions are required to describe damage

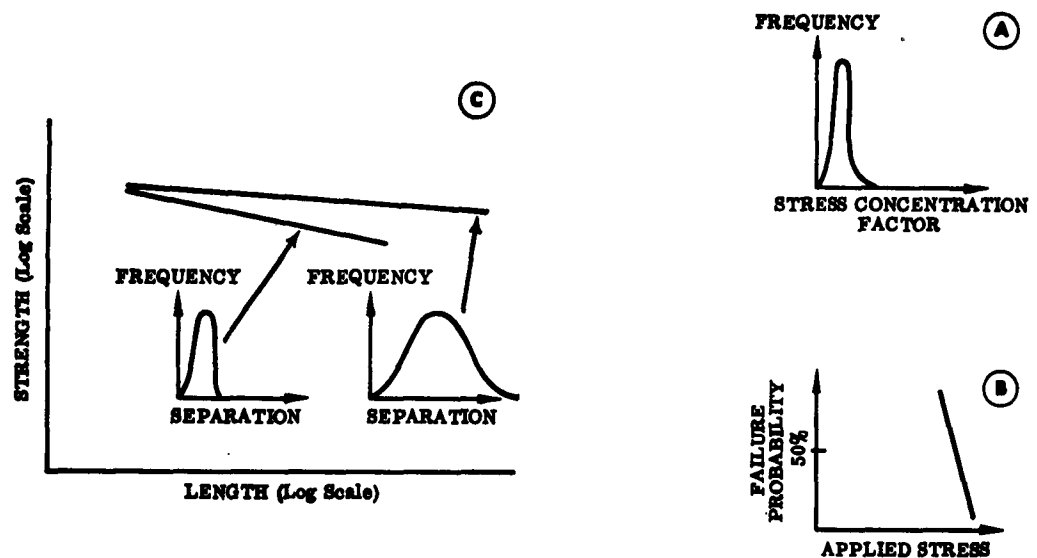


FIG. 11—Effect of Narrow Distribution of Stress Concentration Factors on Strength-Length Plots.

2. Wide separation between flaws on the order of 1 cm as mentioned before.

Using the same arguments, it can be shown that the flaws controlling failure at short gage lengths have the following characteristics:

1. A narrow range of stress concentration factors with typical values between 1.0 and 1.5 for 99 and 1 per cent probability at 0.025 cm length.

2. Narrow separation of flaws, probably less than 0.1 cm apart.

The characteristics of flaws in both E- and S-glasses are remarkably similar (Figs. 5 and 6). This similarity extends

to glass fibers. One is the distribution of severities of defects that can be described in terms of a distribution of stress concentrators. The second is a distribution of spacings between the defects. More than one type of damage has been identified by analysis of the length effect and described qualitatively.

A most significant conclusion from this result is that the single exponent, for example, the  $m$  in the Weibull relation, is inadequate to describe the strength of glass fibers. This can be seen readily by applying one of the failure probability functions to the results



for the length of fibers at the slope change in Fig. 9. The Weibull equation,

$$S_1 = 1 - \exp \left[ -L \left( \frac{\sigma}{\sigma_0} \right)^{m_1} \right], \text{ with } m_1 \approx 100$$

will describe the straight line for short gage lengths, and

$$S_2 = 1 - \exp \left[ -L \left( \frac{\sigma}{\sigma_0} \right)^{m_2} \right], \text{ with } m_2 \approx 6.4$$

which is clearly not the case, or for  $\sigma_0$  to have different values for each part of the curve, which makes  $\sigma_0$  descriptive of the damage rather than a material constant. It follows, therefore, that single exponent distributions are empirical simplifications that can be applied to a single population of defects but do not describe the population fully. Such distributions have been used

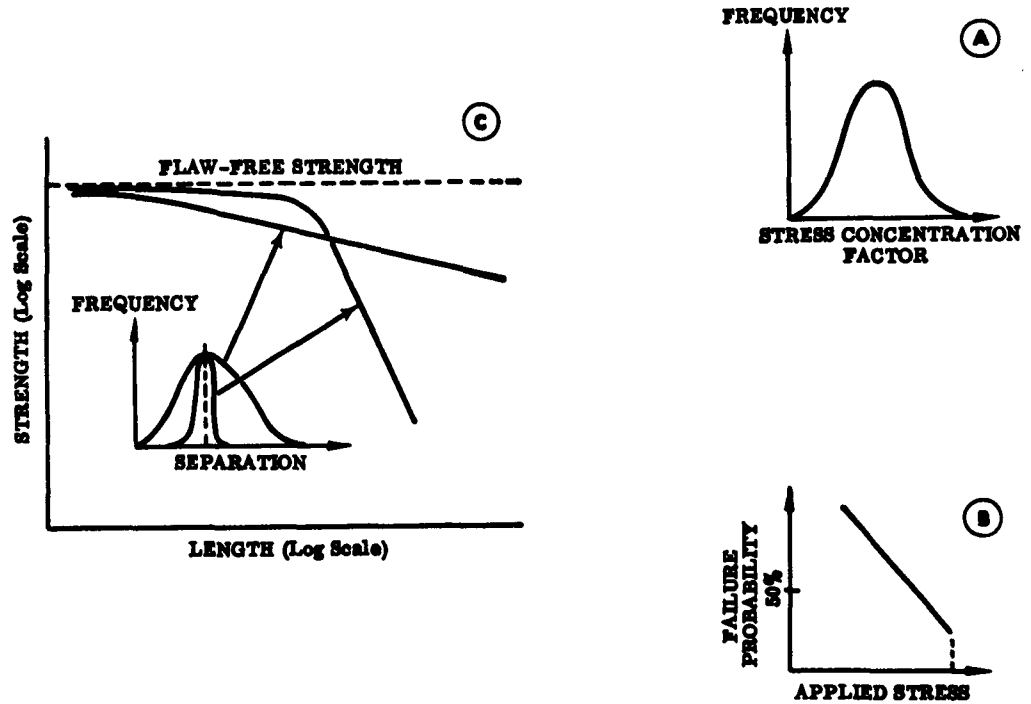


FIG. 12—Effect of Wide Distribution of Stress Concentration Factors on Strength-Length Plots.

will describe the straight line for long gage lengths. The exponent  $m$  in each case describes the slope, because

$$\ln L = m \ln \left( \frac{\sigma}{\sigma_0} \right) - \ln (\ln \frac{1}{1-S})$$

for the plotted strength where the failure probability is equal to 0.5.

However, at the length  $L_B$  where the slope change occurs, the strengths are equal for the two failure distributions. This requires  $m_1$  to be equal to  $m_2$ ,

in prior work without full appreciation of this limitation.

The need for two variables, namely severity of defect and separation, to be defined in order to describe a population of defects, can be made apparent from the following hypothetical cases.

Figure 11 shows the effect of a narrow distribution of flaw severities plotted in terms of frequency versus stress concentration factor (Fig. 11(a)). The corresponding failure probability versus

applied stress plot in Figure 11(b) is steep because the stress concentration factors vary very little (Fig. 11(a)), and the plot is at high applied stress because the average stress concentration factor is very low. Figure 11(c) shows the effect of different frequency-flaw separation curves on the slope of the logarithmic strength-length plot.

Figure 12 shows the effect of keeping the average separation of defects constant while changing the width of this distribution. More severe flaws with a wider distribution are used in this example (Fig. 12(a)) and the corresponding failure probability curve is shown in Fig. 12(b). Figure 12(c) shows the results. Because the probability of finding faults decreases rapidly at short gage lengths for the narrow distribution of flaw separations, the average strength will comprise increasing percentage of high values equal to the flaw-free strength. Thus the curve will show a slope change and approach the theoretical strength asymptotically.

Consideration of these hypothetical curves shows that the downward turn of the logarithmic strength-length plot above a certain gage length (Fig. 9) is dependent on appropriate values of two factors describing the flaws: (1) severity and (2) separation. However, the change of slope need not be an increase (down-turn) as the gage length increases.

Indeed, recent evidence for lengths shorter than 0.1 cm shows that the opposite type of slope may occur below 0.025 cm. Data for both E- and S-glasses show an increasing number of high-strength fibers with values as high as 1,400,000 psi. These can be fitted to the curve only by an upturn in the logarithmic strength-length plot at short gage lengths. The "flaw-free" strength in Fig. 12 could be that of fibers without surface damage, and the higher strength fibers can then be explained as increas-

ing freedom from internal, structural defects. The latter explanation seems appropriate, since strengths of 1,000,000 to 2,000,000 psi are equal to the theoretical strength.

One conclusion from this discussion is that there can be no generalized damage model. A steeper slope, such as those shown in Fig. 5, may be caused by (1) spacing the flaws closer together without any change of flaw severity (Fig. 11), (2) increasing flaw severity without changing the separation, or (3) reducing the spread of interflaw distances leaving the average separation unchanged (Fig. 12).

Although it is not necessary for the behavior of two glasses to be similar, the observations summarized in Figs. 5 and 6 show a remarkable similarity. These results indicate similarities in the distributions of both severity and separation for the two glasses.

Since this section contains several important aspects concerning fiber strength characteristics, a brief summary may be warranted before discussing further results. First, it has been shown that no generalized damage model exists because the strength depends on both severity and distribution of defects, each of which can assume arbitrary values. However, the processes of fiber drawing and of stranding seem to cause defects or flaws typical for each process, thus giving rise to similar strength-length curves for the two glasses investigated, and permit comparison of stress concentration effects on the two glasses. Secondly, the observed length effect on fiber strength precludes application in the statistical distribution function of a common exponent for all gage lengths. This exponent, for instance Weibull's  $m$ , is generally regarded as a descriptive value for "the" strength property and an erroneous picture evolves unless the length effect is taken into account.

**Analysis of Failure Probability:**

The failure probability plots in Figs. 8 and 9 were shown as one straight line

bility plot is shown in Fig. 13 with this simple presentation by two straight (dashed) lines through the data. How-

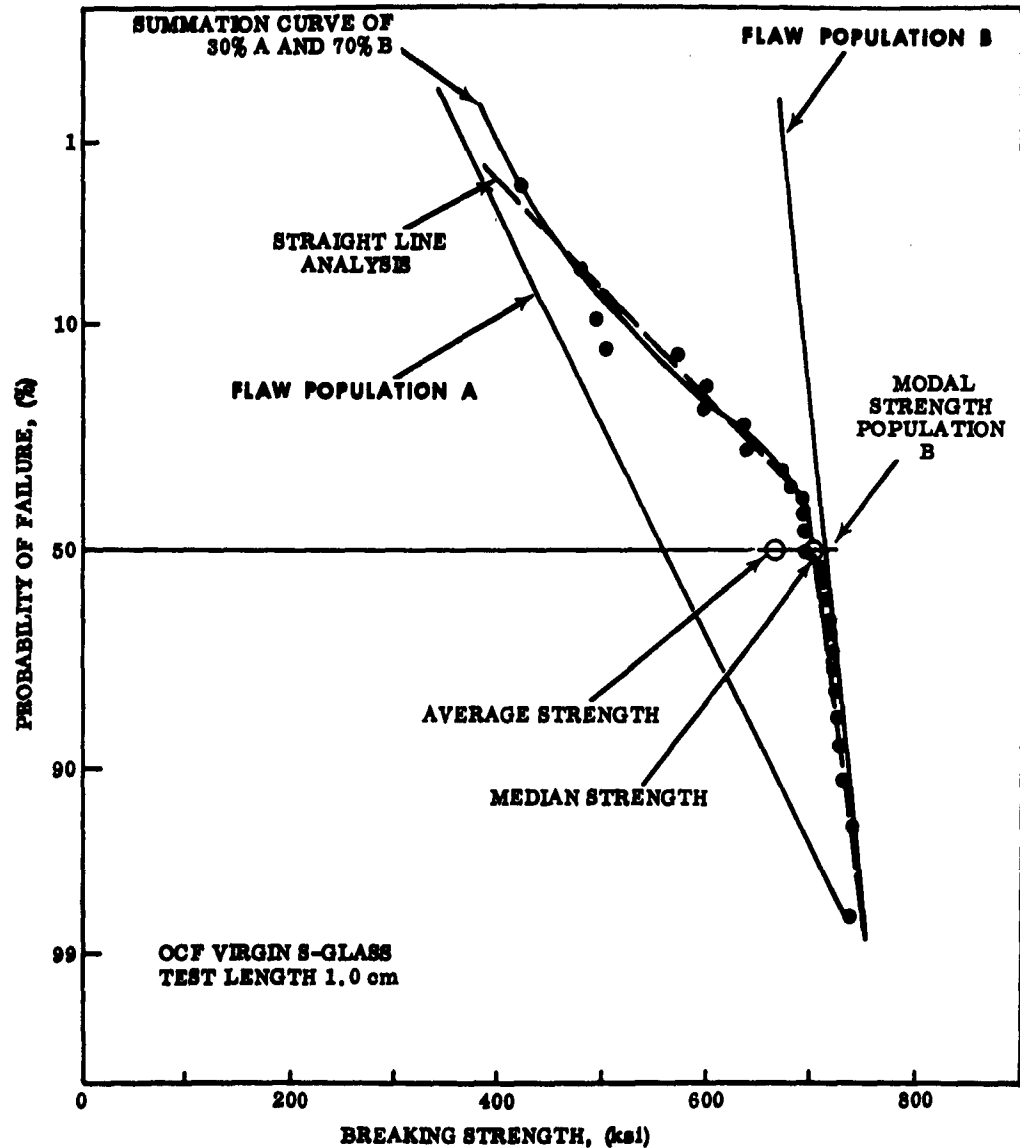


FIG. 13—Graphical Separation of Two Flaw Populations on Gaussian Probability Paper.

for a single distribution, and two intersecting straight lines for a mixed distribution. More careful examination shows that this is a simplification for mixed distributions. A typical failure proba-

ever, a more exact analysis is possible if it is assumed that two populations of flaws control failure and the observed data is the result of failures originating at both types of flaw. The individual

flaw population controlling failure at short gage lengths is represented by *B*, and Population *A* controls failure at

percentage of failures originate as the *A* population of flaws. In Fig. 13, the best fit is obtained when 30 per cent originate

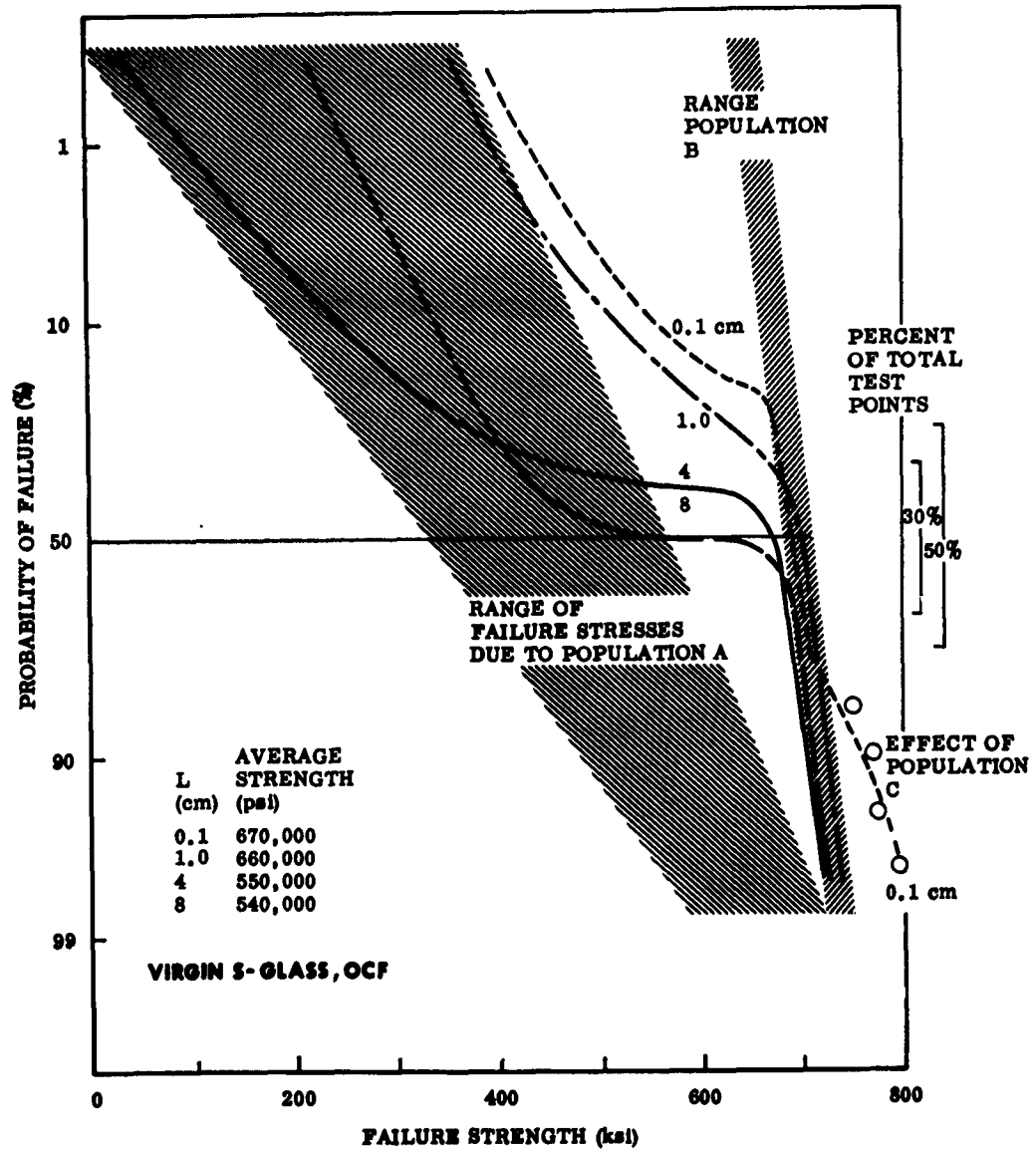


FIG. 14—Bimodal Summation Curves for Virgin S-Glass Fibers Tested at Different Gage Lengths.

long gage lengths. By this it is meant that in the absence of the other type of flaw, the distribution of failure strengths would be as in *A* or *B*. As the gage length increases, an increasing

at *A* flaws and 70 per cent at *B* flaws. The summation curve gives a better fit of the data points than the straight line. Further, it is found that the failure probability curves across the position

of the slope change (Figs. 8 and 9) can be calculated by the summation of appropriate percentages of the fixed Curves *A* and *B*. Better fits are obtained when Population *A* is moved to lower strengths as the gage length increases; this is an inevitable result of multiple *A*-type flaws in the gage length. The most severe *A*-type flaw in the gage length causes failure so that, as the gage length increases, the higher strength associated with milder flaws decreases progressively.

The designations, Populations *A* and *B*, were introduced to categorize conveniently the effect of different stress concentrators on virgin or stranded fibers. The physical nature of flaw types carrying the same label may be quite different. In fact, defects due to stranding override statistically the ones existing on virgin fibers, as is borne out by the position of the respective strength-length curves below the virgin fiber curves (Figs. 5 and 6).<sup>9</sup>

A suggested use of this type of analysis may be for the treatment of experimental strength data. Although no data have been neglected in the present work, there appears to be a widely spread practice to neglect "low" values and ascribe these to accidental damage. The analysis in Fig. 13 suggests a systematic method to perform this separation of data. Thus, low strength values would be neglected only if they depart significantly from the straight-line portion of the total plot that represents the Gaussian distribution.

<sup>9</sup> J. A. Kies' comment on analysis of failure probability: "The analytical method provided here for detecting different coexisting flaw populations may become a powerful tool in guiding the development of better manufacturing and processing methods for glass. Cornelissen et al, Ref. (8), have identified an individual flaw population as being introduced by a certain step in a melting process. They also separated two flaw populations, but used a different technique."

The average and the median (50 per cent probability) values are both equal to the modal strength for the Gaussian distribution, where the failure probability plot is a straight line. For mixed distributions, this is no longer the case, as shown in Fig. 13. Examining the failure distribution plots from short to long gage length of both E- and S-glass showed that, in general, the median strength first decreases slowly from the modal value of flaw Population *B* to the value shown, until 50 per cent failures occur at flaws of type *A*. Then the median strength begins to fall rapidly toward the modal value shown for Population *A*, and ideally beyond that point, as multiple defects prevent realization of the higher strengths on Curve *A*. The median, average, and modal values become equal again for failure controlled by a single Gaussian distribution of *A* flaws.

This trend can be observed in Fig. 14, where the distribution curves of several gage lengths are shown for OCF virgin S-glass, omitting the data points for clarity; the 1-cm curve was discussed in Fig. 13. Figure 14 clearly demonstrates that omission of low-strength values yields what might be called "potential strength" of the virgin glass, while the average strength more realistically presents the "working strength" available in virgin fibers. Presumably, the specimens tested have been handled so that the gage length was not touched prior to testing. Results from virgin E-glass fibers gave similar curves, except that the low-strength tail had relatively higher strength values, that is, less dispersion. It may well be that certain glass compositions are more susceptible to flaw formation than others, in which case reported average strength based solely on selected higher strength values (potential strength) would disguise an important charac-

teristic. It appears, therefore, that omission of low values is justified only if either a small number of data is to be rejected or published strength figures are complemented by description of the method employed.

#### CONCLUSIONS

The following conclusions can be drawn from this work:

1. Careful control permits tension tests of glass fibers to be made down to 0.025-cm gage length.

2. The logarithmic strength-length plot is a valuable tool in the study of flaws in glass fibers.

3. Two types of flaws have been identified in virgin fibers of both E- and S-glass. One type is severe, has wide spacing, and governs failure of long fibers. The other type has narrow spacing, is less severe, and determines failure at short gage length.

4. Some strength values approached the theoretical strength of glass and indicate the presence of flaw-free fiber sections in the short length range of freshly-drawn fibers.

5. Two types of flaws have been identified on fibers from strands. These

flaws originated in the stranding process and are considerably more severe than those of virgin fibers.

6. The single exponent failure probability functions, such as that due to Weibull, are inadequate to describe failure in glass fibers for the conditions investigated. The inadequacy becomes apparent only when the number of flaws in the test volume becomes so small that a second control mechanism begins to assume command.

7. Analysis of failure probability plots allows flaw populations to be separated when mixed control of failure occurs. It also suggests a method to eliminate low values (caused by accidental damage) from a test series.

#### Acknowledgment:

The authors wish to acknowledge the extensive experimental work performed by D. G. Clark and D. Roth of Solar Research Laboratories; the guidance provided by J. V. Long, director of Solar Research; and the encouragement, advice, and suggestions (upon review of this paper) given by J. A. Kies, head of Ballistics Branch, NRL.

#### REFERENCES

- (1) A. A. Griffith, "The Phenomena of Rupture and Flow in Solids," *Philosophical Transactions*, Series A, Vol. 221, Society of London, 1920-1921. "The Theory of Rupture," *Proceedures of International Congress of Applied Mechanics*, Vol. 55, 1924.
- (2) W. Weibull, "A Statistical Theory of the Strength of Materials," *Handlingar*, Royal Swedish Academy of Engineering Sciences, No. 151, 1939.
- (3) J. A. Kies, "The Strength of Glass," *NRL Report 5098*, April, 1958, and *Filament Winding Symposium*, Soc. of Aerospace Material Process Engrs. 1961, p. 273.
- (4) W. F. Thomas, "An Investigation of Factors Likely to Affect the Strength and Properties of Glass Fibers," *Physics and Chemistry of Glasses*, Vol. 1, February, 1960.
- (5) F. O. Anderegg, "Strength of Glass Fibers," *Industrial and Engineering Chemistry*, Vol. 31, 1939.
- (6) D. Sinclair, "A Bending Method for Measurement of Tensile Strength and Young's Modulus of Glass Fibers," *Journal of Applied Physics*, Vol. 21, 1950.
- (7) W. H. Otto, private communication, NARMCO Research & Development, San Diego, Calif.
- (8) J. Cornelissen, H. W. Meyer, and A. M. Kruithof, "Statistical Distribution of the Strength Values of Glass Rods," *Advances in Glass Technology*, 6th International Congress on Glass Washington, D. C., July, 1962.

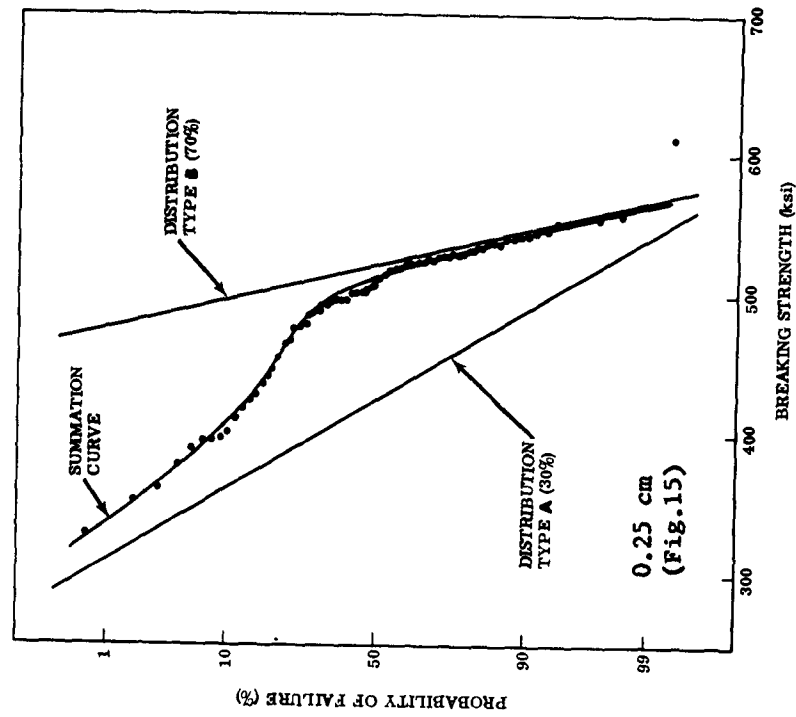


FIG. 16. FLAW ANALYSIS FOR VIRGIN E-GLASS FIBERS

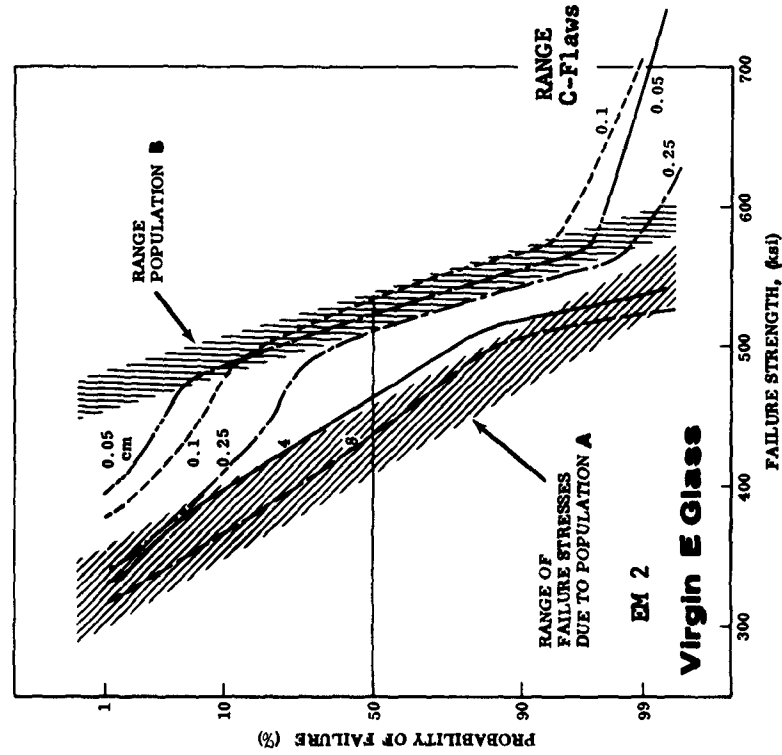


FIG. 15. DISTRIBUTION CURVES FOR VIRGIN E-GLASS FIBERS OF DIFFERENT GAGE LENGTHS

## 1.2 ADDENDUM

The foregoing paper was concerned mainly with surface flaws, while structural (or internal) flaws have been touched only briefly. This addendum serves to fill the gap. As the gage length study continued, it became possible to define the characteristics of surface and structural flaws in more detail. The following is an excerpt from a paper presented at the 1965 SPI meeting<sup>(9)</sup>.

### ANALYSIS OF FLAWS ON GLASS FIBERS

In this Section, the reference strength for calculation of strength reduction factors of flaws is discussed first, followed by a detailed examination of the different flaw types.

The more general term "strength reduction factor" is favored over "stress concentration factor," because it covers all conditions such as lattice irregularity, strength reduction by surface adsorption to reduce fracture strength according to Griffith's relation, and the presence of pits, scratches and other surface defects. The theoretical strength of glass approaches 2,000,000 psi, but glass filaments in the virgin condition have well defined strengths that are considerably lower. For example, E-glass has a typical average strength of 500,000 psi with nearly all values below 600,000 psi. The weight of evidence suggests that inability to realize 2,000,000 psi is a result of lattice irregularities such as imperfect junctions between parts of the silica network. On the other hand, the occurrence of strengths below approximately 600,000 psi is the result of surface defects. Most of the work reported here has been concerned with surface defects, and strength reduction factors have been related to the surface flaw-free strength of 600,000 psi. For example, a sample population with an average strength of 500,000 psi, would have an average strength reduction factor of 1.2.

Figure 15 shows typical failure distribution curves at different gage lengths for E-glass monofilament drawn from OCF marbles, (compare with Fig. 14). Each curve represents approximately 100 tests. Analysis into the individual flaw populations leads to a band of populations A and B. The analysis of the data for gage length 0.25 cm is shown in Fig. 16 (compare with Fig. 13).

Fig. 17 shows an extension of the analysis to the strength-length plot\*. In agreement with Fig. 9, the type of flaw that controls failure changes at the position of the slope change (1 cm). Flaw type A has an average strength reduction factor of 1.36 (strength 440,000 psi) and the flaws are 2 cms apart on the average. These flaws are believed to be deep pits or scratches. Flaw type B has an average strength reduction factor of 1.13 (strength 530,000 psi), and the flaws may be shallow etch pits formed by water vapor attack.

Review of the maximum strength determined during the test of approximately 100 fibers at each length showed an interesting relationship, plotted in Fig. 17 as  $\sigma_{\max}$ . For gage lengths between 0.5 and 8 cms, this maximum remained below the 600,000 psi strength level expected for surface flaw-free

\* The diagram at the bottom is a convenient method to illustrate the change of flaw types with gage length (compare with Fig. 9).



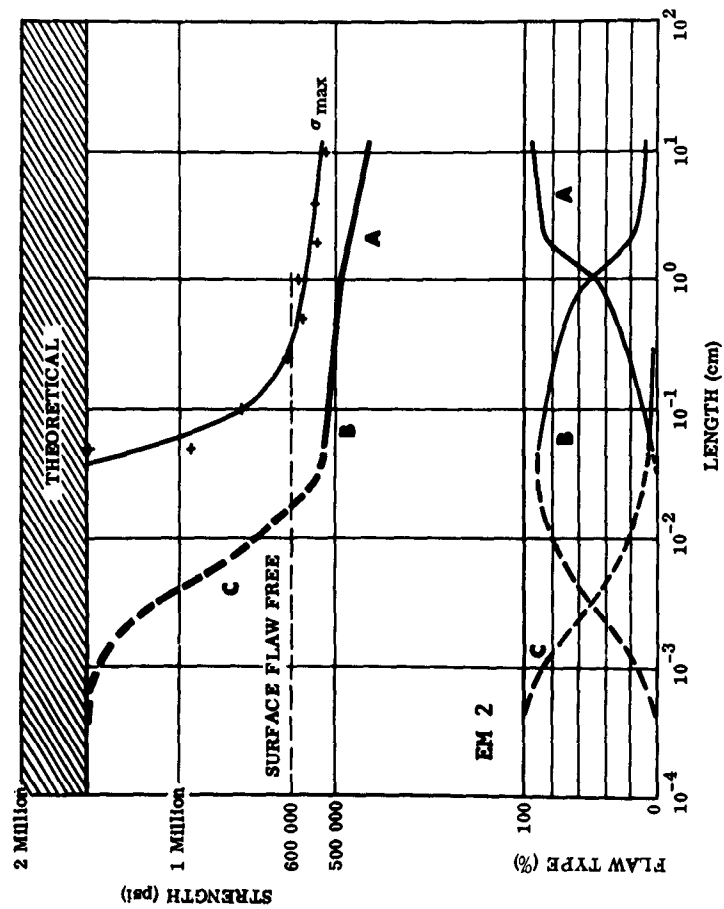


FIG. 17. STRENGTH-LENGTH RELATIONSHIP FOR VIRGIN  
E-GLASS FIBERS TESTED IN LABORATORY  
ATMOSPHERE AT STRAIN RATE  $0.06 \text{ min}^{-1}$

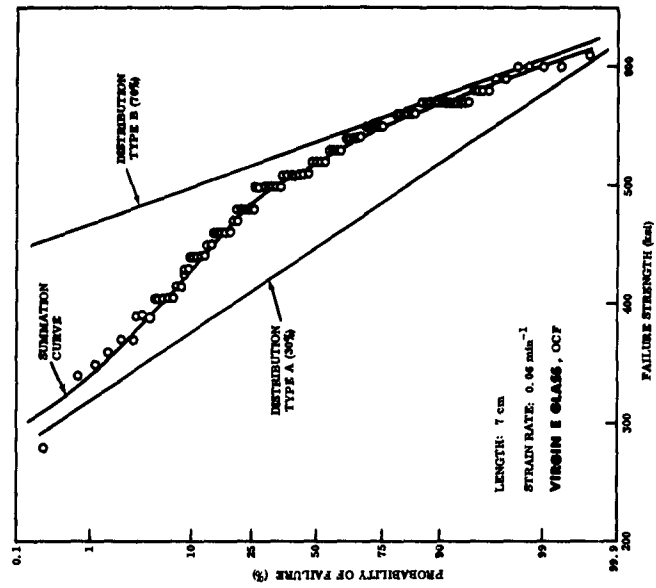


FIG. 18. FLAW ANALYSIS OF OCF DATA ON  
GAUSSIAN PROBABILITY PAPER  
(Lot 5)

E-glass. For shorter gage lengths, an increasing number of much higher strength fibers was found, reaching 1,400,000 psi for one test at 0.05 cms.

The failure probability plots in Fig. 15 show that these data points depart from the stress range expected for type B flaws. The trend to higher strength fibers followed a consistent increase as the gage length was decreased. Accordingly, a new type of flaw has been postulated and is termed type C. Fig. 17 shows the increase in percentage of type C with gage length. Extrapolation of this percentage indicates that type C would control failure at a gage length between  $10^{-3}$  and  $10^{-4}$  cms. This dimension is somewhat greater than would be expected if the strength were controlled by the dimensions of the silica network or chains. It must be postulated, therefore, that the coincidence of breaks in the network at several of the chains creates the type C flaw. The strength-length plot has been completed tentatively (in Fig. 17) to show the effect of type C flaws.

Figure 18 shows recent data from Lindsay, Hood, et al<sup>(10)</sup> analyzed by means of the techniques described earlier. The results from 191 tests by these authors show the same division into failure originating at A and B type flaws. (Compare Figures 16 & 18). The mean strength of the type A-controlled failure is 450,000 psi and the mean strength of the type B-controlled failure is 540,000 psi. These values are extremely close to the values obtained on this glass drawn from OCF marbles at Solar. Lindsay and Hood give the mean strength of the entire population as equal to 506,000 psi with a standard deviation of 67,000 psi. It can be seen now that the high standard deviation results from the mixed distribution, whereas the standard deviation for the separated type B failures is 29,000 psi. Calculation of a standard deviation is, strictly, not justified when the distribution is non-Gaussian. It is interesting to compare these results with Thomas<sup>(4)</sup> who achieved unusually low coefficients of variation by very careful attention to the details of the drawing process, so that his fibers were essentially free of A-type flaws. The average strength observed by Thomas was 530,000 psi with a standard deviation of 8,000 psi\*. Table IV gives a summary of mean strengths, standard deviations and strength reduction factors for the two types of flaws. The consistency within each group is remarkable.

Figure 15 shows the type A flaws have a large range of values. For example, the strength reduction factors of flaws causing failure in a 8 cm gage length vary from 1.13 to 1.82 for probabilities of failure of 99 and 1% respectively. As the flaw separation is approximately 2 cms, more than one type A flaw is present in the gage length. The existence of multiple flaws above 2 cms leads to a gradual decrease in strength because failure occurs at the most severe flaw. This causes the band for type A flaws in Fig. 15 to become broadened.

The same broadening could be observed on data obtained from the S-glass on two shipments of virgin monofilaments mounted on forks by OCF (Fig. 14). Comparison of this data, listed in Table V, with E-glass in Table IV reveals similar trends for the SRF values and standard deviation of the two types of flaws. Numerical (SRF) values for type B coincide, whereas the higher values for A flaws on S-glass are probably related to the sensitivity of this glass composition to fiber drawing parameters. The reference strength of 800,000 psi

\* Similar results were obtained recently by Cameron<sup>(23)</sup>.

TABLE IV

## CHARACTERISTICS OF FLAWS ON E-GLASS FIBERS

at Strain Rate  $0.06 \text{ min}^{-1}$ , 50% RH;  $80^{\circ}\text{F}$ 

Source	No. of Fibers	Mean Strength (psi)	Standard Deviation (psi)	SRF <sup>(1)</sup>	Gage Length (cm)
<u>TYPE A</u>					
SOLAR					
EM II	693	440,000	50,000	1.37	0.05 to 8.0
EM III	160	450,000	46,000	1.34	0.1 to 8.0
Strain Rate Tests	50	475,000	40,000	1.26	20.0
OCF					
Lot 1	178	400,000	48,000	1.5	7.0
Lot 5	191	450,000	55,000	1.34	7.0
<u>TYPE B</u>					
SOLAR					
EM II	693	530,000	25,000	1.13	0.05 to 8.0
EM III	160	530,000	13,000	1.13	0.1 to 8.0
Strain Rate Tests	32	535,000	28,000	1.12	0.25
	50	- -	- -	- -	20.0
OCF					
Lot 1	178	505,000	14,000	1.19	7.0
Lot 5	191	540,000	29,000	1.11	7.0
THOMAS	50	530,000	8,000	1.13	2.5

(1) Reference Strength: 600,000 psi.

TABLE V

## CHARACTERISTICS OF FLAWS ON S-GLASS FIBERS

at Strain Rate  $0.06 \text{ min}^{-1}$ ; 50% RH;  $80^{\circ}\text{F}$ 

Source	No. of Fibers	Mean Strength (psi)	Standard Deviation (psi)	SRF <sup>(2)</sup>	Gage Length (cm)
<u>TYPE A</u>					
SOLAR					
SM I <sup>(1)</sup>	200	465,000	92,000	1.72	0.025 to 8.0
SMII <sup>(1)</sup>	102	490,000	88,000	1.63	0.1 to 8.0
OCF					
Lot 1	120	540,000	78,000	1.43	7.0
Lot 2	123	570,000	75,000	1.40	7.0
<u>TYPE B</u>					
SM I	200	700,000	17,000	1.14	0.025 to 8.0
SM II	102	720,000	20,000	1.11	0.1 to 8.0
OCF					
Lot 1	120	690,000	55,000	1.16	7.0
Lot 2	123	700,000	40,000	1.14	7.0

(1) Fibers supplied by OCF

(2) Reference strength: 800,000 psi.

was determined in the same manner as for E-glass. More recent S-glass data<sup>(10)</sup> show SRF values for A-flaws to be similar to the respective E-glass data. The range of severity as indicated by the standard deviation is still larger, however, for both A- and B-flaws.

#### SUMMARY OF FLAWS ON GLASS FIBERS

The characteristics of flaws on glass fibers have been determined by tensile tests on monofilaments at different gage lengths. The shapes of the distribution curves of strength data have been analyzed to determine the corresponding distribution of flaws. The variation of these distributions with gage length has been analyzed to determine a second characteristic of flaws, that is, the separation of flaws. It has been concluded that three types of flaws exist on monofilaments as revealed by tensile tests in air. For both E- and S-glasses, the flaw types are identical but all strength values are higher for S-glass by 25%. For E-glass the flaw characteristics are:

- Flaw type A - Severe surface flaws that arise from handling and processing, and control the strength primarily in the range below 480,000 psi. These flaws have an average distance apart of 2 cms.
- Flaw type B - Mild surface flaws that control strength in the range 600,000 to 480,000 psi. These flaws are approximately  $10^{-2}$  cms apart. It is likely from the flaw severity that these flaws are etch-pits, but it is not known if these are present as drawn, grow by corrosion in the absence of stress, or grow by a stress corrosion mechanism during the tensile test.\*
- Flaw type C - These flaws control strength above 600,000 psi and can only be observed when gage lengths of less than 0.1 cms are tested. The proportion of failures controlled by C-type flaws increases as the gage length is decreased to 0.025 cms. Extrapolation of this proportion suggests that a gage length of  $10^{-3}$  to  $10^{-4}$  cms would have to be tested to obtain 50% of fibers with strengths of 1,500,000 psi or above, indicating that this is the average separation of C-flaws. It is proposed that C-flaws are internal, structural, defects arising from the heterogeneity of the glass, and thus represent concentrations of terminal cations that interrupt the silica network. These are not flaws in the normal sense of voids, but generate a stress concentration because the weaker bonds at these regions lead to a local reduction of elastic modulus and hence to a stress concentration.

These flaw characteristics have been determined by tests in standard laboratory atmosphere of 50% RH and at a standard strain rate of  $0.06 \text{ min}^{-1}$ . Since flaws are changing with time, humidity and stress, an apparent change of characteristics as revealed by failure strength data is to be expected under other test and environmental conditions. Analysis of published data has shown that these

\* The upper limit of 600,000 psi applies to the present work but is not a fixed value. Other work has shown that 700,000 psi may be more representative. However, such change does not affect the basic considerations expressed here.

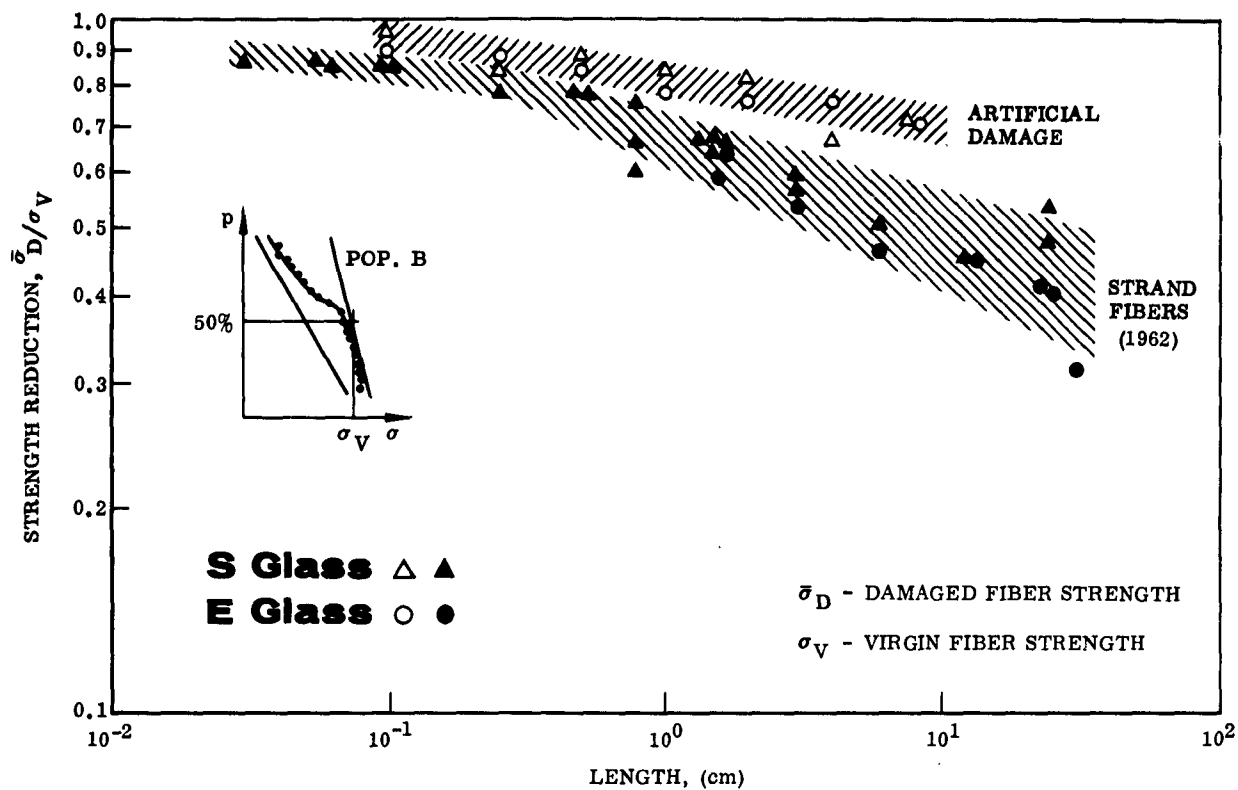


FIG. 19. STRENGTH REDUCTION OF STRAND FIBERS AND ARTIFICIALLY DAMAGED FIBERS

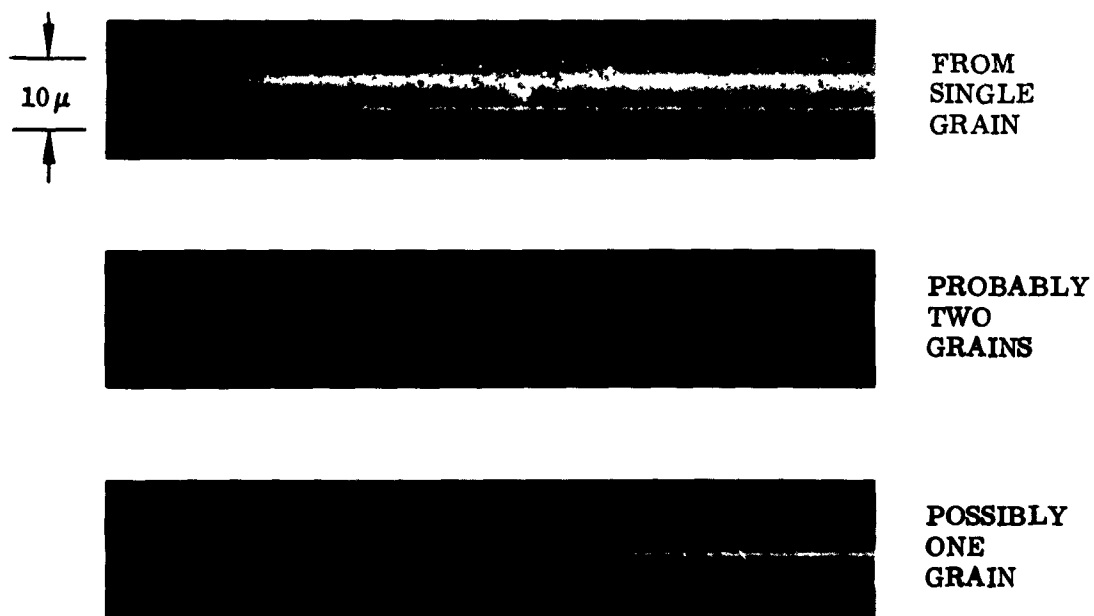


FIG. 20. DAMAGE MARKS FROM GARNET GRAINS ON E-GLASS FIBERS

flaws are characteristic of both E- and S-glasses prepared and tested in several different laboratories.

## II. DAMAGE RESISTANCE OF E- AND S-GLASS FIBERS

In the experiments with artificial damage, fibers of S- and E-glass were subjected to identical procedures. The fiber was pulled through a controlled particle stream at a velocity necessary to achieve the desired hit distribution. Fig. A-4 shows the fiber damage device. The following condition was selected after several preliminary tests:

Particles:	Garnet grain, irregular shape (Fig. A-5)
Size:	Tyler Sieve, -48 + 65; average smallest dimension 250 $\mu$ , largest 500 $\mu$
Specific weight:	4.2 to 4.5 gr/cm <sup>3</sup>
Impact height:	25 cm
Fiber velocity:	10 cm/sec
Average number of hits:	3 to 4 per cm

Virgin control samples were tested in each case to establish a baseline.

The strength loss of the two glasses gives some measure for their relative resistance to damage and data from these controlled experiments can be compared with the strength loss of fibers from strands, provided that the virgin reference strengths are comparable. The reference strength should be independent of gage length for this purpose of cross reference, and the modal strength associated with flaw population B has, therefore, been used. Evaluation of the available probability plots led to the following virgin reference strengths:

<u>Glass</u>	<u><math>\sigma_y</math> (psi)</u>	<u>Remarks</u>
E	525,000	Solar drawn and tested
S	725,000	OCF drawn, Solar tested
994	675,000	High strength data from OCF, used for 994 strand fibers.

Strength reductions, expressed by the ratio: damaged fiber strength/virgin reference strength, were computed on this basis and are shown in Fig. 19 for artificially damaged fibers and fibers damaged in the process of stranding (Figs 5 & 6). The extent of surface damage from the particles used for this condition is shown in the microphotographs, Fig. 20.

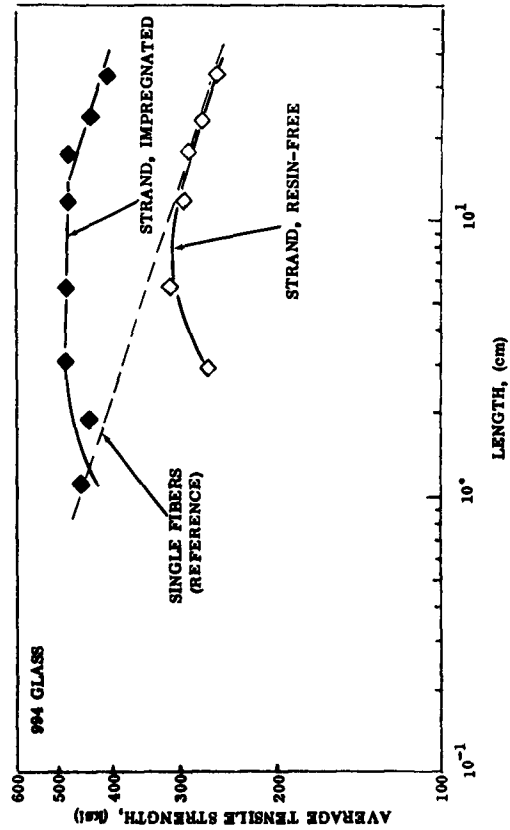
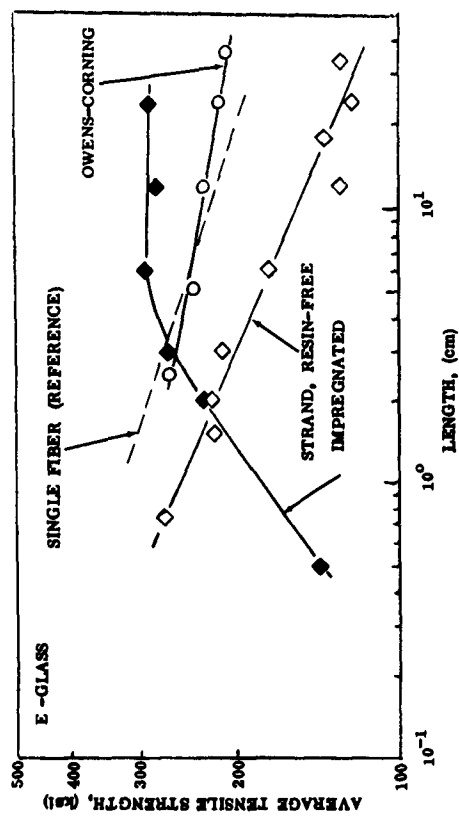


FIG. 21. LENGTH EFFECT ON BREAKING STRENGTH OF STRANDS WITH AND WITHOUT RESIN

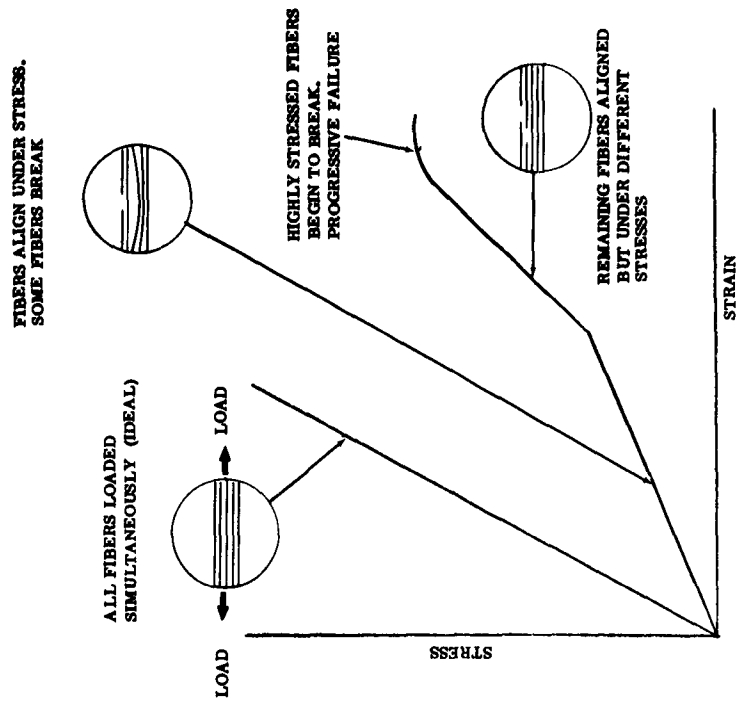


FIG. 22. DEGRADING EFFECT OF POOR FIBER COLLIMATION ON STRAND STRENGTH

The close proximity of the data points of S- and E-glass for the two damage conditions suggests similar resistance to damage. It can be inferred from the experimental results that the stranding process caused similar distributions of both severity and separation of defects on the two glasses. Strand test data presented by OCF at the Polaris meeting, January 1964, substantiated this conclusion. Strength loss was nearly equal for the two glasses, 18 to 19 percent based on 10-inch (25 cm) gage length and virgin control strengths at that length.

### III. EFFECT OF GAGE LENGTH ON STRENGTH OF STRANDS

To provide a link between the strength of single fibers and strands, the investigation of the length effect was extended to strands of the same batch from which fibers were separated for single fiber tests. A limited number of tests was conducted. Results are, therefore, considered to be preliminary, although some definite trends were established.

Data obtained from resin-free and resin-impregnated strands are plotted in Fig. 21. The strength reversal at shorter gage lengths in the 994 (S-glass) plot led to a close examination of the load-elongation curves and it was found that poor fiber collimation was the cause. Relations could be established between progressive loading of poorly collimated fibers and elongation of the entire strand (Fig. 22). This has been discussed in Report No. 4, 1962. It is obvious that different results will be obtained with strands having different fiber collimation and/or with change of pre-tension, as was the case with resin-free strand tests by Owens-Corning, shown in the upper graph of Fig. 21.

Divergent opinions exist over the question whether the average strength values from single-fiber tests can be compared with those from strand tests on the basis of equal gage length. In essence, the argument is whether the total glass length of the strand (i.e., of the 204 fibers) or the nominal gage length must be used in strength-length plots. Examination of the strand strength-length plots (Fig. 21) shows that resin-free strand strength is equal to the average (single) fiber strength in the case of X-994 glass at test lengths where the collimation effect is small. If the total fiber length of the 204 fiber strand were to be used, the measured strengths would have to be plotted more than two decades to the right, at approximately 2000 cm. It can be concluded that the basis of comparison for 994 glass must be gage length. On the other hand, the lower strand strength of Solar's tests on E-glass was due to a severe fiber collimation. Owens-Corning's data for 20-end rovings are plotted in Fig. 21 and fall close to the single fiber curve determined at Solar. If total glass fiber length were the basis of comparison, the Owens-Corning's data would have to be plotted four decades to the right (400 meters total length).

In conclusion, it has been shown that length effects exist for strands as well as for fibers. At long-strand lengths the effect is similar to that on fibers so that strengths match when each is tested at the same gage length.



## PART 2.

### ENVIRONMENTAL EFFECTS ON STRENGTH

The work reported in Part 1 was based on one mode of loading, i.e., a strain rate of  $0.06 \text{ min}^{-1}$ , and one atmospheric condition, i.e., laboratory atmosphere of approximately 50% RH. A change of these two conditions affects the strength, and hence the flaws. These effects have been studied by strain rate tests and static fatigue tests in atmospheres with different humidities. The work was performed in 1964/65 and the referenced reports are those labeled THIRD CONTRACT YEAR.

#### IV. EFFECT OF STRAIN RATE

##### Experimental

Monofilaments of E-glass of standard size (average diameter  $38 \text{ to } 39 \times 10^{-5}$  inches) were drawn from the same batch of OCF marbles used in the strength-length investigation. The monofilaments were approximately 70 inches long and permitted comparable sample populations to be obtained for each of the different test series. Bi-monthly Report No.4, 1964, contains the detailed information on the various tests.

The tensile test equipment used in previous work was modified to provide a wider strain rate range so that rates between  $2 \text{ min}^{-1}$  and  $0.006 \text{ min}^{-1}$  and less could be accomplished. Tests were conducted to assure the validity of the strain rate curves, particularly in the critical high strain rate range.

##### Results

Results from strain rate tests are plotted in two sets of curves: average strength versus strain rate, and failure probability plots. Examples of strength-strain rate curves are shown in Fig. 23. Whereas the 0.25 cm length shows a single trend, it is evident that more than one mechanism must control the curvature of the 20 cm length. The failure probability plots in Fig. 24 are analyzed for characteristic changes and correlated with the strength-strain rate curve. These changes disclose the behavior of flaws under the given test conditions.

The average strength of the 0.25 cm test length was 515,000 psi at the standard strain rate of  $0.06 \text{ min}^{-1}$ . Failure probability plots showed that very few A-flaws were present, and the 515,000 psi average is in agreement with the typical type B average strength of 520-535,000 psi, or a strength reduction factor of approximately 1.15.

The unexpected strength reversal for the 20 cm gage length required additional

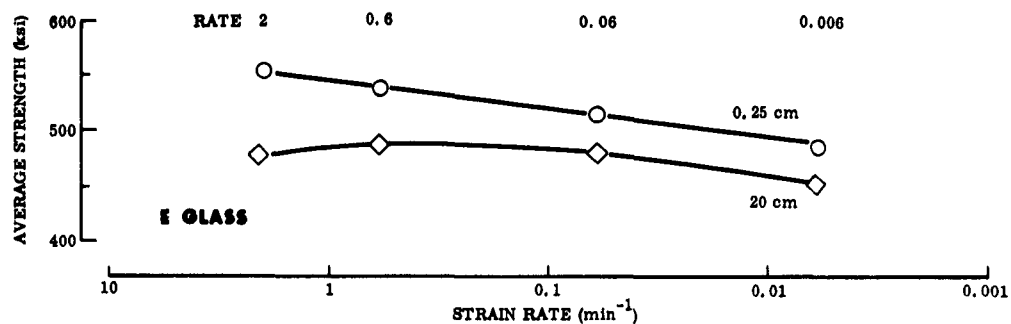


FIG. 23. STRENGTH VERSUS STRAIN RATE CURVES FOR TWO GAGE LENGTHS

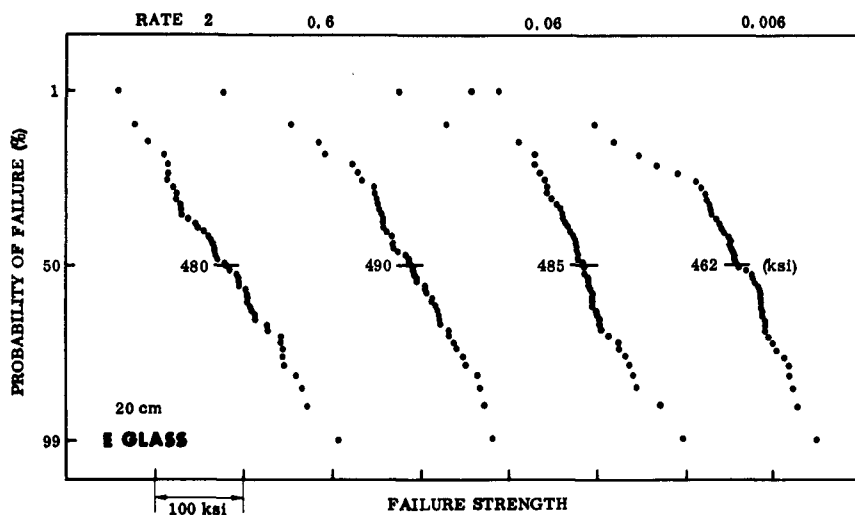


FIG. 24. GAUSSIAN FAILURE DISTRIBUTION PLOTS AT DIFFERENT STRAIN RATES

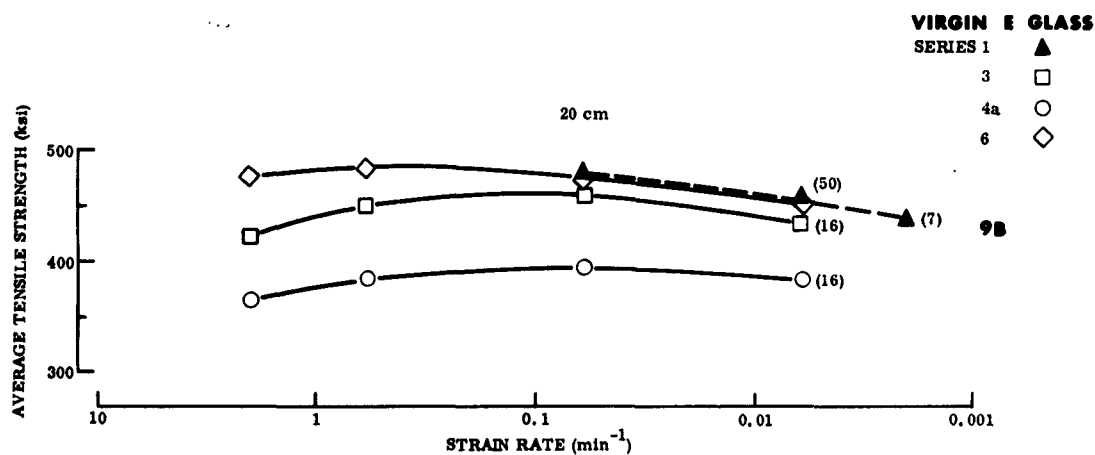


FIG. 25. STRAIN RATE CURVES OBTAINED FROM VARIOUS GROUPS OF 20 cm FIBERS

tests to confirm the effect. Four series of tests were made at 20 cms, but the percentages of types A and B flaws were not very consistent due to variations in fiber quality. As a result, the mean strengths are displaced in Fig. 25, but the shape of the curve is unchanged. In Series 1, a set of specimens was tested at rates down to  $0.002 \text{ min}^{-1}$  and these confirm the gradual strength decrease below a rate of  $0.06 \text{ min}^{-1}$ .

The failure probability analysis of the 20 cm length fibers is confined to Series 6 where adequate data are available. These curves are presented in Fig. 24. The Gaussian distribution for the strain rate 2 has the dispersion characteristic of type A flaws. As the strain rate decreases, up to 13% of a more severe flaw appears that had not been seen in previous tests at the standard rate of  $0.06 \text{ min}^{-1}$ . The major change is an increase in the mean strength of the type A distribution at the rate 0.6, followed by a strength decrease at slower strain rates. The strength reduction factors for the type A flaws are 1.25; 1.21; 1.24; and 1.275 for the four rates from 2 to  $0.006 \text{ min}^{-1}$  respectively.

### Discussion

The physical effects on the flaws during the course of each tensile test are believed to result from interaction with water vapor. This interaction must be a stress corrosion process proportional to the strain rate for short fibers (0.25 cm in Fig. 23). These fibers contain mostly mild B-flaws. The rate of strength loss is approximately 15,000 to 23,000 psi per decade of strain rate.

The curvature of the 20 cm data in Fig. 25 can be explained by a healing process of severe A-flaw caused by water vapor corrosion increasing the root radius faster than the depth increased (Bi-monthly Report No. 4, 1964). This type of mechanism was proposed by Charles(11) for static fatigue tests on glass rods at elevated temperatures. Because of the small size of the glass fibers ( $40 \times 10^{-5}$  inch against 0.1 inch rods used by Charles) and because of the extremely small defects present on high strength glass monofilaments, it is possible to postulate healing during the course of the tensile test. The healing mechanism may be surface diffusion rather than stress-aided corrosion, but the net effect is a difference in rate of change of root radius and depth. The assumption of flaw healing as one of the controlling mechanisms is supported by results from a careful study of the effect of annealing on the strength of E-glass fibers conducted by Cameron(12) at the University of Illinois. Cameron used a gage length of 3/8 inch (approximately 1 cm) with a strain rate of  $0.7 \text{ min}^{-1}$  and tested fibers after anneals at temperature between 150 and  $545^{\circ}\text{F}$ .

Figure 26 shows one set of Cameron's results and shows an apparent strength increase on annealing at  $150^{\circ}\text{F}$ . Another set of results for fibers annealed at  $155^{\circ}\text{F}$  in nitrogen confirmed this strength increase and, in addition, showed the same shape changes in the failure probability plot. When the failure probability plots in Fig. 26 are analyzed for the individual distributions, it is found that the two sets of results behave in the same way. Such consistency of behavior is regarded as a strong indication that the analysis is valid.

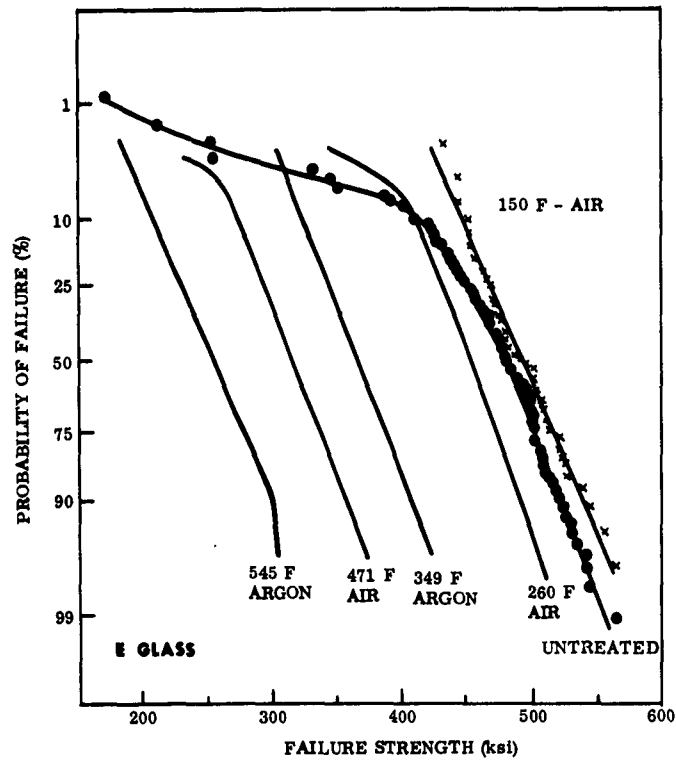


FIG. 26. EFFECT OF ANNEALING ON SHAPE OF FAILURE DISTRIBUTION

- △ SOLAR VIRGIN E GLASS. REF. STRENGTH 510 000 psi Tensile  
 ○ AGC 994 GLASS, 8 inch Spheroids REF. STRENGTH 3980 psig Hydro

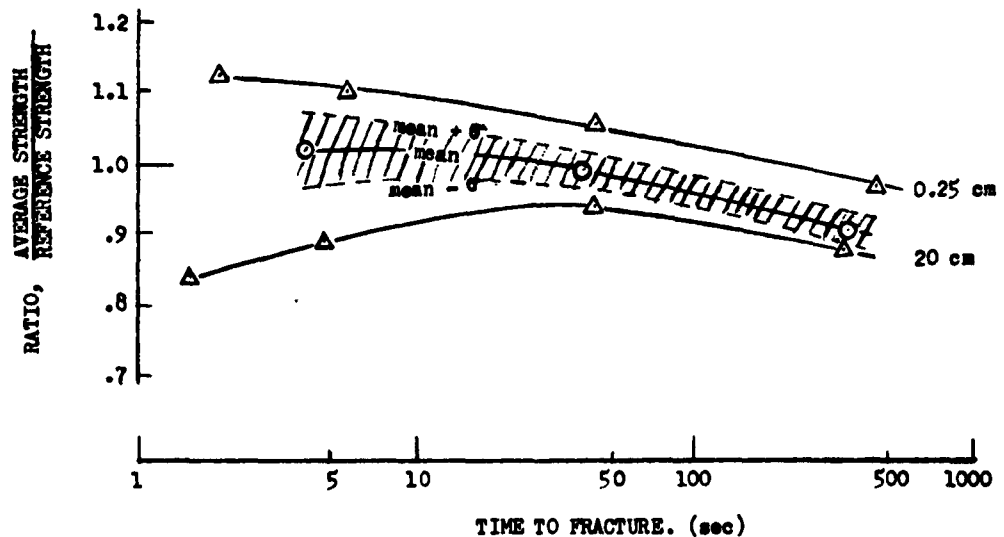


FIG. 27. STRENGTH BEHAVIOR OF FIBERS AND OF PRESSURE VESSELS AS A FUNCTION OF TIME-to-FRACTURE

The non-linear strength - strain rate behavior has been observed also on pressure vessels tested at various rates of pressurization. Aerojet General has hydro-tested two groups of 8-inch spheroids\*. Results of one group are compared in Fig. 27 with Solar's strain rate data and show good agreement; the data from the second group showed still more curvature.

#### Summary

The tensile strength of E-glass fibers decreases slightly with longer test duration, i.e., lower strain rates. Stress corrosion is believed to be the controlling mechanism. Under certain conditions, stress corrosion may heal existing surface flaws and a net increase in average strength occurs as a function of strain rate. Further investigation of stress corrosion has been carried out on static fatigue tests to be reported in the following.

### V. STRESS CORROSION OF E-GLASS FIBERS

Stress corrosion was investigated by static fatigue tests conducted in 50% and 100% RH on virgin E-glass fibers of 2.5 cm gage length. A detailed description of the experimental work is given in Bi-monthly Report No.7 (1965). The test program was coordinated with a similar program conducted by General Electric for the Naval Research Laboratory. Accordingly, Solar proceeded to accumulate data in 100% RH over a wide range of applied stress and the same gage length (i.e., 2.5 cm), as well as a limited number of tests at 50% RH at one intermediate stress level for correlation purposes. The results from static fatigue tests and some tensile tests in various humidities made possible a thorough analysis of the stress corrosion mechanism.

#### 5.1 STATIC FATIGUE TESTS

##### INTRODUCTION

Stress corrosion occurs in metals, ceramics and plastics when these materials are held under load in specific corrosive environments. The environments must not be sufficiently corrosive to cause general attack on the materials, in which case no stress corrosion failures are found. Rather, the chemically-controlled events must occur locally to set up conditions for fracture. In metals, the fracture process may outrun the chemical process so that fracture may stop until the chemical conditions are re-established. In ceramics and glasses, cracks are more difficult to stop, and fracture is usually complete.

The chemically controlled events are not completely understood. Examination of the Griffith's equation has led to two types of explanation. Griffith<sup>(1)</sup>

---

\* Data were presented at the Polaris Meeting, January 1964, by F. T. Clement.

TABLE VI

## THEORETICAL EXPRESSIONS FOR THE STATIC FATIGUE CURVE

Equation*	Investigator and Reference
$\log t = -a + \frac{b}{\sigma}$	Murgatroyd, Ref. 14 Glathart and Preston, Ref. 15 Taylor, Ref. 16
$\log t \simeq a - \frac{b}{\sigma} - \log \sigma$ (for small t)	Stuart and Anderson, Ref. 17
$\log t = -a + \frac{b}{\sigma^2}$	Elliot, Ref. 18
$\log t \simeq -a - b \left(\log \frac{1}{\sigma}\right)$ (for large t)	Charles, Ref. 11

\*  $\sigma$  = Applied stress, t = Time to failure

TABLE VII

## STATIC FATIGUE PROGRAM SUMMARY

Test Series	Applied Stress (ksi)	Number of Test Specimens			Gage Length (cm)	Remarks
		Static Fatigue		Control*		
		at 50% RH	at 100% RH	at 50% RH		
I	320	40	40	32	0.25	Study effect of moisture, and of strength retention of fibers surviving static fatigue tests.
II	320	28	--	32	2.5	
III	480	--	15	15	2.5	Study Strength-Failure Time relation. Note, 50% RH tests conducted at G.E., same gage length.
	440	--	30	30		
	400	--	30	30		
	360	--	30	30		
	320	--	30	30		
	280	--	30	30		
	240	--	20	20		
	200	--	20	20		
	150	--	15	15		
	81	--	5	5		
Fiber Washing	320	--	10 (100% RH only) 10 (100% RH and water coating)	--	2.5	Preliminary investigation of effect of excess water on corrosion mechanism.

\* Control fibers tested at standard tensile strain rate  $0.06 \text{ min}^{-1}$ .

calculated that the stress, S, to propagate a sharp crack of length 2c is given by,

$$S = \sqrt{\frac{E \gamma}{\pi c}}$$

where E is the elastic modulus and  $\gamma$  is the surface energy. The first explanation is that the surface energy term is reduced by the chemical events. But this explanation must assume already existing flaws of length 2c. The second, and more general explanation involves the growth of cracks to a critical size by the chemical process.

Prior stress corrosion (or static fatigue) studies on glass have been reviewed by Mould and Southwick<sup>(13)</sup>. Table VI summarizes the theoretical expressions proposed for the static fatigue curves. None of these expressions distinguish between the relative durations of possible stages in the overall stress corrosion process, such as: incubation; corrosion or flaw growth; and crack propagation or fracture. Indeed, only the theory of Charles<sup>(11)</sup> is based on a physical model. Charles developed a quantitative theory based on the single process of stress accelerated corrosion by which flaw growth to the critical size leads to fracture. Because of this theoretical basis, the theory of Charles has received wide recognition, and will be used as a criterion in this work.

A variety of materials were used in the works cited, although major attention has been devoted to soda-lime glass in the form of rods. The work reported here relates to E-glass monofilaments, and the results obtained are at variance with present theories of stress corrosion of glasses.

## EXPERIMENTAL

### Test Program

Four series of static fatigue tests\* were conducted to study stress corrosion phenomena. The program is summarized in Table VII, listing the applied stress levels, number of test specimens for static fatigue tests and for control fibers tested in tension. Also listed are gage length and purpose of each test series.

### Instrumentation

The static fatigue tester is shown in Fig. A-6. This apparatus permits simultaneous testing of five fibers and can be adjusted for gage lengths from 0.25 cm to 20 cm. Levers carrying the predetermined dead weight load are oil-dampened to prevent accidental failure resulting from shock loads during both fiber loading and fiber fracture.

---

\* To avoid confusion, the following terminology has been adopted for this discussion: "Static Fatigue" means the test; fibers tested in static fatigue are subject to "stress corrosion" (which may only be part of the total failure mechanism). A "stress corrosion process" includes both incubation period and corrosion period, as well as fracture. The term "stress corrosion mechanism," then, denotes a specific sequence of events that occur in the course of the stress corrosion process.

The tester was contained in a humidity-and temperature-controlled chamber (Model Vapor-Temp, Blue M). Actual humidities and temperatures obtained during the nominal 100% relative humidity (RH) were 96 to 99% RH at temperatures between 82 and 86°F. The chamber was not used for the tests at 50% RH.

Test apparatus as well as the chamber were shock-mounted to eliminate effects on fatigue life from vibrational sources, which are most detrimental in long-time tests at low applied stresses. Effectiveness of the damping system was checked by placing a tray of water on the tester. Only very slight ripples could be observed occasionally, and this was taken as an insurance for reliable test results.

Failure times were recorded by five electrical digital clocks operated individually by small mercury switches located on the load-bearing arms of the tester. The clocks recorded the time in minutes with the last digit indicating tenths of a minute in continuous rotation. This allowed time to be interpolated within 2 seconds and was adequate for the purpose of this investigation.

#### Fiber Drawing and Storage

E-glass filaments were drawn at Solar from a conventional one-hole platinum bushing under carefully controlled conditions so that uniform filament strengths could be achieved and fiber diameters be held in close tolerance. Typical strength values were 450,000 to 520,000 psi, with an overall average of 490,000 psi. Diameters were held within  $38$  to  $40 \times 10^{-5}$  inches, determined from measurements under 500x magnification in a Leitz microscope with bi-filar eyepiece. The drawing facilities permitted drawing of 70-inch long monofilaments, measured between bushing and winding drum. Generally, 8 to 10 monofilaments were drawn during one drawing period. The filaments were wound on serrated frames suitable for 2.5 cm free gage length, and were stored in airtight boxes containing Drierite.

#### Control of Filament Strength

One or two monofilaments from each drawing period were checked for tensile strength at 12 locations, using a multiple tensile tester at standard strain rate of  $0.06 \text{ min}^{-1}$  in laboratory atmosphere of approximately 50% RH. These tests were made within 1 to 2 hours after drawing, and served to check drawing performance.

The tensile strength of monofilaments used for static fatigue tests was obtained from 5 specimens from each monofilament, again tested under standard conditions. The strength data were used for correlation between monofilaments and as a baseline for evaluation of strength of fibers surviving static fatigue tests.

#### Sampling Procedures

Because of the importance of sampling in statistical measurements of brittle materials, much attention was paid to the sampling procedures. Three sets of five fibers each were obtained from each 70-inch monofilament. One set was used for the control and reference data mentioned above. The two other sets



were used for the static fatigue tests. In test series I, (Table VII) one set each was assigned to 50% and 100% RH respectively at one stress level. In test series II, one set from each filament was tested at one applied stress, whereas the second set had been used for preliminary tests in 100% RH at different stresses, but are not reported here. Sampling in the latter tests was entirely random, since each specimen of a group of five had been loaded to one of the programmed stresses. However, the long test duration of the low-load fibers proved to be too time-consuming for the overall program and the method had to be discontinued in test series III. In these experiments, all fibers of one group were loaded to the same stress. Since two groups were available from one monofilament, a certain correlation could be achieved by testing the groups at two different stress levels within the programmed stress range (Table VII). To compensate for the simultaneous usage of five fibers from the same source, a large number of tests were made at each stress level. As it turned out, the distribution of failure times of a given group of five fibers was rather wide and, consequently, the effect of biased sampling was minimized.

### Test Procedures

The frame-mounted fibers were inserted simultaneously into the molten sealing wax of the fiber gripping points (Fig. A-6) after the desired humidity in the chamber had been stabilized for some time. Alignment of the specimens was achieved by fixed positioning of the serrated frames which were machined to close tolerance. The temporarily removed Plexiglass bell jar enclosing the tester was replaced immediately and the humidity was restored while the wax cooled. After 5 minutes, the "Zero Position" cam shaft was turned manually through a window in the side of the bell jar, thereby loading the fibers simultaneously in approximately 1/5 second. The clock circuits were activated at the same time by a master switch. Failure times of specimens breaking immediately upon load application (mainly at high stresses) were recorded as "failed within 0 to 2 sec." and are plotted at 1 second on the logarithmic time scale of the respective diagrams.

One of the analytical tools employed in this study required the tensile strength of unbroken test fibers to be determined after a certain exposure time to static fatigue. This was accomplished by means of single lead shots of 0.07 grams average weight being fed into the load baskets (Fig. A-6 shows weights instead of baskets). The shots were fed out of a small glass tube, one at a time, in a controlled succession until the fiber broke (typical failure loads equalled 20 grams).

### RESULTS

Figure 28 shows the customary plot, Applied Stress versus Time-to-Failure on log scale. The number of test points per stress level is given in Table VII. Fibers that failed within 2 seconds after initial loading in the static fatigue test are plotted at the 1 second time mark. Open circles with arrows denote unbroken test specimens that were tensile tested at the plotted times.

In Fig. 29, logarithmic failure times of fibers tested at the various stress levels are plotted on Gaussian probability paper. Best fitting curves are

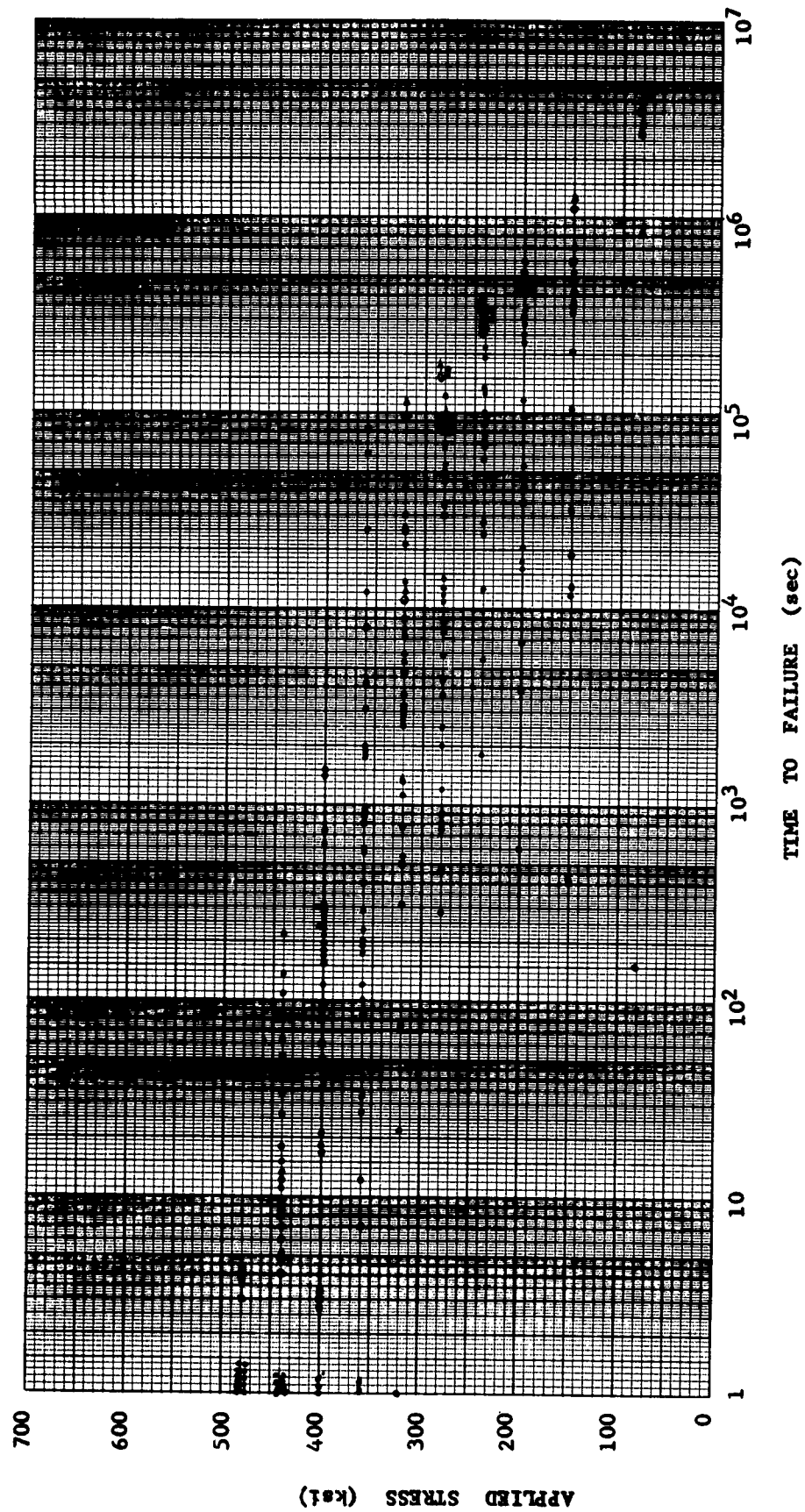


FIG. 28. STATIC FATIGUE DATA FROM 2.5 cm VIRGIN E-GLASS FIBERS IN 100% RH (TEST SERIES III)

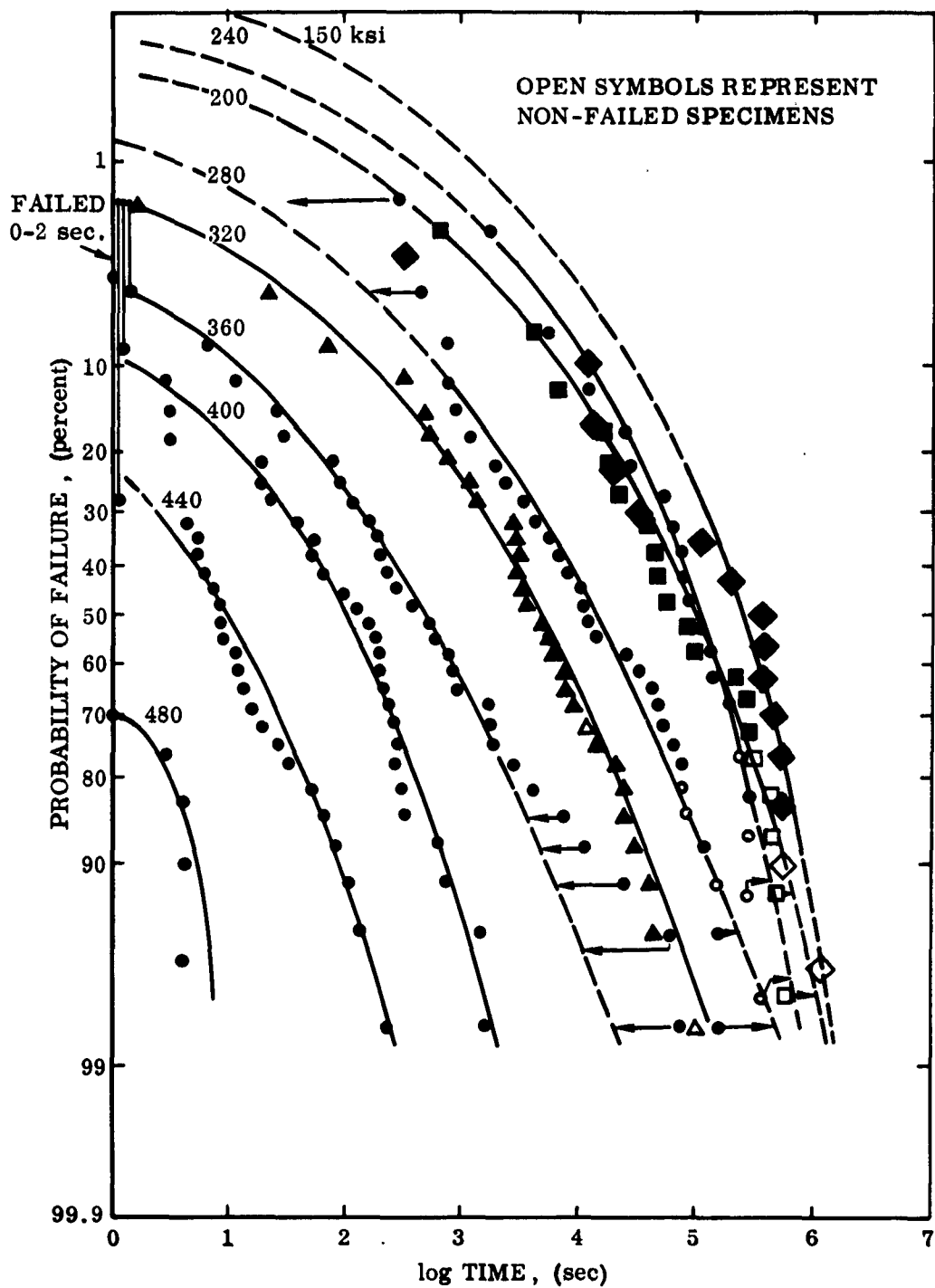


FIG. 29. FAILURE TIME PROBABILITY PLOTS AT VARIOUS APPLIED STRESSES (TEST SERIES III)

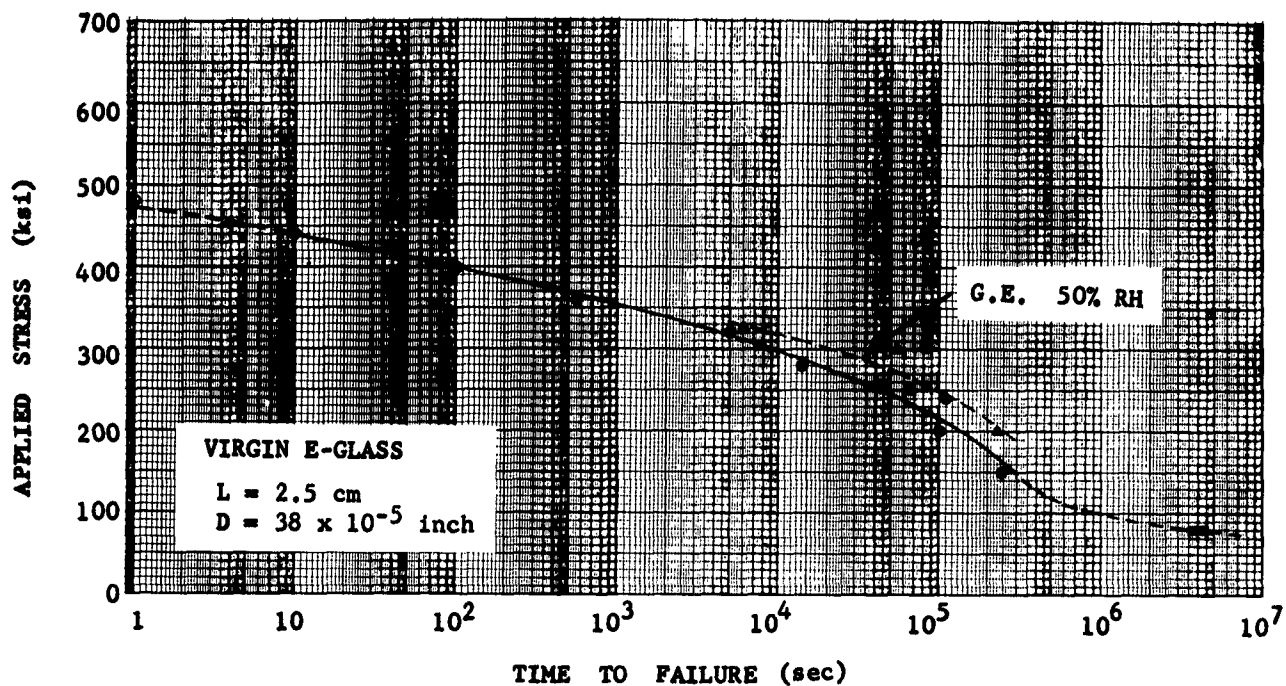


FIG. 30. STATIC FATIGUE CURVE FOR 100% RH

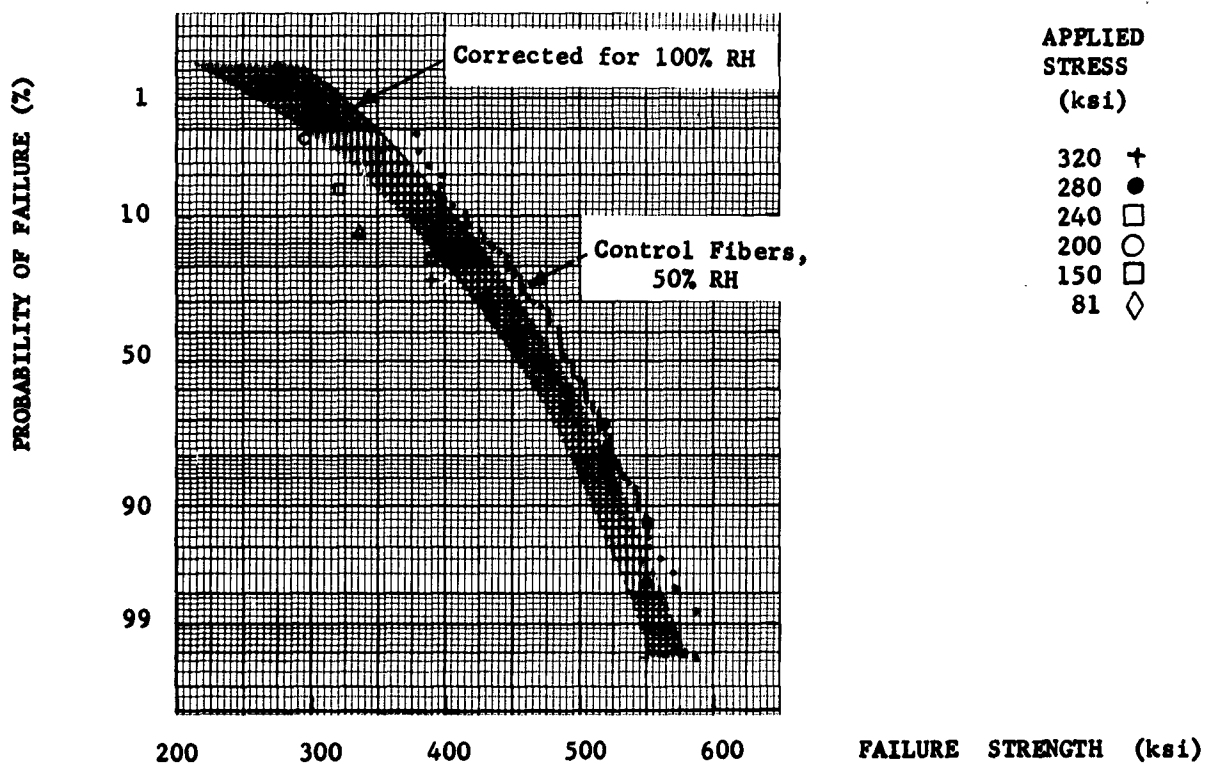


FIG. 31 TENSILE STRENGTH DISTRIBUTION OF UNBROKEN FIBERS (TEST SERIES III)

drawn through the data points, based on the general pattern. Deviations from actual failure times, specifically at 360 ksi, are assumed to have originated in variation of initial filament strength.

Figure 30 shows the static fatigue curve as derived from the best fitting curves of the failure time plots in Fig. 29, at the 50 percent probability level. The 50% time was adopted as a convenient method to deal with the problem of choice of representative values. One of the advantages of this method is that the effect of immediate (0 to 2 sec.) failures, as well as of the non-failed (surviving) specimens, is minimized, specifically if a family of curves is available for evaluation. The data points in Fig. 30 representing G.E.'s results were obtained by the same evaluation method from failure time probability plots. This evaluation was limited to stress levels of 325,000 psi and lower, because of the high mortality rate during loading at the higher stress levels, i.e., 30% mortality on loading, occurred at 440,000 psi in the Solar work, but at 325,000 psi in the G.E. results.

The tensile strength distribution of unbroken (surviving) fibers from Series III is shown in Fig. 31. The strength distribution of the control fibers is shown for comparison, but this was determined at 50% RH and a strain rate of  $0.06 \text{ min}^{-1}$ . Uncertainties in the corrections to be applied to make the control strength data appropriate for 100% RH leads to a band as shown in Fig. 31. For the average strength, the correction is  $0.95 \times$  (strength at 50% RH). Fig. 32 shows additional tensile strength distributions of surviving fibers from Series I and II.

#### ANALYSIS OF RESULTS

Static fatigue data obtained in 50% and 100% RH are analyzed with respect to (1) strength loss with time, (2) effect of humidity on the life of fiber, and (3) strength retention of fibers after prolonged exposure to stress corrosion. Corresponding data from G.E., as well as other Solar data, are used for correlation or clarification.

##### The Static Fatigue Curve

The strength vs failure time plot in Fig. 28 shows the usual spread over 2 to 3 decades of time for each of the stress levels. In order to arrive at a meaningful static fatigue curve, the 50 percent probability of failure time has been used for the different applied stresses. Fig. 29 shows the plots. Best fitting curves are drawn, taking into consideration the recognizable general pattern. The failure time values at 50% probability have been read from the curves to plot the fatigue curve in Fig. 30. This curve is terminated at 440,000 psi because of the high rate of immediate failures at 480,000 psi. The slight curvature of the extrapolated section is necessary because an upper limiting stress must be approached asymptotically. At lower stress levels the curve shows a marked downward curvature. The validity of this curvature is supported by the uniformity of tensile strength data of control fibers, Table VIII. The same tendency is apparent for the G.E. data at approximately 50% RH. Both sets of data were derived by the same method of analysis, e.g., from failure time probability plots. Sample sizes used by the two laboratories were almost identical, and so were the tensile strengths of the respective control fibers, 497,000 psi median strength (G.E.) and 490,000 psi (Solar).

TABLE VIII

## STRENGTH OF CONTROL FIBERS USED IN STATIC FATIGUE TESTS

Static Fatigue Stress (ksi)	Tensile Strength Data of Control Lot		
	Number	Average Strength (ksi)	Coeff. of Variation (%)
All Stress Levels	110	486	10.9
480	15	475	7.6
440	30	503	12.1
400	30	495	8.3
360	30	483	10.3
320	30	505	8.0
280	30	473	10.9
240	20	475	12.6
200	20	486	9.2
150	15	488	7.4
81	5	470	- -

TABLE IX

## STRENGTH RETENTION OF STRESS CORROSION TESTED FIBERS

	①		②			③			④
	Tensile Strength Before Test		Stress Corrosion Test			Tensile Strength After Stress Corrosion Test			Strength Ratio ③/①
	% RH	Average Strength	% RH	Applied Stress	No. of Specim.	% RH	Percent Tested	Average Strength	
Series I	50	510 ksi	50	320 ksi	40	50	37.5	510 ksi	1.00
			100	320	40	100	2.5	550	1.07
Series II	50	480	50	320	28	50	46.5	515	1.07
Series III	50	505	100	320	30	100	6.6	420	0.83
	50	473	100	280	30	100	13.3	515	1.08
	50	475	100	240	20	100	20.0	460	0.97
	50	486	100	200	20	100	25.0	425	0.88
	50	488	100	150	15	100	13.3	380	0.78
	50	470	100	81	5	100	40.0	485	1.03
Average of individual results in Series III:									0.93
Average adjusted to 100% RH of ①:									0.98

The data at 81,000 psi, shown as a band because of statistical uncertainty, indicates a slope reversal of the fatigue curve. This reversal is to be expected since failure from stress corrosion cannot, by definition, occur at zero stress. Corrosion of unstressed E-glass fibers in 100% RH has been found by Thomas(4) to reduce tensile strengths to 70 percent of the initial strength. The loss in strength with time of storage in 100% RH approaches the 70 percent level asymptotically within approximately 80 days.

#### Effect of Humidity

The effect of humidity (50% vs 100% RH) on the fatigue life of fibers has been investigated on a set of comparable sample populations of fibers of 0.25 cm gage length and an applied stress of 320,000 psi, (Test Series I). Evaluation by means of failure time probability plots shows a life increase of 40 percent for the lower humidity. Similar values can be extracted from the curves in Fig. 30, e.g., approximately 25 percent at 325,000 psi, 35 percent at 250,000 psi and 50 percent at 200,000 psi. The increasing percentage indicates a difference in curvature of the two curves, but it is felt that the present data is not reliable enough to determine such details, and clarification would need closely controlled tests in one laboratory.

#### Strength Retention after Exposure to Stress Corrosion

Fibers in static fatigue, not failed at the time of test termination, were loaded to failure. The respective tensile strength data are correlated with the tensile strength of control fibers in two ways: tabulated average strength and failure probability plots. Table IX lists the data of test Series I through III for control fiber strength (column 1), applied stress levels (column 2), and tensile strength after termination of static fatigue tests (column 3). The fourth column, Ratio (Average strength after test/Average strength before test) shows the percent strength retained by the fibers after exposure. The average of 0.93 for Series III has been computed on the basis of the individual results. This value is not directly comparable with the respective values of Series I and II for the following reasons:

- 1) The sampling method led to a closer approach to the 100% life of the fibers. (See Fig. 28 for time of test terminations. Series I and II fibers were sampled closer to the 50 percent life, i.e., approx.  $10^4$  sec.)
- 2) The tensile strength of control fibers was determined in 50% RH instead of 100% RH.

As to item 2, a correction can be applied from available tensile tests results in 50% and 100% RH, (Ref. Bi-monthly Report No. 7 (1965)). It was found that the average tensile strength in 100% RH differed from 50% RH by a factor of 0.95. Application of this factor to the average ratio raises the value from 0.93 to 0.98. Hence the average fiber strength is essentially unchanged by the exposures under load.

The second method of presentation, i.e., failure probability plots, is shown in Fig. 31 for the 100% RH fatigue data. Individual data points of the strength distribution of surviving fibers are related by different symbols to the applied

stress levels at which they were tested. The data points are equally distributed at both sides of the strength band for 100% RH. The low strength data could be interpreted as being obtained during the last phase of the life of the fibers when stress corrosion has progressed. Corresponding plots for the 50% RH data are shown in Fig. 32.

The conclusions drawn from the foregoing analyses can be summarized as follows:

- 1) The static fatigue strengths are not linear functions of log time. A marked downward curvature occurs at lower applied stresses.
- 2) Humidity has a noticeable effect on the static fatigue life of fibers; lower humidity extends the life, as might be expected.
- 3) The initial tensile strength of fibers subjected to stress corrosion is retained over most of the life of the fibers. This was found to be the case for both 50% and 100% RH.

## DISCUSSION

The results and conclusions presented so far will be examined in the light of the current theory on stress corrosion by Charles<sup>(11)</sup>. Charles' work was based on soda-lime glass in the form of rods of 0.10 inch diameter, whereas this investigation is concerned with E-glass filaments 250 times smaller in size. Besides the difference in glass composition\* (E-glass contains only spurious amounts of the critical alkali), there is considerable difference in glass structure due to the different rates of cooling during drawing. The rod structure is close to equilibrium, and surface stresses during cool-down initiate surface cracks of detectable sizes<sup>(20)</sup>. The structure of filaments is "frozen" in an expanded, non-equilibrium state, and the surface is apparently free of detectable surface cracks.

### Current Theory on Stress Corrosion of Glass

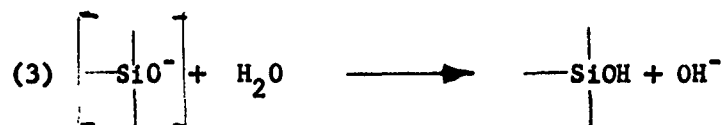
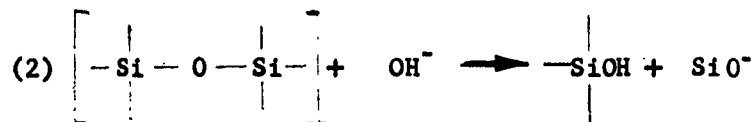
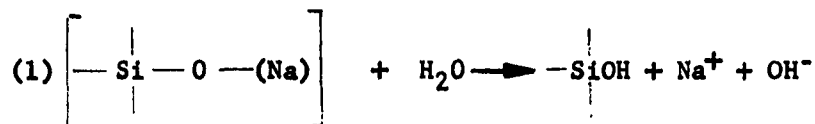
Stress corrosion of glass has been studied primarily for glass rods. Among several investigators, Charles' work has obtained wide recognition; he first studied the corrosion process independently and then investigated the effect of stress.

---

* Soda-lime glass (Corning #0080)		E-glass	
SiO <sub>2</sub>	72%	SiO <sub>2</sub>	54.5%
Na <sub>2</sub> O	17%	CaO	17.0%
CaO	5%	Al <sub>2</sub> O <sub>3</sub>	14.5%
Al <sub>2</sub> O <sub>3</sub>	6%	B <sub>2</sub> O <sub>3</sub>	8.5%
MgO		MgO	4.5%
		Na <sub>2</sub> O	1.0%
		K <sub>2</sub> O	
		TiO <sub>2</sub>	
		FeO <sub>3</sub>	
		2	



Charles has shown that the corrosion of soda-lime glass rods has a temperature dependence leading to an activation energy of 20 kcal/mole, approximately equal to the activation energy for self-diffusion of sodium ions in the glass. This led Charles to postulate a corrosion mechanism involving terminal groups in the silica network:



where reactions (2) and (3) provide an autocatalytic mechanism for continued attack on the silica network. The first reaction must proceed to the degree necessary to create the requisite concentration of hydroxyl ions (or pH) because the second reaction can proceed only at this requisite pH. This explains the observed incubation period in the corrosion penetration versus time plots. Based on these reaction processes, Charles postulated a mechanism of stress corrosion tied to a stress-accelerated corrosion rate. He postulated that the corrosion rate in the x direction at temperature T is given by:

$$\left| v_x \right|_T = k_1 (\sigma)^n + k$$

where  $k_1$  and  $k$  are constants, and  $\sigma$  is the actual stress at the root of a flaw. When the stress-activated corrosion is very much greater than ordinary corrosion, the root of an already existing flaw will be attacked and this will lead to an increase in the severity of the flaw because the stress concentration is a function of ratio, (flaw depth/root radius). If the sides of the flaw are not attacked, but the depth increases, then the stress at the tip of the flaw will increase.

Application of this corrosion rate equation to flaw growth led Charles to a relationship between the time to grow a flaw of critical size and the applied stress. This relationship was:

$$\log t = n \log \frac{1}{\sigma_A} - \log k$$

where  $\sigma_A$  is the applied stress and  $k$  is a constant. This equation provides a convenient way to calculate the exponent,  $n$ , relating stress to corrosion rate.

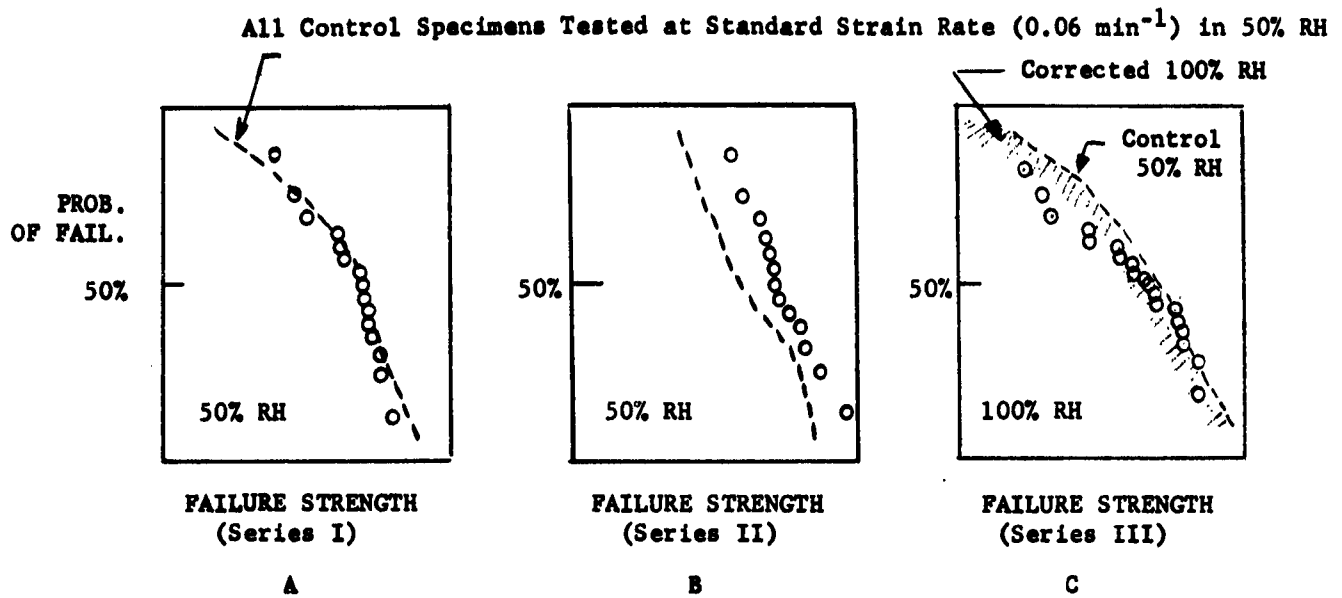


FIG. 32. TENSILE STRENGTH DISTRIBUTIONS OF UNBROKEN FIBERS FROM STATIC FATIGUE TESTS IN 50% and 100% RH

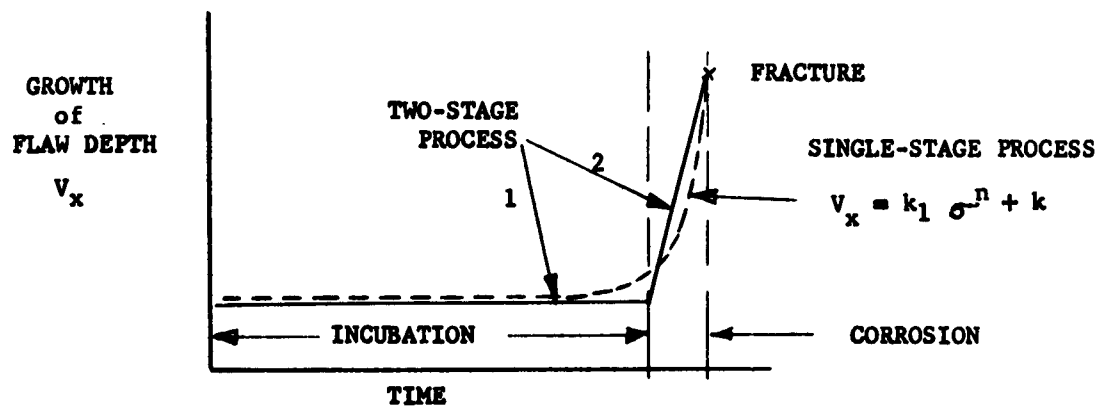


FIG. 33. GROWTH OF FLAW DEPTH WITH TIME

Plot shows how single stress corrosion process following  $V_x = k_1 \sigma^n + k$  fits a two-stage process of incubation followed by corrosion.

Proposed incubation reaction:  $\left[ \text{—Si—ONa} \right] + \text{H}_2\text{O} \rightarrow \text{—Si—OH} + \text{Na}^+ + \text{OH}^-$ .

Corrosion reactions are as postulated by Charles, but occur only in second stage.

## Discussion of Flaw Growth Theory

The flaw growth mechanism of Charles implies that flaws should become more severe with time under load in the static fatigue test. Table IX shows that the average tensile strength of fibers after exposure to 50% and 100% relative humidity has not decreased; exposure times were approximately  $2 \times 10^4$  seconds for Series I and II, and 1 to  $3 \times 10^5$  seconds for Series III. The respective failure strength distributions are shown in Fig. 32. A few fibers in Fig. 32C have strengths less than the control fiber strength adjusted to 100% RH, but others have greater strength (re: Fig. 31). The additional tests conducted at 81,000 psi applied stress showed the same result: two out of five fibers tested were broken after  $2.5$  and  $3.5 \times 10^6$  seconds and showed strengths of 470,000 and 480,000 psi versus 470,000 psi average control fiber strength; the last fiber failed at  $4.2 \times 10^6$  seconds.

These unexpected results show that:

- (i) There is no continuous growth of existing flaws, as suggested by Charles' theory, in times up to at least 95% of the static fatigue life.
- (ii) Both the average strength and strength distribution remain unchanged (Figures 32A and 32B) throughout most of the static fatigue exposure, showing that the flaws are unchanged. The lack of change in the low strength tail shows that the severe flaws are not the origin of static fatigue. The deviations observed in Fig. 32C are consistent with the statement under (i) because sampling took place in the last phase of the statistical life of the fibers.
- (iii) A long incubation period precedes failure, with crack growth restricted to the period immediately preceding fracture.

These results show that the present theory is not adequate because growth of flaws cannot be detected throughout most of the test duration. The deficiencies of the present theory may be related to the following:

- (1) Inglis' (21) criteria for large stress concentrations lead to the relation:

$$\frac{\sigma_f}{\sigma_A} = 2 \sqrt{\frac{\text{depth of critical flaw}}{\text{flaw root radius}}}$$

where  $\sigma_f$  is fracture stress (taken to be 1,500,000 psi) and  $\sigma_A$  is the stress calculated from the applied load. For failure at 300,000 psi applied stress, the stress concentration must reach a value of 5. Assuming very local attack and a flaw root radius of atomic dimensions ( $2\text{\AA}$  assumed), a depth of corrosion of  $12.5\text{\AA}$  is required. Such amounts of corrosion could occur in very short intervals once corrosion starts. Hence corrosion cannot be occurring throughout the entire stress corrosion exposure.

- (2) Calculation of the exponents for the stress-accelerated corrosion has led to typical values for  $n$  between 16 and 26. Such high values give

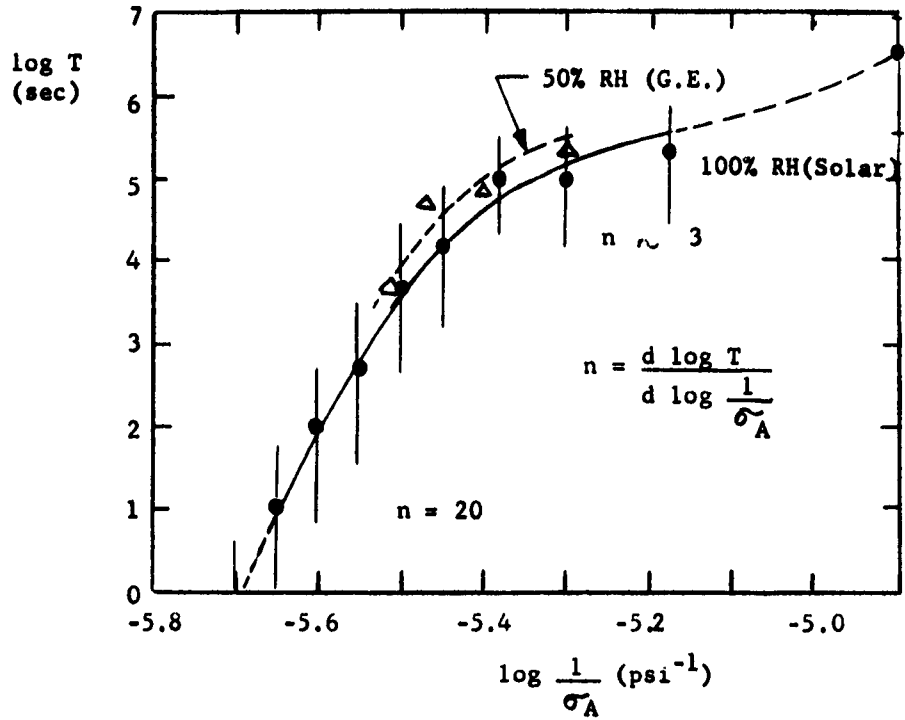


FIG. 34. STATIC FATIGUE FAILURE TIME VERSUS INVERSE APPLIED STRESS FOR VIRGIN E-GLASS FIBERS IN 100% RH (68% of Data falls inside the scatter band shown)

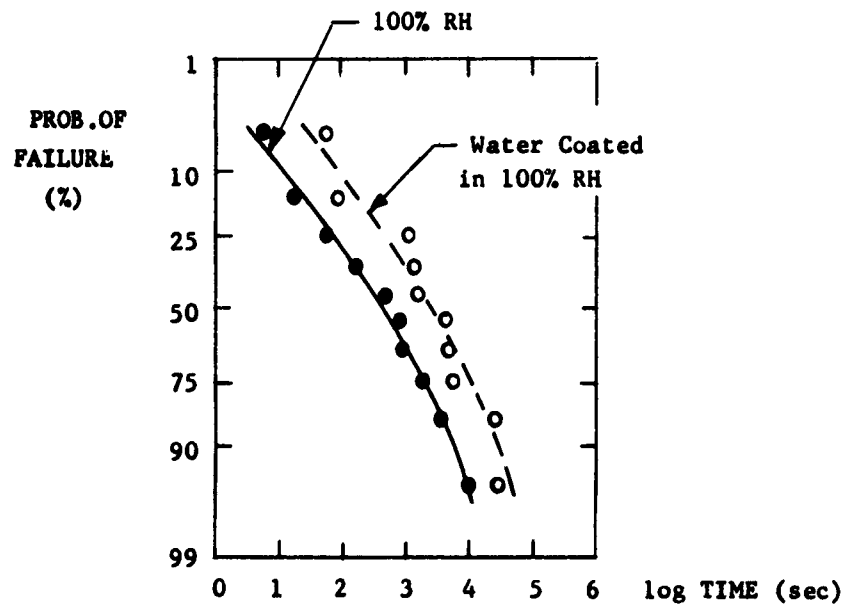


FIG. 35. DELAY OF CORROSION IN STATIC FATIGUE DUE TO PRESENCE OF WATER

an effective incubation period because the corrosion velocity,  $V_x$ , is negligible until a flaw has been deepened or sharpened to raise the stress at the flaw tip (Fig.33). But if the actual mechanism does not require any corrosion until the incubation period is over, then an equation with stress raised to a high power represents an empirical fit of a two-stage process.

- (3) Analysis of static fatigue data by the method of Charles shows that the required linear relationship between log (Time to Failure) and log (Reciprocal Applied Stress), is not obtained. The value of the exponent,  $n$ , varies from 20 at high applied stress to approximately 3 at low stresses, as shown in Fig. 34. The G.E. data, evaluated by the same method of analysis, show the same trend. The limits shown are those of 68 percent of the data and correspond to the one sigma limits in a Gaussian distribution.

#### A Proposed Mechanism of Stress Corrosion

It is proposed that stress corrosion occurs where the so-called C flaws are located at the surface\*. Interaction of water with the cations in the C flaws leads to hydrolysis and an increase in concentration of hydroxyl ions (or of pH). The incubation period continues until the pH reaches the level necessary for corrosion to occur. This incubation period continues for 95% or more of the total static fatigue process duration, (Fig.33).

To support this theory of the incubation, a comparison was made of static fatigue life at 320,000 psi of wet and dry fibers in 99+% relative humidity at room temperature. One set of monofilaments was kept dry (adsorbed water films), and the second set was sprayed to leave water droplets on the surface. It was reasoned that the larger water reservoir in the second case would dilute the  $\text{Na}^+$  and  $\text{OH}^-$  ions, thereby delaying the time at which the critical pH would be reached. Fig. 35 provides preliminary evidence that this effect is occurring, although complete water coverage was not attained. Once the critical pH is reached, attack on the silica network will occur extremely rapidly by the autocatalytic mechanism postulated by Charles, with resulting failure.

The foregoing discussion may be summarized as follows:

Results from static fatigue tests have been examined against the background of Charles' theory of corrosion mechanism on glass. Disagreement was found in the stress versus failure time relation which does not provide a single exponent required for the stress term in the flaw growth equation used by Charles. The equation is designed to govern the entire stress corrosion process from load application to failure; that is, incubation period and corrosion period. Based on these findings, a new mechanism of stress corrosion failure of glass is proposed. The salient features of the proposed mechanism are: 1) a prolonged incubation period extending over approximately 95% of the life of glass fibers is controlled by hydroxyl ion build-up to a critical level of pH; 2) once the critical level is reached, chemical attack occurs rapidly (autocatalytically) until failure occurs; 3) chemical attack originates at preferred sites on the

---

\* For description of flaws, see Part 1, Section I, 3.

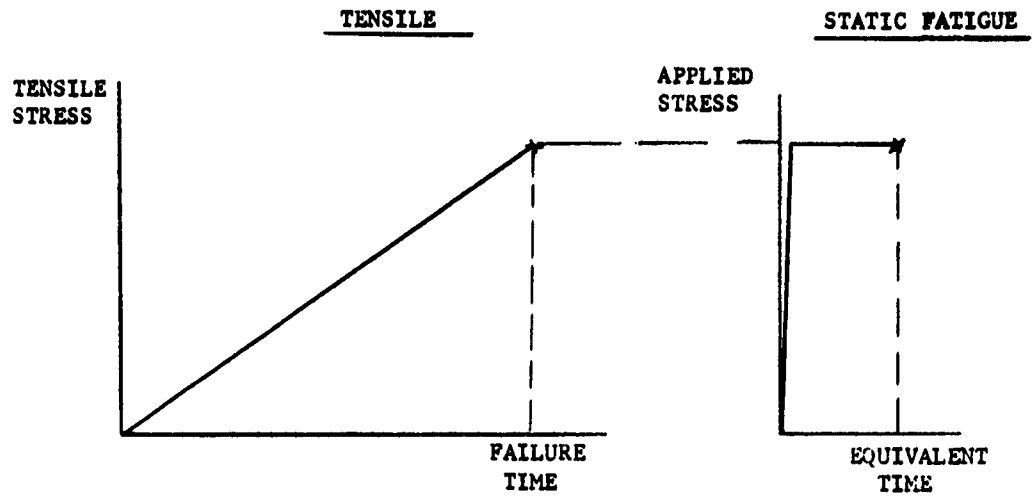


FIG. 36 TIME RELATIONSHIP BETWEEN TENSILE AND STATIC FATIGUE TEST

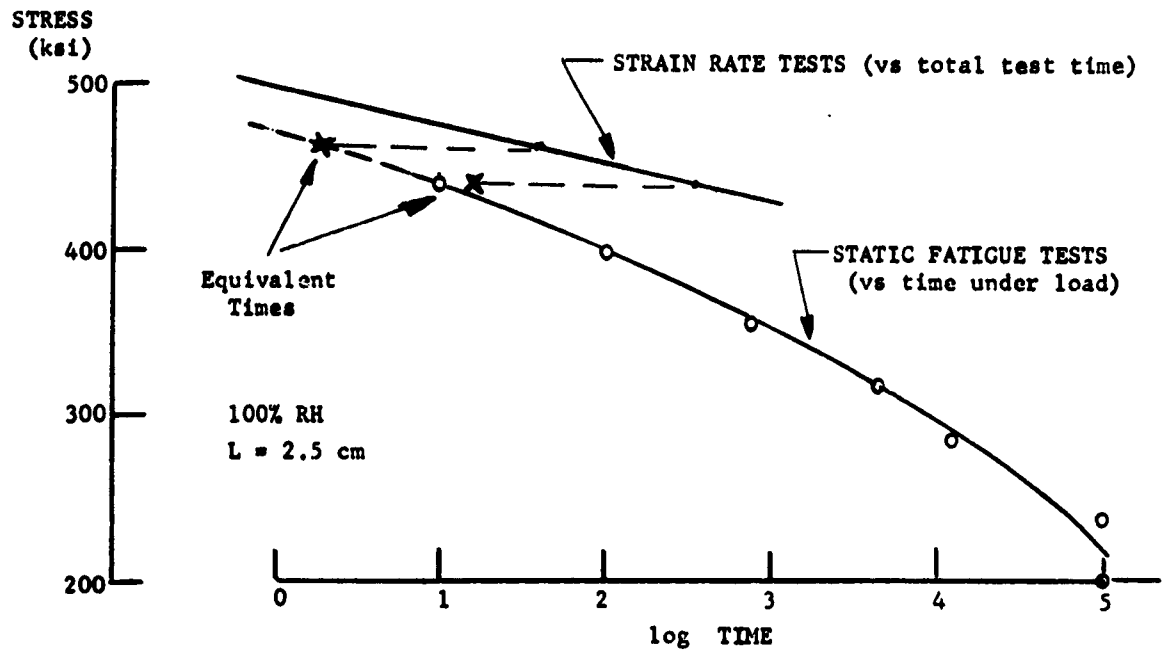


FIG. 37 COMPARISON OF STRAIN RATE AND STATIC FATIGUE DATA

fiber (structural defects or C-flaws) which may or may not coincide with the location of (much larger) surface flaws. 4) The apparent rate of corrosion, if expressed as a power-function of stress, is not determined by a single exponent of this function.

## 5.2 STRESS CORROSION IN TENSILE TESTS

Stress corrosion must be occurring throughout the course of a tensile test\*, but because of the changing stress with time, it is not possible to correlate tensile results with the static fatigue data. Fig. 36 illustrates the problem: what time under a load equal to the tensile strength would be required for static fatigue failure, and does this correspond to the summation of all the stress corrosion experienced under the continuously increasing loads of the tensile test?

A simple assumption was made for the purposes of calculating the stress corrosion damage. This assumption is that the damage fraction is equal to the fraction of the failure time for which the specimen was exposed under that load. In other words, if the failure time under a nominal stress,  $S$ , is equal to  $t_{sn}$  and a specimen is only exposed for a time,  $t_n$ , the fractional life lost is?

$$\frac{t_n}{t_{sn}},$$

$$\text{when } \sum_1^n \frac{t_n}{t_{sn}} = 1.0, \text{ failure will occur.}$$

The damage is assumed to include the incubation and corrosion stages, so that a damage fraction of 0.1 might indicate only that the build-up of hydroxyl ions is a little over 10% complete, but no actual corrosion had occurred.

The biggest assumption in this derivation is that the event occurring during the process at each stress level is the same. But this assumption is not too critical because the major portion of the damage occurs at the highest stresses prior to fracture.

Table X shows a sample calculation for a strain rate of  $0.06 \text{ min}^{-1}$  and a gage length of 2.5 cms. The stress corrosion data used is for 100% RH so that the

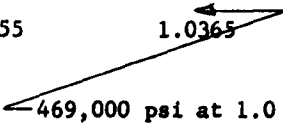
---

\* This was confirmed by tensile tests in three different atmospheric environments: Vacuum, 50% RH, and 100% RH (Bi-monthly Report No.7, 1965). Fibers of 2.5 cm length were tested at strain rates of 0.06 and  $0.006 \text{ min}^{-1}$ . It was found that the average strength decreased by approximately 5 percent if humidity was increased from 50% to 100% RH. At vacuum of  $10^{-6}$  torr, atmospheric water is reduced by a factor of approximately  $10^9$  so that only surface-adhered water is available for stress corrosion. Accordingly, tensile strengths increased by 10 to 12 percent above the 50% RH values. This compares favorably with approximately 15 percent reported by other investigators.

TABLE X

## CUMULATIVE DAMAGE FROM STRESS CORROSION IN TENSILE TEST at 100% RH

Sample Calculation for Standard Strain Rate  $0.06 \text{ min}^{-1}$  and Gage Length 2.5 cm

Stress Range (ksi)	Average Stress Corrosion Failure Time(*) $t_s$ (sec)	Tensile Test Time $t$ (sec)	Loss from Stress Corrosion	
			Fraction of Life Lost $\frac{t}{t_s}$	Total Lost (Cumulative)
0-100	$10^6$	10	0.00001	0.00001
100-200	$3 \times 10^5$	10	0.00003	0.00004
200-300	$5 \times 10^4$	10	0.0002	0.00024
300-400	$1.2 \times 10^3$	10	0.0083	0.00854
400-420	$5 \times 10^1$	2	0.040	0.0485
420-440	15	2	0.133	0.1815
440-460	5	2	0.400	0.5815
460-470	2.2	1	0.455	1.0365
		Total 47 sec		

(\*) From Fig. 30

TABLE XI

## STRESS CORROSION TIME EQUIVALENCE OF TENSILE TESTS

(Gage length constant at 2.5 cm)

Strain Rate, $\text{Min}^{-1}$	Tensile Strength, ksi			Time, Seconds (100% RH)	
	50% RH	100% RH	Calculated*	Tensile Test	Equivalent Time <sup>+</sup>
0.06	496	(462)	469	44	2
0.006	465	(440)	429	425	15

\* See Table X for calculation.

+ Equivalent time is time under load (in static fatigue) equal to tensile strength in 100% RH atmosphere



calculated tensile strength of 469,000 psi is very close to the tensile strength of 462,000 psi. The latter figure has been obtained by applying a 5% correction to a representative tensile strength measured at 50% RH. Table XI presents typical strength data for both 0.06 and 0.006 min<sup>-1</sup> strain rates, and the times of the actual tensile test, as well as the calculated equivalent time.

Data from variable strain rate tensile tests and from the static fatigue tests can now be compared by using these equivalent times. Fig. 37 summarizes these results. It can be seen that the equivalent times bring the tensile data in conformity with the static fatigue data.

### 5.3 CONCLUSIONS

1. Tensile strength measurements of E-glass fibers at various times during static fatigue tests have shown that the initial strength did not deteriorate up to approximately 95% of the life of the fibers. Corrosion must, therefore, occur very rapidly in the last phase of the life.
2. To explain this behavior, it is assumed that chemical processes during the prolonged incubation period must reach a critical stage before the corrosion process can occur.
3. The chemical processes are believed to occur on sites of structural flaws where concentration of terminal cations interrupt the silica network. Interaction of water with cations leads to hydrolysis and an increase in concentration of hydroxyl ions, i.e., an increase in pH. Incubation continues until the pH reaches a critical level for corrosion to occur. Preliminary experiments have supported this view.
4. Structural flaws (defined in earlier work as C-flaws) are distributed densely in the glass fibers. They may be located at the surface or below, and may coincide with much larger surface flaws (A and B-type flaws). Corrosion originates at C-flaws.
5. Analysis of static fatigue data by the method of Charles shows that the required linear relationship between log (Time-to-Failure) and log (Inverse Applied Stress) is not obtained. Some aspects of Charles' stress corrosion mechanism, based on this linear relationship, are subject to doubt.
6. A mechanism of stress corrosion is proposed, based on separation of the two phases--incubation and corrosion. The corrosion phase occupies only a small fraction of the life of the fibers, approximately 5 to 10 percent, and occurs rapidly after chemical processes during the incubation period have reached a critical phase.
7. Stress corrosion in tensile tests becomes effective only at stresses high enough to allow the total corrosion failure process to occur in the time available for fracture. Calculations on the basis of static fatigue data indicate that the process takes place in approximately the last 5 percent of the tensile test time.

## VI. GENERAL CONCLUSIONS

The measured strength of glass fibers ranges from nearly zero to values approaching the theoretical strength of glass, i.e., 1.5 to 2 million psi. These strengths are caused by various types of flaws that can be determined from statistical strength measurements. However, since flaws are changing with time in any given experimental condition, the respective strength values must be related to the specific test and environmental conditions, if the term "strength" is to indicate a property of the material. It appears to be more appropriate to speak about strength properties of glass fibers.

Typical parameters influencing the strength as measured are: gage length, time and mode of loading, and humidity, while melting history of the glass and conditions during fiber forming are factors that set the stage in the first place.

Humidity can be singled out as the most important parameter since it leads to stress corrosion, and hence to the aforementioned change of flaws. It has been shown that stress corrosion is the limiting factor, not only in static fatigue (delayed failure), but also in tensile tests whenever water vapor is available. The corrosion process seems to initiate at structural flaws where concentrations of terminal cations interrupt the silica network. Structural flaws are distributed densely in the glass and, if coinciding with larger surface defects, could lead to preferential flaw growth, depending upon the location in the flaw.

The experimental and analytical methods developed for the purpose of this work have been applied to examine glass fibers, as well as available strength data from other laboratories. The results were consistent with the findings on Solar-drawn glass. Thus, the methods have proven to be a powerful tool in the study of strength properties of materials subject to statistical strength measurements.

## VII. RECOMMENDATIONS

The outcome of this work indicates a need for improvement of test procedures, for further studies of strength properties and for improvement of composites as follows:

- 1) It seems almost mandatory to standardize tensile tests in order to provide for comparable strength data. Primary points to be considered are: gage length, strain rate, and relative humidity; other points are: treatment of data (i.e., omission of low values) and presentation of data.
- 2) Strength properties have been studied fairly comprehensively for E-glass (tensile and static fatigue) but less so for S-glass (tensile only).

Additional studies of S-glass and other new glasses, as well as other materials in filament form are recommended to enlarge the body of knowledge and thus further the understanding of fiber problems.

- 3) The mechanism of stress corrosion of glass fibers is perhaps the least understood. Extension of this work is recommended, and could include critical tests designed to increase the static fatigue life of the fibers. Results from such tests could be used to improve the wet strength of reinforced composite structures.

# REFERENCES

- (1) A. A. Griffith, The Phenomena of Rupture and Flow in Solids, Philosophical Transactions, Series A, Vol.221, Society of London, 1920-1921. The Theory of Rupture, Procedures of International Congress of Applied Mechanics, Vol.55, 1924.
- (2) W. Weibull, A Statistical Theory of the Strength of Materials, Handlingar, Royal Swedish Academy of Engineering Sciences, No.151, 1939.
- (3) J. A. Kies, The Strength of Glass, NRL Report 5098, April 1958, and Filament Winding Symposium, Soc. of Aerospace Material Process Engrs. 1961, P. 273.
- (4) W. F. Thomas, An Investigation of Factors Likely to Affect the Strength and Properties of Glass Fibers, Physics and Chemistry of Glasses, Vol. 1, February 1960.
- (5) F. O. Anderegg, Strength of Glass Fibers, Industrial and Engineering Chemistry, Vol.31, 1939.
- (6) D. Sinclair, A Bending Method for Measurement of Tensile Strength and Young's Modulus of Glass Fibers, Journal of Applied Physics, Vol.21, 1950.
- (7) W. H. Otto, private communication, NARMCO Research & Development, San Diego, Calif.
- (8) J. Cornelissen, H. W. Meyer and A. M. Kruithof, Statistical Distribution of the Strength Values of Glass Rods, Advances in Glass Technology, 6th International Congress on Glass, Washington, D.C., July 1962.
- (9) G. K. Schmitz and A. G. Metcalfe, Characterization of Flaws on Glass Fibers, SPI Reinforced Plastics Division, Proceedings, 1965.
- (10) E. M. Lindsey, J. C. Hood, et al, Glass Reinforcement for Filament Wound Composites, Office of Tech. Services, Dept. of Commerce, TR-64-8-104 (Final Report, December 1963)
- (11) R. J. Charles, Static Fatigue of Glass I and II, Journal of Applied Physics, Vol.29, No. 11 (1958).
- (12) N. M. Cameron, The Effect of Annealing on the Room Temperature Strength of Glass Fibers, University of Illinois, T & AM Report No. 207, (1962).
- (13) R. E. Mould and R. D. Southwick, Strength and Static Fatigue of Abraded Glass under Ambient Conditions: II, Effect of Various Abrasions and the Universal Fatigue Curve, J. Am. Ceram. Soc., Vol.42, No. 12 (1959).
- (14) J. B. Murgatroyd, Mechanism of Brittle Rupture in Glass, J. Soc. Glass Technol. Vol.28 (130) 406-31T (1944); Ceram. Abstr. (Sept. 1946).
- (15) J. L. Glathart and F. W. Preston, The Fatigue Modulus of Glass, J. Appl. Phys. 17, 1946.
- (16) N. W. Taylor, Mechanism of Fracture of Glass and Similar Brittle Solids, J. Appl. Phys. Vol.18, No. 11 (1947); Ceram. Abstr. (Aug. 1948).
- (17) D. A. Stuart and O. L. Anderson, Dependence of Ultimate Strength of Glass Under Constant Load on Temperature, Ambient Atmosphere, and Time, J. Am. Ceram. Soc. Vol.36 No. 12 (1953).
- (18) H. A. Elliot, Stress Rupture in Glass, J. Appl. Phys. Vol.29 (1958).
- (19) D. L. Hollinger, T. J. Jordan, et al, General Electric Company, Advanced Engineering and Technology Dept., Private Communication (1965), and Bi-Monthly Reports Numbers 3 and 4, Contract Nonr 4486(00)(X).
- (20) N. M. Cameron, An Introduction to the Factors Influencing the Strength of Glass Fibers, University of Illinois, T & AM Report No.186, (1961).
- (21) C. E. Inglis, Stresses in a Plate Due to the Presence of Cracks and Sharp Corners, Proc. Inst. Naval Architects, March 14 (1913).
- (22) A. G. Metcalfe and G. K. Schmitz, Effect of Length on the Strength of Glass Fibers, ASTM Proceedings, Vol.64 (1964). Reprinted with permission of ASTM from its copyrighted Proceedings.
- (23) N. M. Cameron, An Investigation into the Effect of Environmental Treatments on the Strength of E- Glass Fibers, Univ. of Illinois, T & AM Report No.274 (1965).

## **APPENDIX A**

### **Photographs of Test Instrumentation**

- FIG. A-1 SINGLE FIBER TESTER SET-UP FOR SHORT FIBER TESTING**
- FIG. A-2 MULTIPLE FIBER TESTER**
- FIG. A-3 TEST LABORATORY WITH FIBER DRAWING FACILITIES  
FOR 70-inch MONOFILAMENTS**
- FIG. A-4 FIBER DAMAGE APPARATUS WITH SLED-MOUNTED FIBER AFTER DAMAGE**
- FIG. A-5 GARNET GRAINS USED FOR ARTIFICIAL FIBER DAMAGE**
- FIG. A-6 STATIC FATIGUE TESTER**
- FIG. A-7 VACUUM EQUIPMENT FOR ENVIRONMENTAL TESTING**
- FIG. A-8 MULTIPLE TENSILE TESTER INSTALLATION IN VACUUM CHAMBER**
- FIG. A-9 TYPICAL FIBER MOUNTING FRAMES FOR DIFFERENT TEST EQUIPMENT**

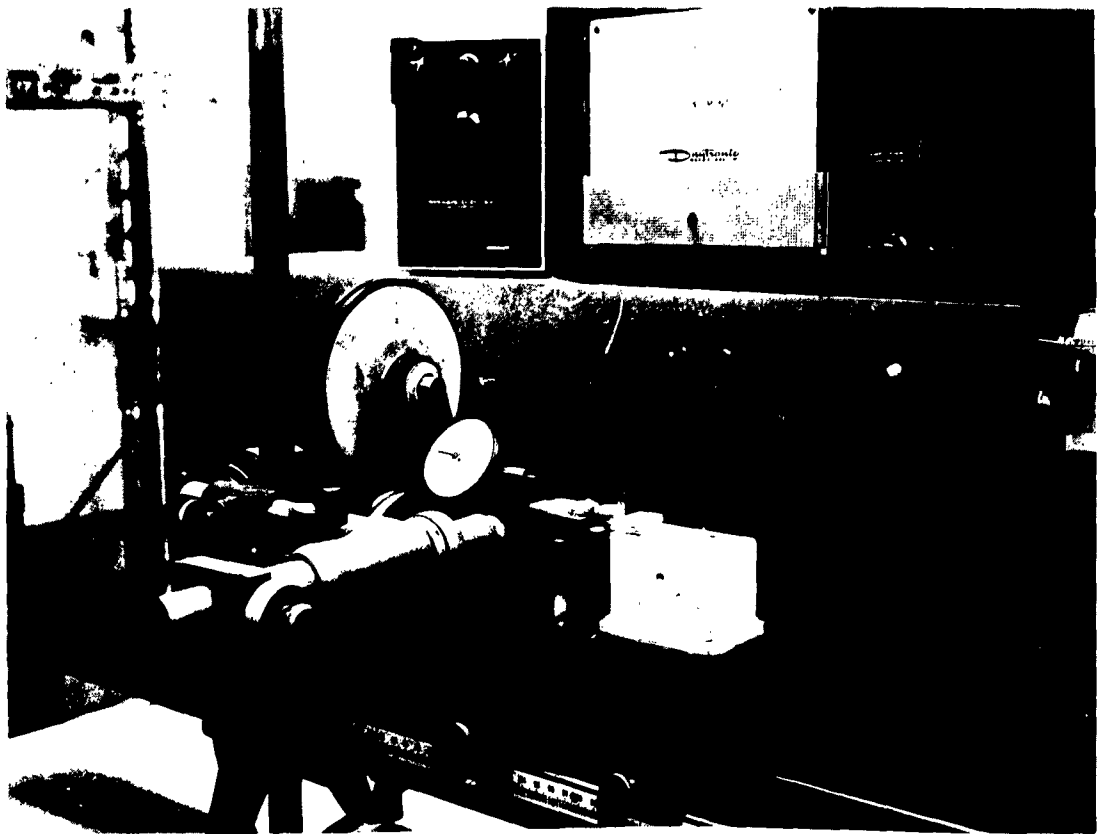


FIG. A-1. SINGLE FIBER TESTER SET-UP FOR SHORT FIBER TESTING



FIG. A-2. MULTIPLE FIBER TESTER



FIG. A-3. TEST LABORATORY WITH FIBER DRAWING FACILITIES FOR 70-inch MONOFILAMENTS

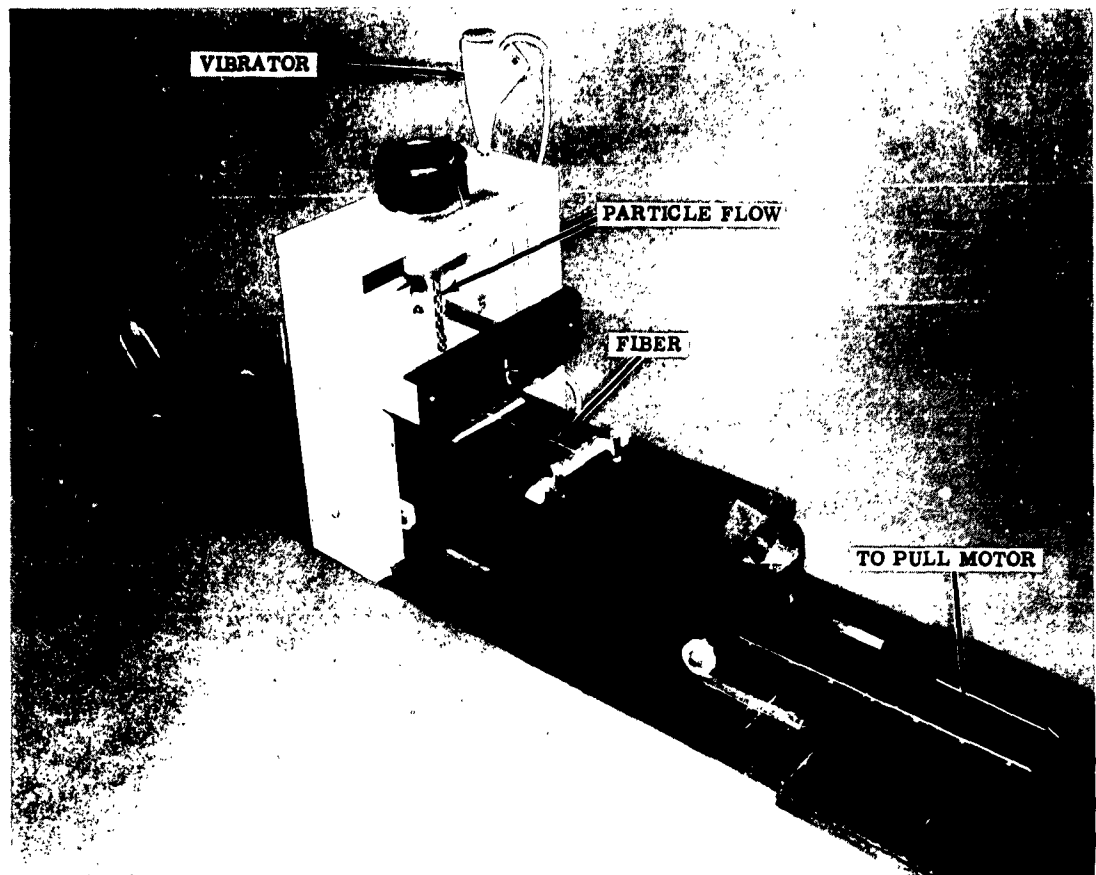


FIG. A-4. FIBER DAMAGE APPARATUS WITH SLED-MOUNTED FIBER AFTER DAMAGE

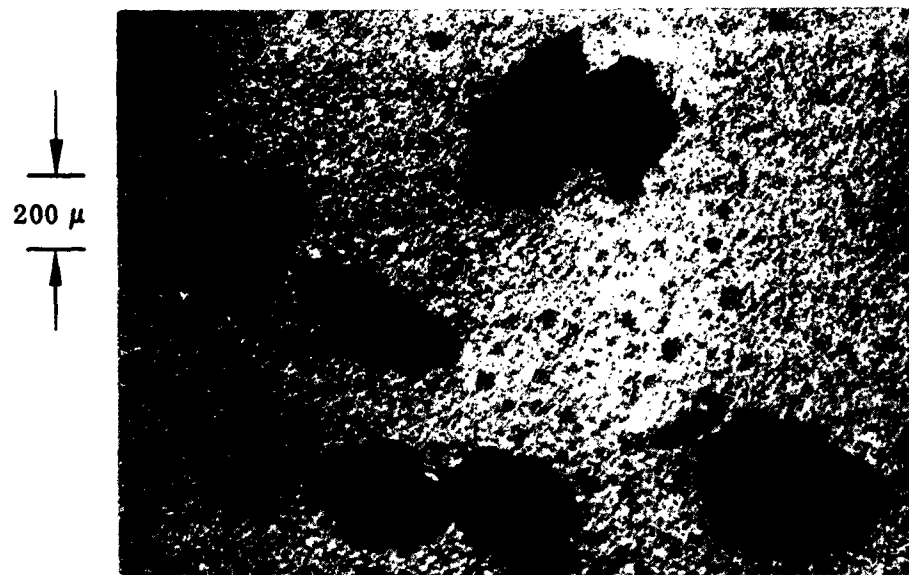


FIG. A-5. GARNET GRAINS USED FOR ARTIFICIAL FIBER DAMAGE



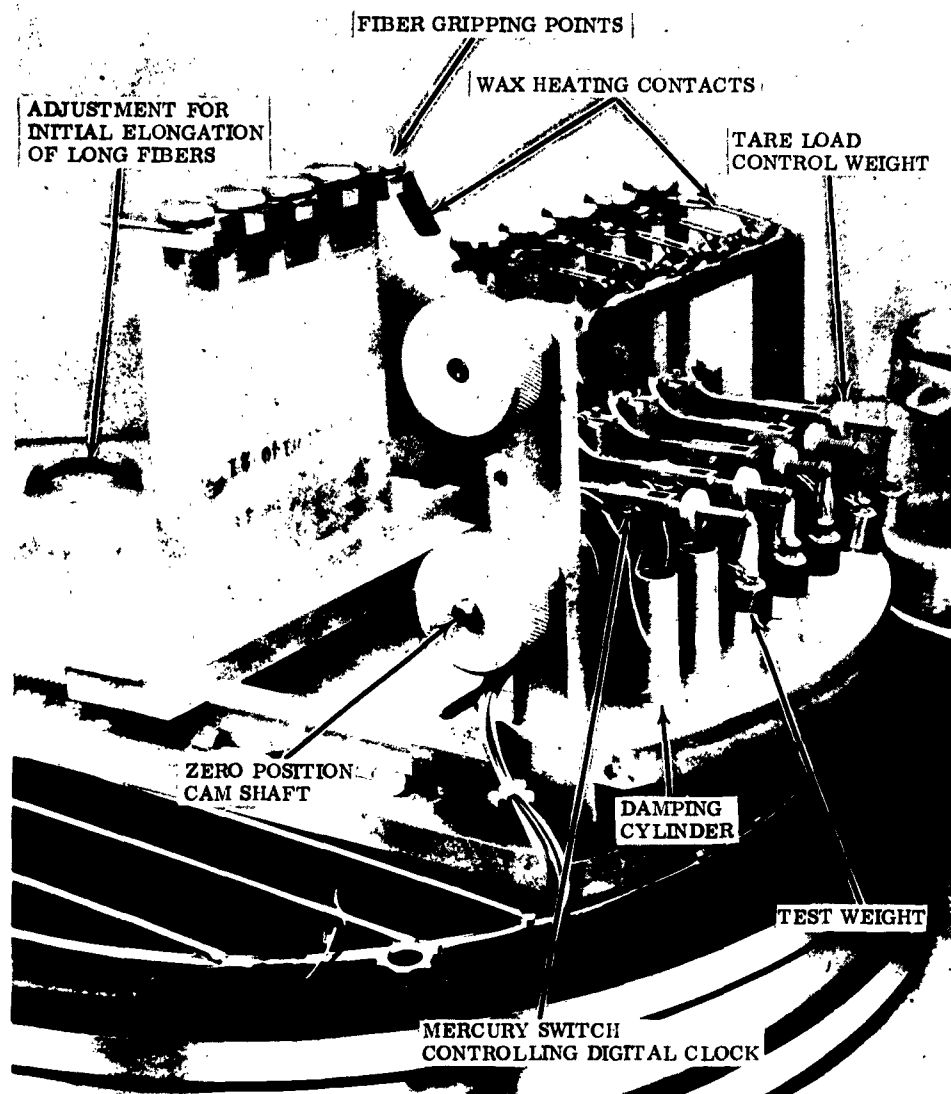


FIG. A-6. STATIC FATIGUE TESTER

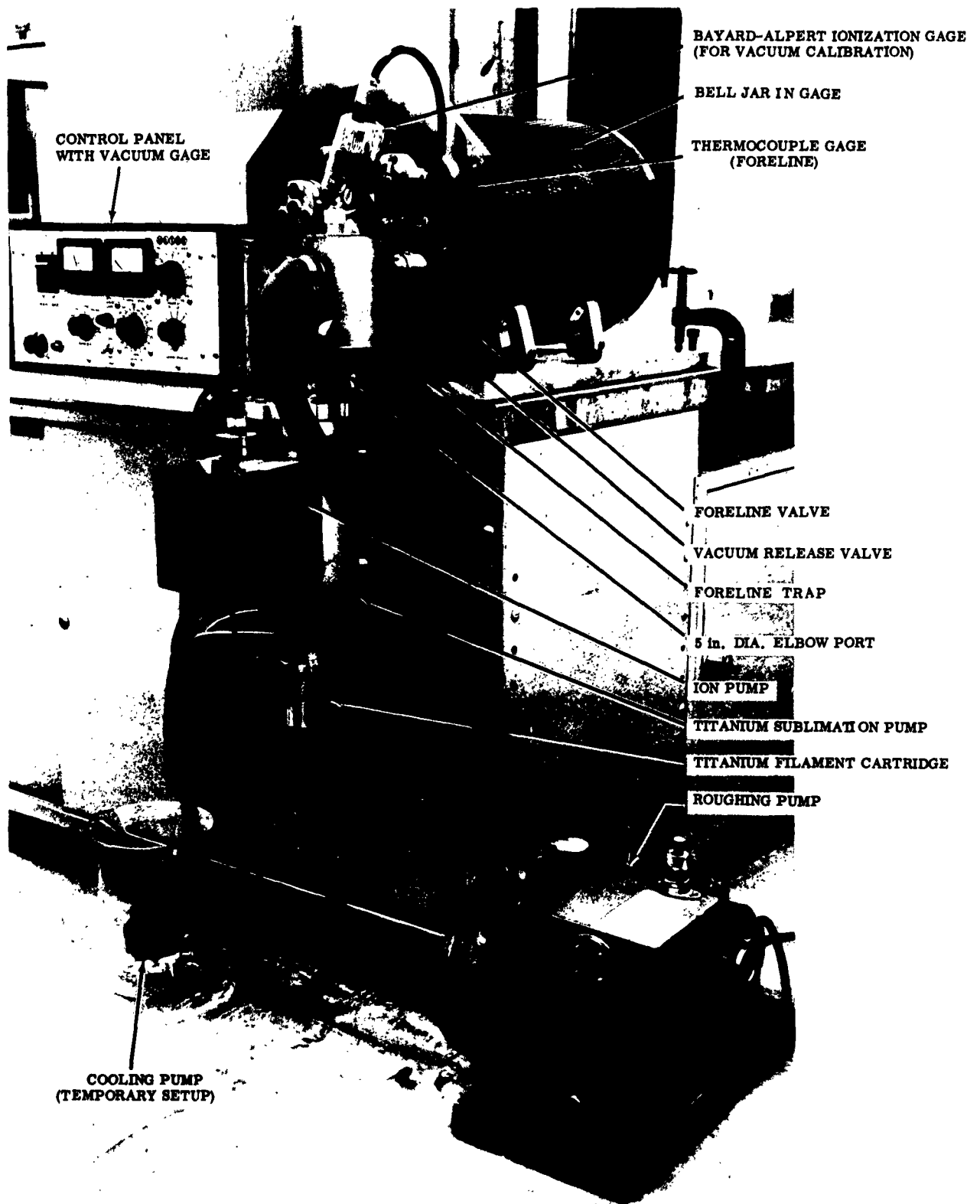


FIG. A-7. VACUUM EQUIPMENT FOR ENVIRONMENTAL TESTING

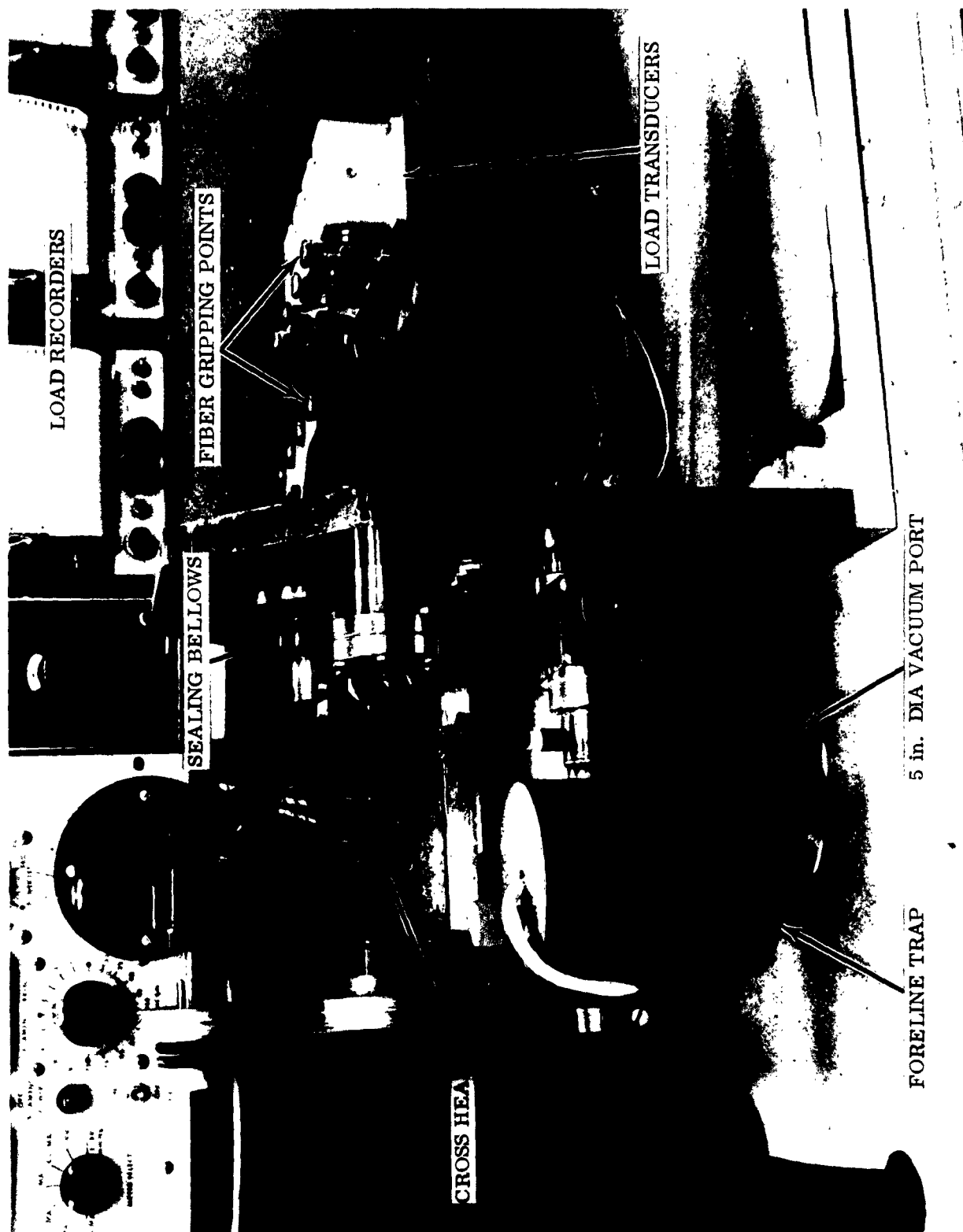
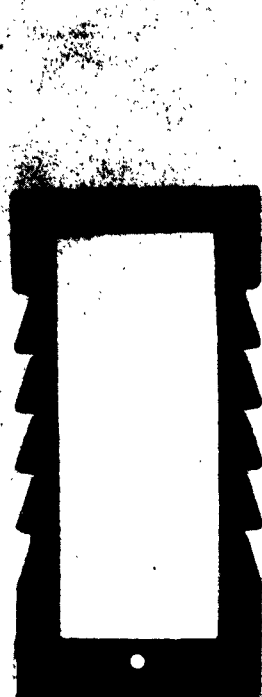
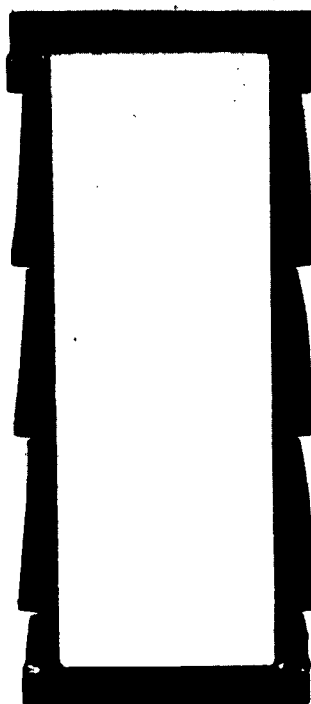


FIG. A-8. MULTIPLE TENSILE TESTER INSTALLATION IN VACUUM CHAMBER



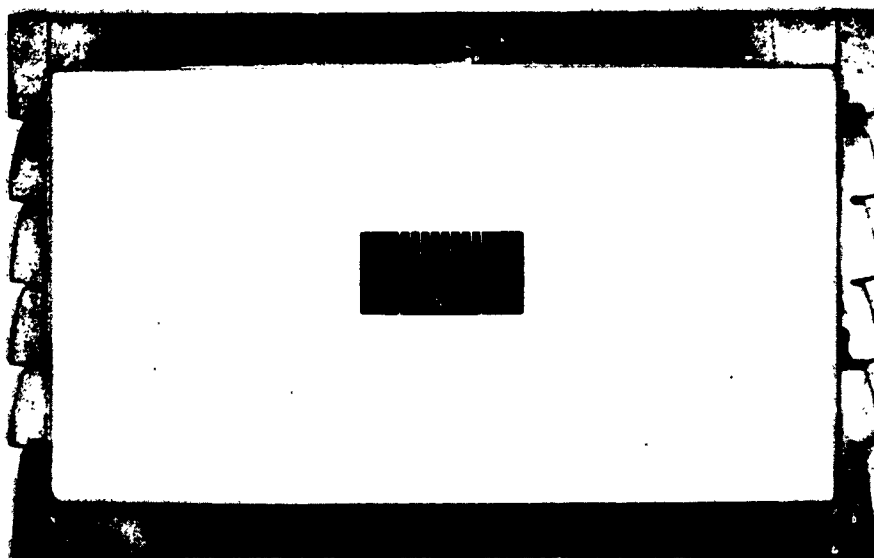
**SINGLE TESTER**  
( $L < 1$  cm)



**MULTIPLE TESTER**  
( $L = 2.5$  cm)



**STATIC FATIGUE TESTER** ( $L = 2.5$  cm)



**SINGLE TESTER AND STATIC FATIGUE TESTER** ( $L = 20$  cm)

**FIG. A-9. TYPICAL FIBER MOUNTING FRAMES FOR DIFFERENT TEST EQUIPMENT**

## APPENDIX B

### APPLICATION OF SINGLE FIBER DATA TO REINFORCED PLASTICS STRUCTURES

The following is part of the discussion of the SPI paper<sup>(9)</sup> by J. A. Kies, NRL.

The discovery and characterization of several kinds of flaw populations in glass offers the hope that through a study of changes in the individual populations we can better learn the effect of different manufacturing, handling, or environmental variables and how to improve the fibers and composites. The authors have made outstanding progress in developing testing and analytical techniques for this purpose.

The usual doubt or misunderstanding by the public of the utility of this kind of work stems mostly from the fact that we do not have a simple direct way of predicting the effect of filament strength as measured on the strength of reinforced plastics. This is complicated by the fact that in reinforced plastic structures the fiber strength is not the only factor and a variety of different failure modes are encountered in service.

Some progress is being made in relating filament strength to composite strength. As an illustration of this possibility, the following mathematical and mechanical model is offered.

Assume that we are interested in the failure of filament wound pressure bottles operating at high stresses. It has been demonstrated fully that one of the important modes of failure initiation is the sometimes violent unwinding or peel back of thin strips, especially in the outer hoop windings of cylinders. If we use a Weibull type distribution function for the strength of fibers, we can compute the probability of finding "n" fiber breaks in a bundle and within an element of length  $\Delta L$  sufficiently small so that the fiber breaks cooperate to form a broken bundle sufficiently big to start peeling away. When this is done we can arrive at a formula such as follows:

$$\left( \frac{\sigma_g}{\bar{\sigma}} \right)^m = \frac{L_1}{0.693 r D} \log_e (1 - x) \quad (1)$$

where  $\sigma_g$  is the median stress for failure in the glass in the composite layer.  $\bar{\sigma}$  is the median stress for failure of single filaments of length  $L_1$  outside the composite. It is assumed that the Weibull coefficient,  $m$ , is characteristic of fibers both in and out of the composite.  $D$  is the fiber diameter and  $r$  is a nondimensional measure of  $\Delta L$  so that  $\Delta L = r D$ . This is

the distance along which the fiber does not provide much strength in the vicinity of a break.

$$x = \left( \frac{arD}{WL} \right)^{1/Na^2} \quad (2)$$

where "a" is the width and depth of a square bundle that contains  $Na^2$  broken fibers within length element  $\Delta L = rD$ . W and L are the width and length of the layer of windings in which failure can occur.

$$N = \frac{4f}{\pi D^2} \quad (3)$$

N is the number of fibers per unit cross sectional area in the parallel winding and f is the volume fraction of glass. In a previous paper at S.P.I., Kies and Bernstein discussed the condition for peel back. In the present application the critical size of the bundle or strip is accordingly -

$$a = \frac{6 K_{IIc}^2}{\sigma_y^2 f^2} \quad (4)$$

where  $K_{IIc}^2$  is a measure of the composite toughness. Tests at NRL showed  $K_{IIc}^2 = 30 \times 10^6$  (psi  $\sqrt{\text{in.}}$ )<sup>2</sup> for S glass in 826/CL resin. Assembling all of this together leads to

$$= \bar{\sigma} \left\{ \frac{L_1}{0.693 r D} \log_e \left[ 1 - \left( \frac{3r D K^2}{\sigma_g^2 f^2 WL} \right) \frac{\pi D^2 f^3 \sigma_g^4}{144 K^4} \right] \right\}^{1/m} \quad (5)$$

To a fair degree of approximation we can compute from Eq. (5) that in the composite the effective strength of the glass,  $\bar{\sigma}$ , is proportional to the strength of the fibers  $\bar{\sigma}$  measured at length  $L_1$ . It is also a function of fiber diameter D, resin toughness K abbreviated for  $K_{IIc}$ , the glass fraction "f", the size of the composite piece WL, and, very importantly, of the debonded length rD at the break of a fiber. The minimum r is 2 for 90 percent stress pick-up.

$\bar{\sigma}_g$  is more sensitive to r than to any of the other variables and to a good approximation

$$- \frac{d(\log \bar{\sigma}_g)}{d(\log r)} = \frac{1}{m} \quad (6)$$

Thus, if resin porosity or moisture creates debonding around fiber breaks  $\Delta L = rD$  becomes large and the strength degrades according to the same law as

that describing the effect of test length on the strength of fibers which is in the Weibull formula -

$$-\frac{d(\log \bar{\sigma})}{d(\log L_1)} = \frac{1}{m}$$

## CONCLUSIONS

In conclusion I want to emphasize that for a certain prevalent mode of failure in highly stressed pressure bottles the Weibull coefficient  $m$  for glass fibers and their strength  $\bar{\sigma}$  which is a function of test length  $L_1$  are in theory important contributors to the strength and reliability of the pressure vessel. If in Eq. (5)  $r$  is kept small, say  $r = 2$  or  $L = 2D$  and the service stress  $\sigma_s$  on the glass is kept moderate to low because perhaps of other modes of failure dominating, then the coefficient  $m$  for the fibers does not control and

$$-\frac{d(\log \sigma_s)}{d(\log WL)} = \frac{1}{Rm}$$

$R$  in such cases can be about 50 so that mechanical damage to the glass would have to be very severe indeed before  $Rm$  is reduced to, say, 20 where it would have a noticeable effect. Fibers after process can be expected to degrade so that  $m = 4$  to 6.

Under good conditions, degrading beyond this does not seem to happen, and since  $Rm$  is the controlling coefficient we do not find the effects of abrasion reflected to a very high degree in the strength and scatter for composite structures. On the other hand the inherent strength  $\bar{\sigma}(L_1)$  is more directly reflected, and stronger glass will enable us to better withstand stress concentrations although the apparent strength of a structure indicates that only a fraction of  $\bar{\sigma}(L_1)$  for small  $L_1$  is being achieved.

Derivation of the above formulas and numerical work to show the effects of the parameters will be published elsewhere.

Other distribution functions simpler than Weibull's result in less complication and easier computation than Equation (5). One such under further study as to its applicability is -

$$s = \left( \frac{\sigma}{\sigma_0} \right)^m \frac{A}{\omega} \quad (7)$$

for the probability of failure at stress below  $\sigma$  somewhere in area  $A$  of the glass and where  $\omega$  is an elemental area of arbitrary but small size. Qualitatively the implications are the same and instead of Eq. (5) we then have Eq. (8) as follows:

$$\frac{\sigma_g}{\bar{\sigma}} = \left\{ \frac{L_1}{0.693 r D} \left( \frac{3 r D K^2}{\sigma^2 f^2_{WL}} \right) \frac{\tilde{n} D^2 f^3 \sigma_g^4}{144 K^4} \right\}^{1/m} \quad (8)$$

The constant 0.693 results from choosing median strengths  $\sigma_g$  and  $\bar{\sigma}$ . In the future one should study the effect of non-uniform tensioning in the fibers of a structure; then for Eq. (7) we would have

$$S = \int \left( \frac{\sigma}{\sigma_0} \right)^m \frac{dA}{\omega}$$



## APPENDIX C

- List of Reports
- Reference Chart for Test Series and Failure Probability Plots

# LIST OF REPORTS

NRL Project 62 R05 19A, Contract Nonr 3654(00)(X)

	Tech.Memo No.	Report	Date Issued	Subjects
(1962)	196	Bi-monthly 1	15 Jan. 62	Preliminary Work
	197	2	26 Mar. 62	Single Fibers Separated from Strands, Tests
	198	3	1 June 62	
	199	4	21 Aug. 62	Strand Tests
	200	5	25 Oct. 62	Fiber Slip.; Theor.Analys. of Bimodal Distributions
	215	Final Report (1)	12 Apr. 63	Discussion of Diff.Distrib. Functions
(1963)	216	Bi-monthly 1	17 Apr. 63	Program Outline 1963; Prelim. Fiber Damage
	217	(Second Contract Year) 2	24 June 63	Solar E-Glass Drawing Performance
	218	3	22 Aug. 63	Virgin E- and S-Glass; Discuss. Analys. of Flaw Distr.
	219	4	24 Oct. 63	Virgin E- and S-Glass Completed
	238	5	30 Dec. 63	Artificial Fiber Damage, E- and S-glass
	239	Final Report 2	25 Mar. 64	Summary of Gage Length Study
(1964/65)	245	Bi-monthly 1	15 Mar. 64	Program Outline, 1964; Prelim. Strain Rate Tests
	246	(Third Contract Year) 2	15 May 64	Strain Rate Tests
	247	3	14 July 64	Strain Rate Tests; Static Fatigue Test Equip.
	248	4	10 Sept. 64	Summary Strain Rate Tests
	249	5	14 Nov. 64	Static Fatigue Tests, Series I; Vacuum Equip.
	250	6	15 Jan. 65	St. F. Tests, Series II; Eval. of St. F. Data
	251	7	15 Apr. 65	Summary of St. F. and Environ. Tensile Tests
	258	Final Summary Report	20 May 65	Summary of Entire Work

REFERENCE CHART FOR TEST SERIES AND FAILURE PROBABILITY PLOTS

Final Summary Report	Bi-Monthly Report		Yearly Report		Failure Probability Plots
	(Test Series)	(Tech.Memo.No.)	(Test Series)	(Tech.Memo.No.)	
PART 1.					
Section I	EM1	216	EM I	239	239
	EM2	219	EM II	239	239
	ES1	197	Series I	215	197
	ES2	197	Series II	215	197
Section II	SM1	218	SM I	239	239
	SS1-A	198	X-994, Series I	215	198
	SS1-B	199	X-994, Series II	215	199
	SS2	--	S-994 (9/19/62)	215	215
Section III	Artificial Damage, E S	238 238	EM III SM II	239 239	239 239
	Strand Tests, E-glass	199	E-glass	215	--
	994-glass	199	994-glass	215	--
PART 2.					
Section IV	Strain Rate, Series 1	246	--	--	--
	3	246	--	--	246
	4a	247	--	--	247
	6	248	--	--	248
Section V	Static Fatigue, Series I	249	--	--	249
	II	250	--	--	250
	III	251	--	--	251
	Tensile, (not specified)	251 251	-- --	-- --	251 251

DISTRIBUTION LIST

Contract NONR-3654(00)(X)A2

Office of Naval Research (2)  
American Embassy  
London, England

Commanding Officer  
ONR Branch Office  
1030 E. Green Street  
Pasadena 1, California

Contract Administrator  
Southeastern Area  
Office of Naval Research  
2110 G Street, N. W.  
Washington, D. C. 20037

Director, U. S. Naval Res. Lab. (6)  
Attn: Technical Information Officer

Office of Technical Services  
Dept. of Commerce  
Washington, D. C. 20230

Defense Documentation Center, (10)  
Cameron Station, Bldg 5  
5010 Duke St.  
Alexandria, Va.

U.S. Naval Research Laboratory  
Washington 25, D. C.  
Attn: Dr. G. R. Irwin  
Code 6200

U.S. Naval Research Laboratory  
Washington 25, D. C.  
Attn: Mr. P. Waterman (2)  
Code 5360

U.S. Naval Research Laboratory  
Washington 25, D.C.  
Attn: Mr. J. A. Kies (10)  
Code 6210

U.S. Naval Research Laboratory  
Washington 25, D. C.  
Attn: Dr. Irvin Wolock  
Code 6213

U.S. Naval Research Laboratory  
Washington 25, D. C.  
Attn: Mrs. Doris Baster  
Code 2027

Department of the Navy  
Bureau of Naval Weapons  
Washington 25, D. C.  
Attn: Mr. H. Bernstein (3)  
Code SP-2714

Department of the Navy  
Bureau of Naval Weapons  
Washington 25, D.C.  
Attn: Mr. Phillip M. Goodwin  
Code RRMA-3

Department of the Navy  
Bureau of Naval Weapons (2)  
Washington 25, D.C.  
Attn: Technical Library

Bureau of Naval Weapons Rep.  
P. O. Box 504  
Sunnyvale, California

Commander  
U.S. Naval Ordnance Laboratory  
White Oak, Maryland

Bureau of Naval Weapons Resident Rep.  
P.O. Box 1947  
Sacramento, California

Bureau of Naval Weapons Br. Rep.  
Allegany Ballistics Laboratory  
Cumberland, Maryland  
Attn: Code 4

**DISTRIBUTION LIST (Cont.)**

**Contract NONR-3654(00)(X)A2**

**Commander  
U.S. Naval Ordnance Test Station  
China Lake, California  
Attn: Mr. S. Herzog  
Code 5557**

**Bureau of Naval Weapons Res. Rep.  
(Special Projects Office)  
c/o Hercules Powder Company  
Bacchus Works  
Magna, Utah**

**BuShips Code 634 C 3  
Washington 25, D.C.  
Attn: W. Graner**

**Department of the Army  
Office, Chief of Ordnance  
Washington 25, D.C.**

**Department of the Navy  
Bureau of Naval Weapons (2)  
Washington 25, D.C.  
Attn: RMMP**

**Commander  
Army Rocket and Guided Missile Agency  
Redstone Arsenal, Alabama**

**Mr. W. Cohen, Code LPS  
National Aeronautics & Space Admin.  
1512 H. Street, N.W.  
Washington 25, D.C.**

**Commander  
Aeronautical Systems Division (2)  
ASRCNC-1  
AF Systems Command  
U.S. Air Force  
Wright-Patterson AFB, Ohio**

**National Aeronautics & Space Admin.  
Lewis Research Center  
21000 Brookpark Road  
Cleveland 35, Ohio  
Attn: Chief Librarian**

**National Bureau of Standards  
Washington 25, D.C.  
Attn: M. Kerper**

**Commander  
Air Force Ballistic Missile Division  
Hq. Air Res. and Devel. Command  
P. O. Box 262  
Inglewood, California**

**Dr. N. LeBlanc (2)  
Allegheny Ballistics Laboratory  
Cumberland, Maryland**

**Commanding General  
Aberdeen Proving Ground  
Maryland**

**Dr. Brelant  
Aerojet-General Corporation (2)  
Azusa, California**

**Commanding Officer  
Picatinny Arsenal  
Dover, New Jersey**

**Dr. F. J. Climent  
Aerojet-General Corporation (2)  
P.O. Box 1947  
Sacramento, California**

**Commander  
Army Ballistic Missile Agency  
Redstone Arsenal, Alabama**

**Mr. George Moe  
Lockheed Aircraft Company  
LMSD Headquarters  
P.O. Box 504  
Sunnyvale, California**

**Commander  
Armed Services Technical Info. Agency  
Arlington Hall Station (10)  
Arlington 12, Virginia**

**Solar  
A Division of International  
Harvester Company  
San Diego 12, California  
Attn: John V. Long**

**DISTRIBUTION LIST (Cont.)**

**Contract NONR-3654(00)(X)A2**

**Professor H. H. Johnson  
Dept. of Eng. Mechanics & Mat'ls  
Thurston Hall  
Cornell University  
Ithaca, New York**

**University of Dayton  
Research Institute  
Dayton 9, Ohio  
Attn: Miss Barbara Henn, Librarian**

**Scientific & Tech. Info. Facility  
P.O. Box 5700  
Bethesda, Maryland  
Attn: NASA Rep. (S-AK/DL)**

**Aerojet-General Corporation  
P.O. Box 296  
Azusa, California  
Attn: Librarian**

**Jet Propulsion Laboratory  
4800 Oak Grove Drive  
Pasadena 3, California  
Attn: I.E. Newlan  
Chief, Reports Group**

**Allegany Ballistics Laboratory  
Hercules Powder Company (2)  
Cumberland, Maryland  
Attn: Tech. Library**

**Solid Propellant Information Agency  
Applied Physics Laboratory (3)  
The Johns Hopkins University  
Silver Spring, Maryland  
Attn: G. McMurray**

**Hercules Powder Company  
Bacchus Works  
Magna, Utah  
Attn: Librarian**

**Professor John Outwater  
University of Vermont  
Burlington, Vermont**

**Professor H. T. Corten  
University of Illinois  
Urbana, Illinois**

**Lockheed Missiles & Space Co.  
A Div. of Lockheed Aircraft  
1122 Jagels Road  
Sunnyvale, California  
Attn: Technical Library**

**Aerojet-General Corporation  
P. O. Box 1947 (5)  
Sacramento, California  
Attn: Dr. W.O. Wetmore**

**Aerospace Corporation  
P.O. Box 95085  
Los Angeles 45, California  
Attn: Library  
Technical Documents Gr.**

**Defense Metals Information Cntr.  
Battelle Memorial Institute  
505 King Avenue  
Columbus 1, Ohio**

**Black Sivalls and Bryson  
Oklahoma City, Oklahoma  
Attn: Manager of Engineering**

**B. F. Goodrich Company  
500 S. Main  
Akron, Ohio  
Attn: Mr. H. W. Stevenson**

**Goodyear Aircraft Corporation  
Akron 15, Ohio  
Attn: Mr. R. Burkley**

**DISTRIBUTION LIST**

**Contract NONR-3654(00)(X)A2**

**Narmco Industries, Inc.  
Research and Development Division  
8125 Aero Drive  
San Diego, California  
Attn: Mr. W. Otto**

**Pittsburg Plate Glass Co.  
7204 Chestnut Street  
Washington D. C. 20015  
Attn: Mr. Richard E. Harmon**

**General Electric Company  
Schenectady, New York  
Attn: Mr. T. Jordan**

**J. G. Shonts  
Lockheed, Dept. 88-20  
Missile & Space Division  
Sunnyvale, California**

**Hercules Powder Company  
P. O. Box A  
Rocky Hill, New Jersey**

**Rocketdyne Engineering  
A Div. of North American Aviation, Inc.  
6633 Canoga Park Blvd.  
Canoga Park, California  
Attn: Mr. E. Hawkinson**

**Lockheed Missiles and Space Company  
A Division of Lockheed Aircraft Corp.  
3251 Hanover Street  
Palo Alto, California  
Attn: Mr. M. Steinberg**

**Plastic Evaluation Center  
Picatinny Arsenal  
Dover, New Jersey  
Attn: ORD-BB**

**Owens-Corning Fiberglass Corp.  
Wash. Rep. R. J. Weber (2)  
900 17th Street, N. W.  
Washington, 6 D. C.**

**Syracuse University  
Wood Products Eng. Dept.  
Syracuse 10, New York  
Attn: E. A. Anderson, Chairman**

**H. I. Thompson Fiberglass Co.  
1602 West 135th Street  
Gardena, California**

Unclassified

Security Classification

## DOCUMENT CONTROL DATA - R&amp;D

(Security classification of title, body of abstract and indexing annotation must be entered when the overall report is classified)

1. ORIGINATING ACTIVITY (Corporate author)		2a. REPORT SECURITY CLASSIFICATION	
SOLAR, A Division of International Harvester Co.		Unclassified	
		2b. GROUP	
3. REPORT TITLE			
EXPLORATION AND EVALUATION OF NEW GLASSES IN FIBER FORM			
4. DESCRIPTIVE NOTES (Type of report and inclusive dates)			
FINAL SUMMARY REPORT 16 Nov. 1961 through 15 Feb. 1965			
5. AUTHOR(S) (Last name, first name, initial)			
Schmitz, Gunther K.			
6. REPORT DATE		7a. TOTAL NO. OF PAGES	7b. NO. OF REFS
May 20, 1965		98	23
8a. CONTRACT OR GRANT NO.		9a. ORIGINATOR'S REPORT NUMBER(S)	
Nonr 3654(00)(X)		RDR 1423-8	
b. PROJECT NO.			
NRL Project 62 R05 19A			
c.		9b. OTHER REPORT NO(S) (Any other numbers that may be assigned this report)	
d.		Tech. Memo No. 258	
10. AVAILABILITY/LIMITATION NOTICES			
All distribution of this report is controlled. Qualified DDC users shall request through U. S. Naval Research Laboratory, Washington 25, D.C., Mr. J. A. Kies, Code 6210			
11. SUPPLEMENTARY NOTES		12. SPONSORING MILITARY ACTIVITY	
		U. S. Naval Research Laboratory Washington 25 D.C. Code 6210	
13. ABSTRACT			
<p>The strength of E- and S-glass fibers was investigated by tensile tests and static fatigue (constant load) tests. The principal variables were: gage length, strain rate, applied stress in static fatigue, and humidity. The gage length study led to identification of two types of surface flaws and a structural flaw type related to the heterogeneity of the glass network. Severity and distribution of flaws were derived from failure probability plots and strength-length plots at one strain rate in laboratory atmosphere. The effects of strain rate and of humidity on the flaw characteristics was studied.</p> <p>Extensive static fatigue tests provided insight into the stress corrosion processes. Fibers retained the initial tensile strength over 95percent of the static fatigue exposure. It was postulated that chemical events during this incubation period had to reach a critical stage before stress corrosion could occur, and that corrosion originated on sites of structural flaws located near the surface. These findings are in disagreement with the current theory on stress corrosion and a new model is proposed.</p> <p>Additional work included investigation of damage resistance of the two glasses, and a study of the effect of gage length on strength of E- and S-glass strands.</p>			

Unclassified

Security Classification

(e)



14. KEY WORDS	LINK A		LINK B		LINK C	
	ROLE	WT	ROLE	WT	ROLE	WT
1. Strength of Glass Fibers a. E- and S-glass b. Tensile c. Strain Rate d. Static Fatigue e. Humidity						
2. Surface and Structural Flaws a. Identification by Gage Length Change b. Flaw Behavior						
3. Stress Corrosion a. Constant Load (Static Fatigue) b. Varying Load (Tensile Tests) c. Varying Humidity						
4. Proposed New Stress Corrosion Mechanism						
5. Developed new experimental and analytical methods.						

## INSTRUCTIONS

1. **ORIGINATING ACTIVITY:** Enter the name and address of the contractor, subcontractor, grantee, Department of Defense activity or other organization (*corporate author*) issuing the report.

2a. **REPORT SECURITY CLASSIFICATION:** Enter the overall security classification of the report. Indicate whether "Restricted Data" is included. Marking is to be in accordance with appropriate security regulations.

2b. **GROUP:** Automatic downgrading is specified in DoD Directive 5200.10 and Armed Forces Industrial Manual. Enter the group number. Also, when applicable, show that optional markings have been used for Group 3 and Group 4 as authorized.

3. **REPORT TITLE:** Enter the complete report title in all capital letters. Titles in all cases should be unclassified. If a meaningful title cannot be selected without classification, show title classification in all capitals in parenthesis immediately following the title.

4. **DESCRIPTIVE NOTES:** If appropriate, enter the type of report, e.g., interim, progress, summary, annual, or final. Give the inclusive dates when a specific reporting period is covered.

5. **AUTHOR(S):** Enter the name(s) of author(s) as shown on or in the report. Enter last name, first name, middle initial. If military, show rank and branch of service. The name of the principal author is an absolute minimum requirement.

6. **REPORT DATE:** Enter the date of the report as day, month, year, or month, year. If more than one date appears on the report, use date of publication.

7a. **TOTAL NUMBER OF PAGES:** The total page count should follow normal pagination procedures, i.e., enter the number of pages containing information.

7b. **NUMBER OF REFERENCES:** Enter the total number of references cited in the report.

8a. **CONTRACT OR GRANT NUMBER:** If appropriate, enter the applicable number of the contract or grant under which the report was written.

8b, 8c, & 8d. **PROJECT NUMBER:** Enter the appropriate military department identification, such as project number, subproject number, system numbers, task number, etc.

9a. **ORIGINATOR'S REPORT NUMBER(S):** Enter the official report number by which the document will be identified and controlled by the originating activity. This number must be unique to this report.

9b. **OTHER REPORT NUMBER(S):** If the report has been assigned any other report numbers (*either by the originator or by the sponsor*), also enter this number(s).

10. **AVAILABILITY/LIMITATION NOTICES:** Enter any limitations on further dissemination of the report, other than those

imposed by security classification, using standard statements such as:

- (1) "Qualified requesters may obtain copies of this report from DDC."
- (2) "Foreign announcement and dissemination of this report by DDC is not authorized."
- (3) "U. S. Government agencies may obtain copies of this report directly from DDC. Other qualified DDC users shall request through \_\_\_\_\_."
- (4) "U. S. military agencies may obtain copies of this report directly from DDC. Other qualified users shall request through \_\_\_\_\_."
- (5) "All distribution of this report is controlled. Qualified DDC users shall request through \_\_\_\_\_."

If the report has been furnished to the Office of Technical Services, Department of Commerce, for sale to the public, indicate this fact and enter the price, if known.

11. **SUPPLEMENTARY NOTES:** Use for additional explanatory notes.

12. **SPONSORING MILITARY ACTIVITY:** Enter the name of the departmental project office or laboratory sponsoring (*paying for*) the research and development. Include address.

13. **ABSTRACT:** Enter an abstract giving a brief and factual summary of the document indicative of the report, even though it may also appear elsewhere in the body of the technical report. If additional space is required, a continuation sheet shall be attached.

It is highly desirable that the abstract of classified reports be unclassified. Each paragraph of the abstract shall end with an indication of the military security classification of the information in the paragraph, represented as (TS), (S), (C), or (U).

There is no limitation on the length of the abstract. However, the suggested length is from 150 to 225 words.

14. **KEY WORDS:** Key words are technically meaningful terms or short phrases that characterize a report and may be used as index entries for cataloging the report. Key words must be selected so that no security classification is required. Identifiers, such as equipment model designation, trade name, military project code name, geographic location, may be used as key words but will be followed by an indication of technical context. The assignment of links, roles, and weights is optional.